Analysis of premature loss of the extraembryonic Amnioserosa in *Drosophila* morphogenetic mutants

by

Roopali Chaudhary

A thesis
presented to the University of Waterloo
in fulfillment of the
thesis requirement for the degree of
Master of Science
in
Biology

Waterloo, Ontario, Canada, 2009

I hereby declare that I am the sole author of this thesis. This is a true copy of the thesis, including any required final revisions, as accepted by my examiners.

I understand that my thesis may be made electronically available to the public.

Abstract

During Drosophila embryogenesis, an extra-embryonic tissue, known as the amnioserosa (AS), is required for the morphogenetic processes of germ band retraction (GBR) and dorsal closure (DC). Being extra-embryonic, the AS is not part of the embryo proper but is eliminated via programmed cell death (PCD) in the late stages of embryogenesis. Programmed elimination of the AS during normal development can be prevented by directly inhibiting apoptosis, either through the deletion of the pro-apoptotic genes *hid*, *grim* and *reaper*, or through the expression of the pan-caspase inhibitor P-35. PCD in the AS can also be prevented by indirect inhibition of apoptosis via inactivation of autophagy, either through activation of the InR/PI3K pathway, or through activation of the Ras signalling pathway. The timing of AS elimination is critical to development as mutants associated with premature AS loss fail in GBR. To better characterize this premature AS death, a detailed phenotypic analysis of the AS behaviour in the GBR mutant *hindsight* (*hnt*) was performed. Direct inactivation of apoptosis failed to rescue the GBR defects in *hnt* mutant, though the premature AS death was completely rescued. Inactivation of autophagy, however, rescued AS cell behaviour and contacts during GBR, with partial rescue of the GBR defects in the *hnt* mutant. The nature of premature AS loss is characterized as a possible model for anoikis, a form of cell death that is triggered through reduced cell-cell or cell- matrix contact.

Acknowledgments

I would like to thank my supervisor, Dr. Bruce H. Reed for giving me the opportunity to work in his lab. Bruce's willingness to share his extensive knowledge and his guidance throughout my project is greatly appreciated. Thank you for allowing me to return to your lab, and for believing in my abilities. It has been a wonderful experience to pursue science under your guidance.

I would like to express my gratitude to my committee members, Dr. Bernie Duncker and Dr. Mungo Marsden, for their valuable suggestions and guidance throughout this work.

A big "Thank you" goes out to the past and present members of the Reed Lab. In particular, I would like to thank Nilufar Mohseni for her wonderful friendship and advice on an array of topics. I would also like to thank Stephanie McMillan for her "mind-blasting" friendship, and for always extending her ears to listen to me.

I would especially like to thank my family for their constant support and encouragement throughout the course of my Masters. I would like to thank my dad, Sohan Lal Chaudhary, and my mom, Neelam Chaudhary, for always standing by my side. I would also like to thank my brother, Rohit and my wonderful sister, Shefali, for making me laugh during times of frustration.

A great appreciation is extended to all of the above people whose support and encouragement helped me accomplish this work.

Table of Contents

List of Figures

List of Tables

Abbreviations

AEL	After Egg Laying
ARM	Armadillo
AS	Amnioserosa
Atg	Autophagy genes
boss	Bride of Sevenless
crq	Croquemort
da	Daughterless
DC	Dorsal Closure
DEcad	*Drosophila* E-cadherin
DIAP	*Drosophila* Inhibitor of Apoptosis Protein
$dInR^{ACT}$	Activated Insulin Receptor
ftz	Fushi tarazu
ftzUA	Fushi tarazu GAL4 driver with Ubiquitin DE-cad^{GFP} and UAS-$actin^{GFP}$
GBR	Germband Retraction
GFP	Green Fluorescent Protein
hid	Head Involution Defective
hnt	Hindsight
IAP	Inhibitor of Apoptosis Protein
IRS	Insulin Receptor Substrate
JNK	Jun N-terminal Kinase
kr	Kruppel
LE	Leading Edge

mCD8	Myristoylated CD8 protein
MDCK	Madin-Darby Canine Kidney
PKA	Protein Kinase A
PKB/Akt	Protein Kinase B
PI3K	Phosphotidylinositol-3-kinase
PIP_2	Phosphotidylinositol-4,5-bisphostphate
PIP_3	Phosphotidylinositol-3,4,5-trisphosphate
Ras^{V12}	Activated Ras
rpr	Reaper
RREB	Ras Responsive Element Binding protein
TOR	Target of Rapamycin
TUNEL	Terminal Deoxynucleotide Transferase mediated dUTP-biotin nick end-Labelling
UAS	Upstream Activating Sequences

Chapter 1 – Introduction

Morphogenesis is the creation of biological structure, or 'morphology', through the regulation of the spatial relationships between cells and among group of cells over time (Gilbert, 2003). Morphogenesis can involve modifications in cell shape, cell-cell adhesion, cell proliferation, and cell death (Davies, 2005). Coupled with cellular growth and cell fate determination, morphogenetic movements are an integral part of broader developmental programs that specify the final form of tissues and organisms (Stronach and Perrimon, 2001). In general, tissue morphogenesis is essential for embryonic development and adult tissue physiology.

This study concerns the analysis of a morphogenetic mutant in the model genetic organism *Drosophila*. The mutant in question, known as *hindsight*, disrupts morphogenesis and cell death during embryonic development. While these mutant phenotypes are related, the topics of morphogenesis and programmed cell death are reviewed separately in this introduction.

1.1 Morphogenesis in the *Drosophila* embryo

The first two hours of *Drosophila* embryonic development involve rapid nuclear division and result in a syncytium containing approximately 5000 nuclei. The vast majority of these nuclei migrate to the blastoderm cortex where they are "cellularized" by invaginations of plasma membrane. The completion of cellularization at the end of the third hour of embryonic development creates the cellular blastoderm embryo. Gastrulation of the *Drosophila* blastoderm involves the internalization of cells through the formation of the ventral and cephalic furrows, as well as the anterior and posterior

midgut invaginations. Gastrulation segregates three distinct layers of cells—the endoderm, ectoderm, and mesoderm (Gilbert, 2003).

Morphogenesis begins soon after the formation of the *Drosophila* cellular blastoderm. There are four main morphogenetic movements in the post-gastrulation embryo: germband extension, germband retraction, dorsal closure and head involution. (The "germband" is generally considered to be the part of the embryo that gives rise to the thoracic and abdominal segments (Irvine and Wieschaus, 1994)). Germband extension starts shortly after the onset of gastrulation and continues through the fourth hour of development concomitant to posterior midgut invagination (Irvine and Wieschaus, 1994). During germband extension, also known as germband elongation, the length of the germband increases along the anterior-posterior axis through the intercalation of cells along the dorsoventral axis (Schöck and Perrimon, 2002). The developing embryo, however, is encased by the vitelline membrane, which creates a spatial restriction for the elongating germband. As a consequence, the elongating germband appears to push itself around the posterior end of the embryo, essentially folding over top of itself (Irvine and Wieschaus, 1994) (Table 1.1; Figure 1.1). By the end of elongation, the posterior tip of the germband has traveled approximately 70% of the embryo length towards the head region (da Silva and Vincent, 2007).

The germband remains in the extended state for about three hours, during which segmentation of the epidermis occurs (Ashburner, 1989) (Table 1.1). The second morphogenetic event, germband retraction, begins at the end of this three-hour period when the embryo is approximately 7 hours old (stage 12) (Table 1.1). The event or signal that triggers the onset of germband retraction is not known. During GBR, also known as

germband shortening, the process of germband elongation is reversed, and as the germband shortens, the caudal end of the germband returns to its final posterior position (Yip, Lamka, and Lipshitz, 1997) (Figure 1.1). Unlike germband elongation, the mechanism of GBR is not associated with intercalation, but involves regulated cell shape changes in the lateral epidermis (Schöck and Perrimon, 2002). During retraction, the germband doubles along its dorsoventral axis, while decreasing by 50% along its anterior-posterior axis (Schöck and Perrimon, 2002). As the germband retracts, the extra-embryonic amnioserosa (AS) unfolds and is exposed on the dorsal side of the embryo (Figure 1.1). (The ontogeny and characteristics of the AS are described in section 1.1.1).

Following GBR the AS is completely exposed on the dorsal surface of the embryo, and dorsal closure (DC) is initiated (Table 1.1). Unlike germband extension and retraction, there is no pause between retraction and DC. DC occurs from 10 to 13.3 hours of development and during this time the AS is flanked by lateral epidermal cells (Figure 1.1). During DC, the two lateral epithelial sheets advance to close the opening transiently covered by the AS (Toyama *et al.*, 2008) (Figure 1.1). The dorsal-most row of cells of each lateral epithelial sheet (the row of cells which abut the AS) is collectively known as the leading edge (LE) (Reed, Wilk and Lipshitz, 2001). As DC progresses, the LE cells extend filopodia and lamellipodia that contact the AS as well as each other (Reed, Wilk and Lipshitz, 2001). LE cells are also associated with high Jun N-terminal Kinase (JNK) signalling, while the AS cells have little or no JNK signalling activity; the maintenance of this high/low JNK signalling boundary between the LE and AS cells has been suggested to be necessary for the proper progression of DC (Reed, Wilk, and Lipshitz, 2001). During DC, the LE cells elongate in the dorsoventral axis of the embryo, while the AS

cells contract (Gorfinkiel and Arias, 2007) (Figure 1.1). The co-ordinated activity of both cell types contributes to the completion of DC (Kiehart *et al.*, 2000). DC is completed when the LE cells approach each other, meet and fuse at the dorsal midline; a process known as zippering (Reed, Wilk and Lipshitz, 2001). As the LE cells zipper, the AS cells are internalized, and die through programmed cell death (Gorfinkiel and Arias, 2007).

The last morphogenetic event to be discussed is head involution. The regulation and mechanism of head involution is generally considered to be more complex than germband extension, GBR, or DC. In general, head involution is not well understood, although there is some evidence that DC and head involution may be linked in terms of both mechanism and regulation (VanHook and Letsou, 2008). Head involution involves the progression of the epidermis over the head segments, which simultaneously move into the embryo (VanHook and Letsou, 2008). Head involution is complete when the head epithelium completely covers the anterior end of the embryo (VanHook and Letsou, 2008) (Figure 1.1).

Upon completion of these main morphogenetic events, the mature *Drosophila* embryo has adopted its final form—that of the first instar larva.

Table 1.1: Stages of development in *Drosophila* embryo (modified from Ashburner, 1989)

STAGE NUMBER	HOURS AFTER EGG LAYING (AEL)	DEVELOPMENT
1-5	0 – 2:50 hr	Fertilization to cellularization of the embryo
6	2:50 – 3 hr	Onset of gastrulation; the three germ layers are formed
7	3 – 3:10 hr	Gastrulation complete; germband elongation begins
8	3:10 – 3:40 hr	Rapid germband elongation
9	3:40 – 4:20 hr	Slow germband elongation
10-11	4:20 – 7:20 hr	Germband elongation ends; segmentation of the epithelia
12	7:20 – 9:20 hr	Germband retraction begins
13	9:20 – 10:20 hr	Germband retraction ends
14	10:20 – 11:20hr	Dorsal closure initiates; head involution begins
15	11:20 – 13 hr	End of dorsal closure and head involution
16-17	13 – hatching (21-22 hr)	Mid gut constrictions; muscle movements; trachea fill with air; first instar larva hatching

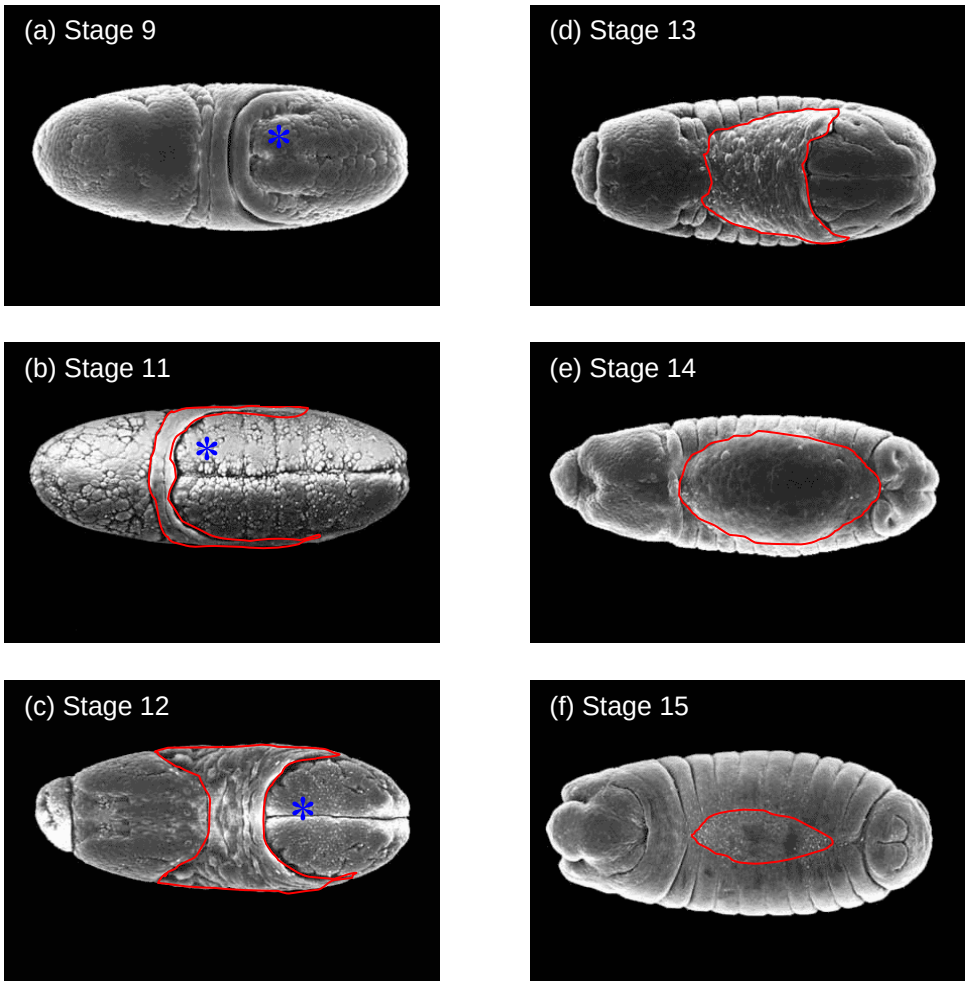

Figure 1.1: Morphogenesis in the *Drosophila* embryo; SEM images; dorsal view. (a) Gastrulation completed and germband (blue asterisks *) has been differentiated (approximately 3.5 hrs old). Germband extension is initiated. Refer to Table 1.1 for details. (b) Germband extension is completed (approximately 7.5 hrs old). The germband is folded on top of itself, and the AS (indicated in red) fills the space between. The asterisk represents the future posterior ventral epidermis of the embryo. (c) Mid-GBR (9 hrs old); the germband shortens and the AS begins to be exposed on the dorsal side of the embryo. (d) Near the end of GBR (approximately 9.5 hrs old) where the folded AS peels off the caudal region of the embryo. (e) Beginning of DC (approximately 10.5 hrs old); the AS is fully exposed on the dorsal side of the embryo. (f) Late DC stage (approximately 12.5 hrs old); the LE cells start to zipper up around the AS, while being internalized into the embryo proper; head involution is also almost completed with the epithelium almost covering all the anterior region. All embryos are oriented with the anterior to the left. (Modified from Turner and Mahowald, 1979).

1.1.1 The Amnioserosa, an extra-embryonic tissue involved in morphogenesis

The amnioserosa (AS) plays a pivotal role in guiding major morphogenetic movements, including GBR and DC (Jacinto and Martin, 2001; Reed *et al.*, 2004). The AS is a squamous epithelial monolayer that derives from the dorsal-most region of the cellular blastoderm (Frank and Rushlow, 1996).

The AS forms during gastrulation from columnar epithelial cells generated at cellularization (Pope and Harris, 2008). As germband extension begins, the AS cells flatten and elongate to fill the space between the dorsal and ventral half of the germband as it folds on top of itself (Frank and Rushlow, 1996). Interestingly, the cells of the presumptive AS do not undergo any post-blastoderm mitotic divisions, whereas most other tissues generally undergo two or three divisions post-blastoderm (Foe, 1989). At the end of germband extension and during the early stages of GBR, the posterior most AS cells maintain adhesions with the caudal end of the germband, and form a layer of overlapping cells on the germband epithelia (Schöck and Perrimon, 2002). As GBR continues, the AS and the germband move as one coherent sheet (Figure 1.1); the overlap of the AS on the germband gradually decreases as the contact with the yolk sac increases (Schöck and Perrimon, 2002). The AS is fully exposed on the dorsal side of the embryo by the end of GBR and the beginning of DC (Figure 1.1). As DC proceeds, 10% of the AS cells are basally extruded from the epithelium; these extruded cells undergo apoptosis upon losing contacts with neighbouring cells (Mohseni *et al.*, 2009). The remaining 90% of AS cells undergo programmed cell death following DC (Mohseni *et al.*, 2009). Since the AS is eliminated during the normal course of embryogenesis and is not part of the embryo proper, the tissue is considered extra-embryonic.

The AS tissue is essential for the completion of GBR and DC; it plays crucial roles in generating force between the epithelial cells and the AS (Lamka and Lipshitz, 1999; Schöck and Perrimon, 2002), as well as providing signals for the proper completion and co-ordination of the morphogenetic events (Lamka and Lipshitz, 1999; Reed *et al.*, 2004). The AS maintains important connections with the yolk sac, as well as with the LE cells which contribute to the completion of GBR and DC (Reed *et al.*, 2004). Premature loss of the AS leads to a lack of completion of these morphogenetic events and embryonic lethality.

1.2 Programmed cell death

Programmed cell death (PCD) plays a critical role in morphogenesis where it can have two main purposes: first, to control cell populations while forming a new shape, and second, to remove damaged cells during morphogenetic events (Davies, 2005). PCD is a genetically regulated process that is involved in a variety of developmental events (Baehrecke, 2002). There are three main kinds of PCD—apoptosis, autophagy, and non-lysosomal cell death (Debnath, Baehrecke, and Kroemer, 2005).

Apoptotic cell death is the most common form of PCD and has been studied extensively. Apoptosis is often described as a "suicide" program, that, when activated, leads to the caspase-mediated death of individual cells (Alberts *et al.*, 2008). The morphological manifestation of this evolutionarily conserved process comprises shrinkage, chromatin condensation, nuclear fragmentation, and membrane blebbing (Debnath, Baehrecke, and Kroemer, 2005). Apoptotic corpses are engulfed by phagocytic macrophages. Apoptosis plays major roles in tissue homeostasis and removal

of cells during embryonic development (Baehrecke, 2002).

Autophagic cell death, on the other hand, is less well characterized and is more highly debated than apoptosis. Autophagy, meaning "self-eating", is a process by which a cell undergoes partial auto-digestion under starvation conditions (Tsujimoto and Shimizu, 2005). Autophagy has been shown to have cytoprotective functions, yet it is also linked to PCD – a situation that has often been viewed as paradoxical in the field (Klionsky, 2007; Yoshimori, 2007). Autophagy is a ubiquitous process that occurs in low levels in eukaryotic cells to recycle cytoplasmic components (Yoshimori, 2007). Basal levels of autophagy are associated with the clearance of misfolded or toxic proteins and damaged organelles, especially mitochondria (Klionsky, 2007; Yoshimori, 2007). Autophagy is upregulated in response to several conditions of cellular stress, the most notable being starvation. While the removal of individual cells is believed to be achieved through the caspase-dependent apoptosis, elimination of whole tissues is often attributed to autophagy (Mohseni *et al.*, 2009).

The morphological manifestation of autophagy greatly differs from apoptosis. Cells undergoing autophagy have an excess number of autophagic vacuoles and autophagolysosomes that are used for self degradation (Baehrecke, 2005). Autophagy is independent of phagocytes; the cells undergoing autophagy are not engulfed by phagocytic macrophages as in apoptosis. Autophagic cell death is known to play a role in the development of insects and mammals, including humans (Scott, Juhasz, and Neufeld, 2007).

The third type of PCD, non-lysosomal cell death, is the least characterized of the three forms of PCD. Non-lysosomal cell death is rarely observed in development. Non-

lysosomal cell death is associated with swollen organelles and lysosome-independent formation of "empty spaces" in the cytoplasm (Baehrecke, 2005).

1.3 The Regulation of Apoptosis

Apoptosis can be activated through an extrinsic or an intrinsic pathway. Extrinsic activation of apoptosis is induced by extracellular signals, such as death ligands, binding to death receptors on the cell membranes (Shiozaki and Shi, 2004). On the other hand, intrinsic activation of apoptosis is triggered by internal signals, such as DNA damage or viral infection, which leads to the release of intermembrane mitochondrial proteins (Shiozaki and Shi, 2004). Regardless of the method of activation of apoptosis, it results in a cascade of signalling events that lead to the activation of intracellular proteases called caspases (Davies, 2005).

Caspases are cysteine proteases which cleave protein substrates to dismantle the cell. Caspases exist in inactive forms called procaspases, which are catalytically cleaved to form active enzymes (Debnath, Baehrecke, and Kroemer, 2005). Caspases are classified into two groups—apical or initiator caspases, and effector or executioner caspases (Cashio, Lee and Bergmann, 2005; Debnath, Baehrecke, and Kroemer, 2005). Initiator caspases are activated in response to cell death stimuli which then, in turn, activate downstream effector caspases via proteolytic cleavage (Cashio, Lee and Bergmann, 2005). Effector caspases are responsible for the degradation of a wide spectrum of substrates leading to the typical apoptotic morphological manifestations.

The cell membrane of apoptotic cells undergoes a change in chemical composition, signalling neighbouring cells or macrophages to engulf the apoptotic

corpses, and thereby preventing an inflammatory response (Martin and Baehrecke, 2004). Unlike healthy cells, apoptotic corpses contain the lipid phosphatidylserine within the outer leaflet of the cell membrane; this acts as a recognition signal for phagocytic macrophages (Martin and Baehrecke, 2004).

Apoptosis is an all-or-nothing event and its onset is tightly regulated. One component of apoptosis regulation involves the negative regulation of active caspases through Inhibitor of Apoptosis Proteins (IAPs) (Hay and Guo, 2006). IAPs bind to the active site of caspases, and use their E3-ubiquitin ligase activity to promote degradation of these caspases (Cashio, Lee, and Bergmann, 2005; Kornbluth and White, 2005).

Several techniques have been developed to detect the onset of apoptosis in cells and tissues. These methods include detection of DNA fragmentation by terminal deoxynucleotide transferase (TdT)-mediated dUTP-biotin nick end-labelling (TUNEL) (Debnath, Baehrecke, Kroemer, 2005), anti-active caspase antibodies, and acridine orange staining.

1.3.1 Apoptosis in Drosophila and in the Amnioserosa

Embryonic apoptosis is characterized by extensive cell death throughout the developing embryo. PCD via apoptosis is required during *Drosophila* embryogenesis in a number of developmental events, including segmentation of the epithelia (Pazdera, Janardhan and Minden, 1998), the elimination of the AS tissue from the embryo proper (Mohseni *et al.*, 2009), and formation of the central nervous system as well as head development in embryos (Rusconi, Hays and Cagan, 2000).

In *Drosophila*, unlike other organisms, many cells experience chronic activation of an initiator caspase (Hay and Guo, 2006). Cells survive this continuous death stimulus

through the expression of *Drosophila* IAPs (DIAPs). In this system, cell death is activated by disrupting DIAP-caspase interactions through the targeting of DIAPs for ubiquitin-mediated degradation, thus freeing caspases and inducing apoptosis (Hay and Guo, 2006). DIAPs are targeted for degradation upon interactions with the products of the *H99* genes: *head involution defective* (*hid*), *grim*, and *reaper* (*rpr*) (Bangs, Franc, and White, 2000). The *H99* genes are regulated independently of each other resulting in the precise control of developmental apoptosis (Figure 1.2).

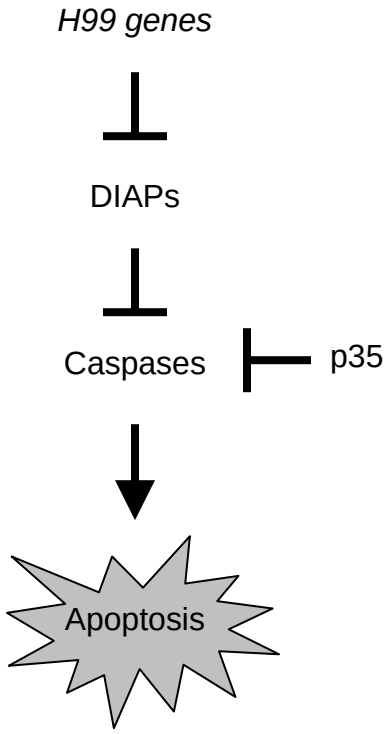

Figure 1.2: Induction of apoptosis in *Drosophila*. The *H99* genes, *hid*, *rpr* and *grim*, inhibit the DIAPs which, in turn, negatively regulate caspases. Activated caspases induce apoptosis. Caspases can also be inhibited by ectopic expression of the baculovirus derived protein known as p35.

The pro-apoptotic *H99* genes, *hid*, *grim*, and *rpr*, are located in a cluster on the third chromosome. A chromosomal deletion in the region, known as *Df(3L)H99* (hereafter referred to as *H99*), has been shown to eliminate virtually all caspase-

dependent programmed cell death in *Drosophila* embryos (Cashio, Lee, and Bergmann, 2005; Mohseni *et al.*, 2009). The absence of PCD in homozygous *H99* mutant embryos results in the persistence of the AS as an intact coherent tissue several hours beyond its normal time of degeneration (Mohseni *et al.*, 2009).

Many viruses express anti-apoptotic genes that efficiently inhibit apoptosis; this is likely a strategy that evolved to keep host cells alive while viral replication is completed (Tschopp *et al.*, 1998). The baculovirus protein, p35, acts as a broad-spectrum caspase inhibitor (Bangs, Franc, and White, 2000) (Figure 1.2). Embryos that ectopically express p35 phenocopy *H99* mutants and are associated with a persistent AS (Mohseni *et al.*, 2009).

1.3.2 Anoikis

An interesting sub-category of apoptosis is a mechanism whereby cell death is induced upon the loss of cell-cell or cell-matrix adhesions, or due to inappropriate cell-matrix interactions (Frisch and Screaton, 2001). This type of apoptotic cell death is called "anoikis", a Greek word meaning "homelessness" (Frisch and Screaton, 2001).

The initiation and execution of anoikis is mediated by different pathways, all of which merge into the activation of caspases and downstream molecular pathways, resulting in DNA fragmentation and cell death (Yin and Thummel, 2004). Anoikis following a loss of cell anchorage is of physiological relevance for development, tissue homeostasis and disease.

1.4 The Regulation of Autophagy

Evolutionarily conserved pathways regulate autophagy in response to nutrient

conditions, including the Target of Rapamycin (TOR) kinase pathway (Levine and Yuan, 2005). The TOR kinase pathway provides the major negative control of autophagy (Codogno and Meijer, 2005). Downstream of TOR kinase are the evolutionarily conserved autophagy-related genes, *Autophagy genes* (*Atg*), which encode proteins required for the induction of autophagy, and the formation and recycling of the autophagosome (Levine and Yuan, 2005). Upstream of the TOR kinase pathway are the members of the insulin receptor/phosphotidylinositol-3-kinase (InR/PI3K) pathway, which also play a major role in repressing autophagy (Britton *et al.*, 2002).

Upon binding of insulin-like molecules, the insulin receptor (InR) autophosphorylates, and in turn phosphorylates InR substrate (IRS) proteins within the cell. The IRS proteins bind downstream targets, resulting in the initiation of a conserved kinase cascade, including PI3K. PI3K phosphorylates phosphatidylinositol-4,5-bisphosphate (PIP_2), to form phosphatidylinositol-3,4,5-trisphosphate (PIP_3). Interactions of protein kinase B (PKB)/Akt with PIP_3 at the cortex leads to the activation of PKB/Akt (Figure 1.3) resulting in the initiation of a signalling cascade inducing cell survival (Britton *et al*., 2002). Activation of Akt, in turn, activates TOR kinase pathway (Berry and Baehrecke, 2007), thus downregulating autophagy (Figure 1.3).

Another method through which the PI3K pathway is induced is through activation of Ras upon nutrient signalling (Berry and Baehrecke, 2007). Ras controls the activity of a number of effector pathways. Ras proteins are small GTPase switch proteins that function in transducing external signals in a cell through a common cascade of serine/threonine kinases (Lodish *et al.*, 2004). Activation of Ras, in turn, activates PI3K which inhibits autophagy.

Ras activation also positively controls the activity of the cAMP-dependent protein kinase (PKA) (Figure 1.3), which negatively regulates the sublocalization of Atg protein to the preautophagosomal structure, a precursor for the formation of autophagosomes (Klionsky, 2007; Stephan and Herman, 2006). Thus the activation of Ras inhibits autophagy through multiple pathways.

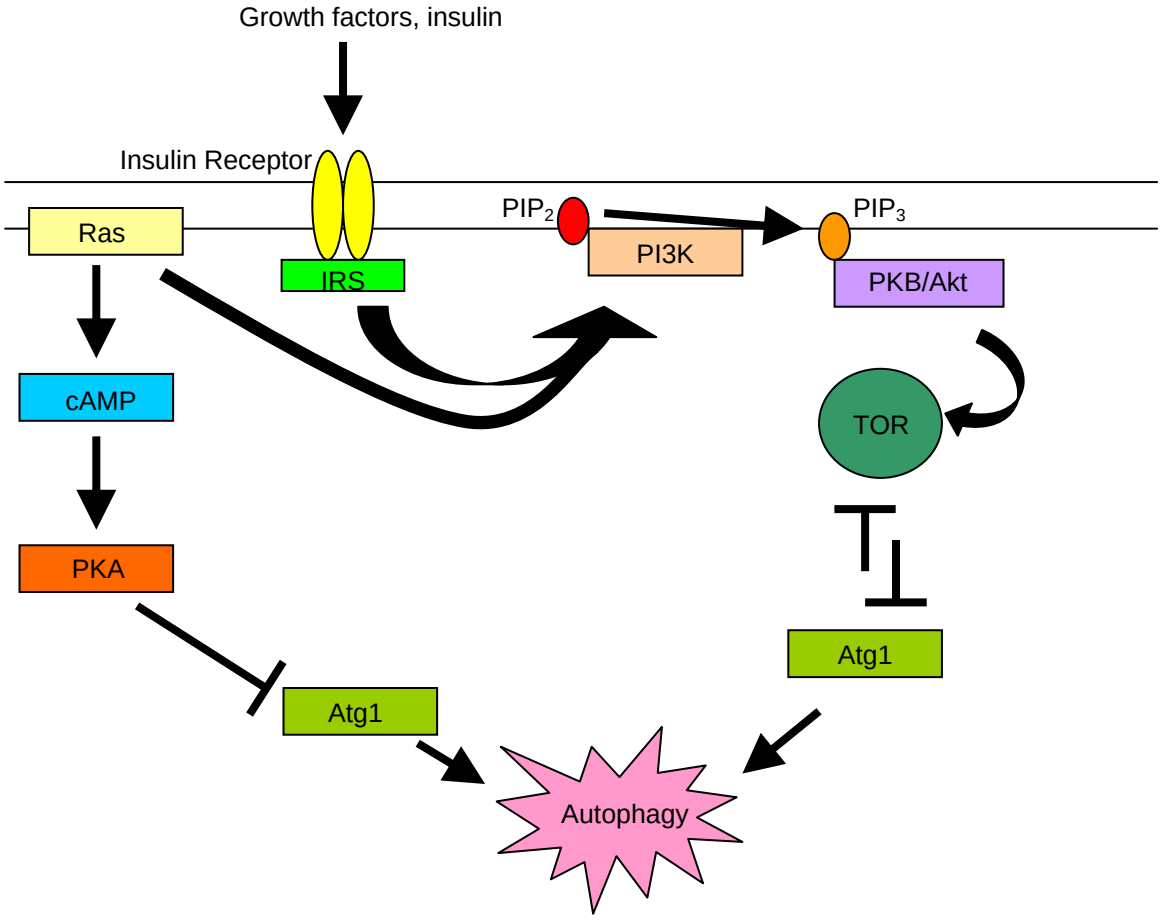

Figure 1.3: Induction of autophagy in *Drosophila*. Two main pathways are discussed in this study, namely the insulin receptor/phosphatidylinositol -3-kinase (InR/PI3K) pathway and the Ras activated pathway.

1.4.1 Autophagic cell death

Autophagy is also induced by up-regulating several *Atg* genes (Debnath, Baehrecke, and Kroemer, 2005). Clonal ectopic expression of Atg1, an autophagy

specific protein kinase, has been associated with increase in cell death in larval fat bodies and larval imaginal discs (Scott, Juhasz, and Neufeld, 2007). This study shows that the death of larval wing discs was delayed by the pan caspase inhibitor, p35, but the cells were eventually eliminated in an *Atg1* overexpression background, suggesting a role of excess autophagy leading into caspase dependent apoptosis or an autophagic cell death.

Autophagy can be downregulated by activating the InR/PI3K pathway. Using *Drosophila* embryos expressing a constitutively active form of InR, Mohseni *et al.* (2009) have shown that the downregulation of AS autophagy results in a strong persistent AS phenotype. The presence of this persistent AS phenotype suggests that autophagic cell death may be involved in the elimination of the AS (Mohseni *et al.*, 2009). Another method of downregulating autophagy is associated with the activation of Ras (Berry and Baehrecke, 2007). *Drosophila* larval salivary gland degradation is inhibited by expression of activated *Ras* (Berry and Baehrecke, 2007); also the AS (Mohseni *et al.*, 2009), again providing evidence for autophagic cell death or autophagy leading into apoptosis.

1.5 Premature amnioserosa loss in *hindsight*, a morphogenetic mutant

The morphogenetic mutant used in this study, *hindsight* (*hnt*), fails in the completion of GBR and is associated with premature AS loss. The gene *hnt* encodes for a nuclear zinc-finger protein, HNT, which is expressed in the AS, the midgut, as well as the tracheae of the embryo (Yip, Lamka and Lipshitz, 1997). HNT is also expressed in the photoreceptor cells of the developing adult retina (Pickup *et al.*, 2002).

Expression of HNT in these epithelia regulates several local and global

morphogenetic processes. HNT expression in the AS is required for the proper completion of GBR (Yip, Lamka, and Lipshitz, 1997). During tracheal and eye development, HNT expression has been suggested to maintain the state of differentiation as well as epithelial integrity (Wilk *et al.*, 2000; Pickup *et al.*, 2002). Mutations in *hnt* result in failure of GBR and DC, and undergo premature AS loss that is associated with a failure to downregulate JNK signalling in the AS (Lamka and Lipshitz, 1999; Reed, Wilk, and Lipshitz, 2001).

A study of several GBR mutants by Frank and Rushlow (1996) suggests that this category of embryonic mutant is, in general, associated with the premature loss of the AS. In this study, a subset of the mutants, including *hnt*, show *reaper* positive cells in the area of the AS by RNA *in situ* hybridization. This suggests that the premature loss of AS in *hnt* mutants is attributable to premature *reaper*-mediated apoptosis (Frank and Rushlow, 1996), suggesting a role for HNT promoting AS survival.

Rescue of the GBR defect in the *hnt* mutant has been observed following heat shock overexpression of InR, suggesting that HNT acts upstream of InR (Lamka and Lipshitz, 1999). InR is an active component of the InR/PI3K signalling cascade, which ultimately decreases autophagy; thus suggesting a role for HNT in regulating autophagy.

HNT is also expressed in the adult ovaries, and several genetic screens have identified *hnt* mutants through disrupting cell shape changes that occur in the follicular epithelium during the development of the egg chamber. Recent studies using somatic mosaics to create patches of ovarian follicular cells mutant for *hnt* show an increase in cell-cell adhesion molecules, including Armadillo, *Drosophila* homolog for β-catenin, and *Drosophila* E-Cadherin (Melani *et al.*, 2008) within the *hnt* mutant patch. The study

also showed that reduction of expression of the mammalian homolog of HNT, Ras-response element binding protein (RREB-1), in mammalian epithelial cells led to the formation of immobile, tightly adherent cell colonies (Melani *et al.*, 2008). This suggests that HNT negatively regulates these important cell-cell adhesion molecules.

1.6 Objectives

The gene *hnt* encodes a nuclear zinc-finger protein whose expression is required in the AS for the proper completion of GBR. Previous work in our lab has established that the bulk of the AS undergoes apoptotic cell death in a manner that is dependent on autophagy (Mohseni *et al.*, 2009). Prior to this study, the generally accepted explanation as to why *hnt* mutant embryos fail in GBR has involved the loss of the AS through premature cell death (Frank and Rushlow, 1996; Lamka and Lipshitz, 1999). The nature of the AS loss in *hnt* mutants, however, has not been described in detail and the most accurate descriptions refer to the loss of "AS integrity". Since the AS is required for GBR (possibly through the generation of mechanical force, or in a cell signalling capacity, or both), the primary role of *hnt* in the AS has been proposed to be of a pro-survival or anti-apoptotic nature. The role of *hnt* in the AS, however, has not been carefully examined and such interpretations remain suppositional.

This study encompasses three general aims regarding *hnt*, its role in morphogenesis and the maintenance of AS integrity. The first objective of this study was to better characterize the premature degeneration of the AS in *hnt* mutants using GFP-based live imaging techniques. The second objective was to determine if AS loss was indeed a premature onset of AS death as it occurs during development, and the third

objective was to determine if *hnt* is involved in the regulation of cell adhesion in the AS during GBR and DC.

Chapter 2 – Materials and Methods

2.1 UAS-GAL4 expression system

The yeast UAS-GAL4 system is a popular method used in *Drosophila* to promote ectopic gene expression. The ectopic gene can be expressed under spatial or temporal control (Brand and Perrimon, 1993). The ability to express a gene in a directed fashion is a useful means of analyzing its role in development (Brand and Perrimon, 1993). The GAL4 protein is a yeast transcription factor that binds to a specific target DNA sequence: the Upstream Activating Sequence (UAS). GAL4 responsive sequences are not found in the *Drosophila* genome, rather are introduced using genetically engineered transposable elements, usually *P*-elements. A promoter or enhancer directs the expression of GAL4 activating transcription of the gene downstream of the UAS sequence (Brand and Perrimon, 1993). The advantage of using the UAS-GAL4 system is that the activator (GAL4) and the target sequence (UAS) are separated into distinct transgenic lines. Generating a UAS-GAL4 combination is a simple matter of performing a genetic cross between the two transgenic lines. Only the progeny carrying both constructs would have targeted gene expression. In this way, the UAS-GAL4 system can be used to ectopically express any gene of interest, including lethal mutations (Brand and Perrimon, 1993) (Figure 2.1). To refine the pattern of GAL4-dependent expression, a negative regulator of GAL4, GAL80 protein was used. GAL80 protein binds to the activation domain of GAL4 protein, inhibiting the transcriptional activation of downstream UAS genes (Perler, 2004). Expressing GAL80 in a pattern that overlaps GAL4 expression inhibits expression from UAS-GAL4 expression system.

Figure 2.1: UAS-GAL4 gene expression system. To activate ectopic gene expression of target gene, a GAL4 enhancer trap line is crossed with a UAS transgenic line. Progeny of the genetic cross express the target gene under the spatial/temporal control of GAL4.

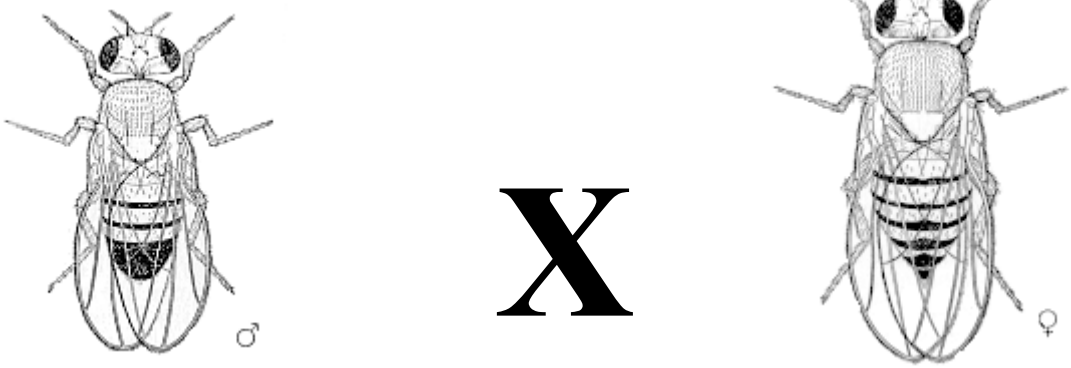

Enhancer trap GAL4 X UAS – gene X

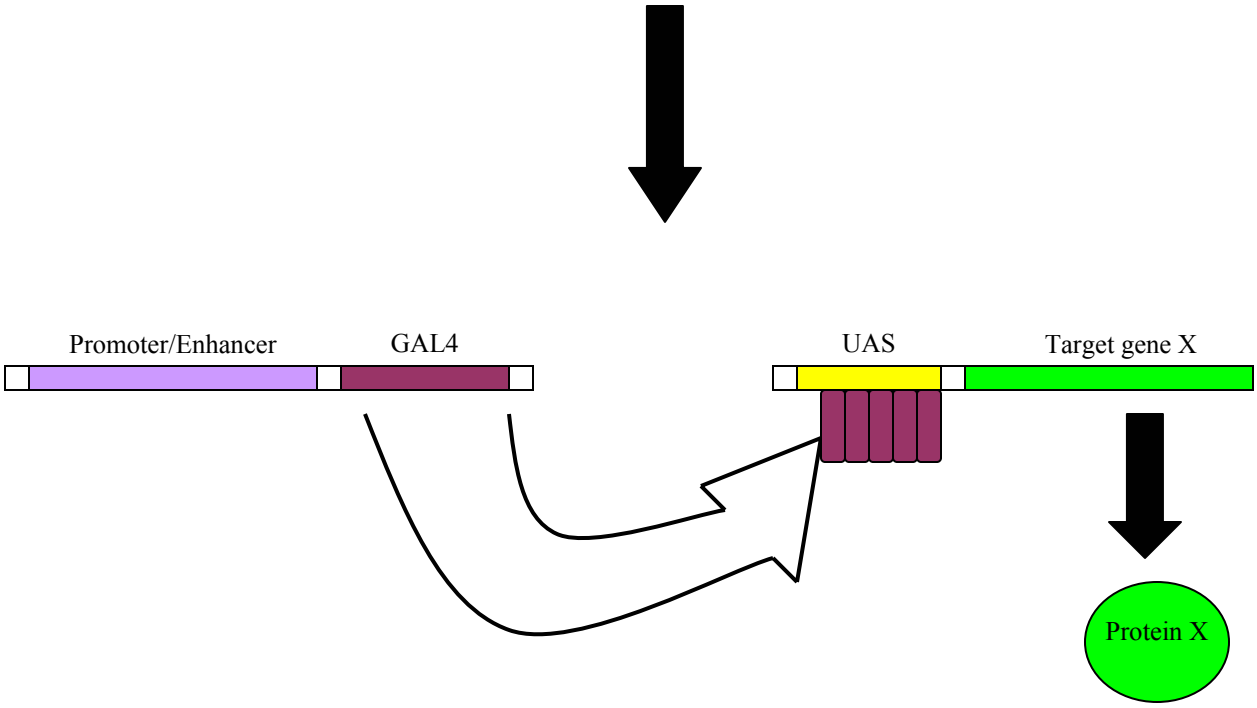

Tissue specific GAL4 expression **Transcriptional activation of *gene X***

2.2 *Drosophila* mutant lines and genetic crosses

The genotypes and source of all *Drosophila* transgenic stocks used in this study are summarized in Table 2.1. The nomenclature of these stocks is ordered by chromosome number separated by a semi-colon (;) i.e. in order of X; 2; 3 chromosomes. The mating scheme to recognize H99/ED225 mutants is summarized in Figure 2.2. The mating scheme to recognize hnt^{308} mutants using GAL80 is summarized in Figure 2.3. The $tubulin^{GAL80}$ suppression of GAL4 induced GFP expression was tested by collecting embryos from the crossing scheme illustrated in Figure 2.3. The embryos were separated on basis of presence or absence of GFP expression, and allowed to grow at normal conditions. The non-GFP expressing embryos yielded female adult progeny comprised of the duplication (straight wings) or the balancer chromosome (curly wings), and male adult progeny with the duplication (straight wings). The GFP expressing embryos yielded no adult progeny.

2.3 Cuticle preparations

Embryos were collected overnight on grape juice agar plates at 25°C. Embryos were aged for another 24 hours at the same temperature to allow for any viable embryos to complete embryonic development and hatch as larvae. The unhatched embryos were collected in a mesh using PBT and dechorionated in 50% commercial bleach for 3 mins. The dechonionated embryos were then flushed with water to remove any residual bleach. The embryos were transferred to a drop of Hoyer's mountant on a glass slide and covered with a glass coverslip. The slide was baked overnight at 60°C. Cuticle preparations were

visualized using the Zeiss Axiovert 200 microscope, and images were captured using the OpenLab Software by Improvision.

Table 2.1: A list of all genotypes used in this study. The parental genotypes of all transgenic lines used in genetic crosses in this study are listed, along with the source of the genetic stocks. The nomenclature is written in order of chromosomes, and chromosome location is indicated on the bottom right corner. The genotypes *FM7*, *CyO*, *Gla*, *TM3* and *TM6UW23-1* represent balancer chromosomes which prevent recombination and, thus, are used to maintain a heterozygous stock.

	GENOTYPE (Chromosome)	SOURCE
(1)	yw^{67} (X)	Bloomington Stock Center
(2)	$whnt^{308}$/w ;; puclacZ/TM3 (X ;; 3)	Reed Lab*
(3)	da^{GAL4} (3)	Bloomington Stock Center
(4)	$whnt^{308}$/w ;; da^{GAL4} (X ;; 3)	Reed Lab**
(5)	$whnt^{308}$; Dp(1;2)4FRDup/CyO (X ; 2)	Reed Lab*
(6)	w ;; UAS-GFP^{nls}+LP-1^{GAL4}/TM3 (X ;; 3)	Reed Lab*
(7)	$whnt^{308}$/w ; Dp(1;2)4FRDup/+ ; UAS-GFP^{nls}+LP-1^{GAL4}/+ (X ; 2 ; 3)	Reed Lab**
(8)	$whnt^{308}$; Dp(1;2)4FRDup/CyO,$cMar14^{GAL4}$ (X ; 2)	Reed Lab*
(9)	w ; ftz^{GAL4}UASnuc^{lacZ}+Ubi-$DEcad^{GFP}$/CyO (X ; 2)	Reed Lab*
(10)	w^{1118} ;; UAS-GFP^{nls} (X ;; 3)	Bloomington Stock Center
(11)	w ; ftz^{GAL4}UASnuc^{lacZ}+Ubi-$DEcad^{GFP}$/+ ; UAS-GFP^{nls}/+ (X ; 2 ; 3)	Reed Lab**
(12)	w ; UAS-$hnt^{RNAi(2A)}$; UAS-$hnt^{RNAi(2B)}$ (X ; 2 ; 3)	Lipshitz Lab
(13)	$ywhnt^{1142}${FRT101}/FM7 (X)	Lipshitz Lab
(14)	w ; crq^{GAL4}+UAS$mCD8^{GFP}$/Gla (X ; 2)	Reed Lab*
(15)	y(w) ;; LP-1^{GAL4}+Df(3L)ED225/TM6UW23-1 (X ;; 3)	Reed Lab*
(16)	$whnt^{308}$/y(w) ;; LP-1^{GAL4}+Df(3L)ED225/TM3 (X ;; 3)	Reed Lab**
(17)	y(w) ;; UAS$mCD8^{GFP}$+Df(3L)H99/TM6UW23-1 (X ;; 3)	Reed Lab*
(18)	UAS-p35 (2)	Bloomington Stock Center

(19)	*(y)w ; CyO,Kr^{GAL4}+UAS-GFP/+ ; LP-1^{GAL4}/(LP-1^{GAL4})* (X ; 2 ; 3)	Reed Lab*
(20)	*whnt^{308} ; Dp(1;2)4FRDup/CyO,Kr^{GAL4}+UAS-GFP ; (LP-1^{GAL4})* (X ; 2 ; 3)	Reed Lab**
(21)	*tub$^{GAL80\text{-}LL\text{-}1}$; Pin^{Yt}/CyO* (X ; 2)	Bloomington Stock Center
(22)	*tub$^{GAL80\text{-}LL\text{-}1}$; UAS-p35* (X ; 2)	Reed Lab**
(23)	*w ;; UAS-dInR^{ACT} "G"* (3)	Bloomington Stock Center
(24)	*tub$^{GAL80\text{-}LL\text{-}1}$* (X)	Bloomington Stock Center
(25)	*Ly/Tm3* (3)	Kyoto Stock Center
(26)	*tub$^{GAL80\text{-}LL\text{-}1}$;; Ly/Tm3* (X ;; 3)	Reed Lab**
(27)	*tub$^{GAL80\text{-}LL\text{-}1}$;; UAS-dInR^{ACT} "G"* (X ;; 3)	Reed Lab**
(28)	*UAS-Ras^{V12}* (3)	Bloomington Stock Center
(29)	*tub$^{GAL80\text{-}LL\text{-}1}$;; UAS-Ras^{V12}* (X ;; 3)	Reed Lab**
(30)	*ftz^{GAL4}UASnuc^{lacZ}/CyO* (2)	Reed Lab*
(31)	*UAS-hnt$^{6\text{-}1}$* (3)	Lipshitz Lab
(32)	*ftz^{GAL4}+Ubi-DEcad^{GFP}+UAS-actin^{GFP}/CyO* (2)	Reed Lab*
(33)	*w ;; arm$^{GFParm[83]}$* (3)	Bloomington Stock Center
(34)	*ftz^{GAL4}+UASnuc^{lacZ}/CyO ; arm$^{GFParm[83]}$/(arm$^{GFParm[83]}$)* (2 ; 3)	Reed Lab*

* recombinant chromosome or multiple insertion stocks made in Reed Lab

** crossing schemes for construction of the multiple insertion stocks are presented in Appendix A

Figure 2.2: Crossing scheme to recognize *H99/ED225* mutants. Each of the deficiencies, *Df(3L)H99* and *Df(3L)ED225* are embryonic lethal as homozygotes, and thus are maintained as a heterozygous stock. The *LP-1*^{GAL4} driver is AS specific, and allows expression of the *UAS-mCD8*^{GFP}. Only progeny from the cross that contain both GAL4 and UAS constructs have GFP detection, thus allowing the deficiencies to be recognized in embryos. Only the male progeny are illustrated.

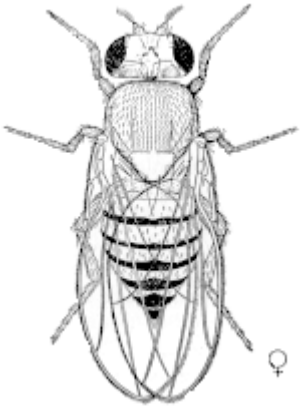

X

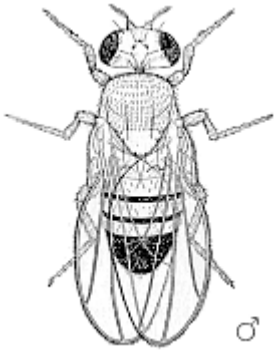

$whnt^{308}$;; $LP\text{-}1^{GAL4}$ + Df(3L)ED225 / y(w) (TM3)

y(w) ;; $UASmCD8^{GFP}$ + Df(3L)H99 / TM6UW23-1

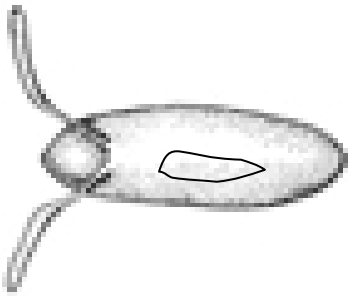

$whnt^{308}$;; $LP\text{-}1^{GAL4}$ + Df(3L)ED225 / TM6UW23-1

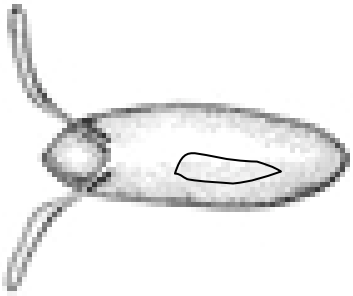

$whnt^{308}$;; $UASmCD8^{GFP}$ + Df(3L)H99 / TM3

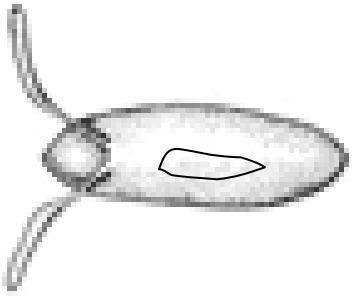

$whnt^{308}$;; TM6UW23-1 / TM3

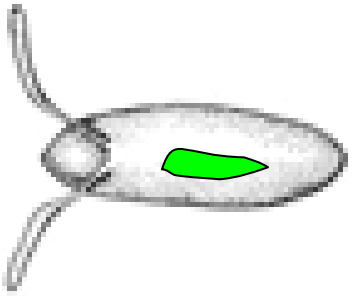

$whnt^{308}$;; $LP\text{-}1^{GAL4}$ + Df(3L)ED225 / $UASmCD8^{GFP}$ + Df(3L)H99

Figure 2.3: Crossing scheme to recognize *hnt*^{308} mutants using *tub*^{GAL80}. An example of how GAL80 was used to recognize *hnt*^{308} mutants. GAL80 binds and inhibits GAL4 activity, and thus prevents the expression from UAS downstream genes. This procedure was also utilized with various constructs on the second and third chromosomes.

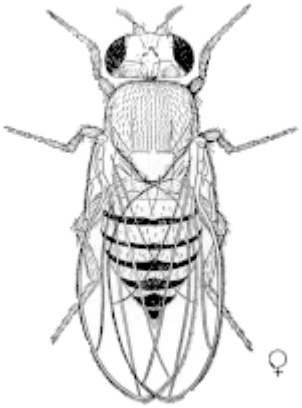

$\frac{whnt^{308}}{whnt^{308}}$; $\frac{Dp(1;2)4FRDup}{CyO,Kr^{GAL4}+UAS\text{-}GFP}$

X

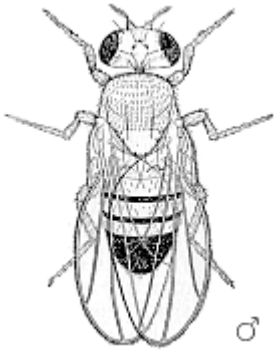

$tub^{GAL80\text{-}LLI}$

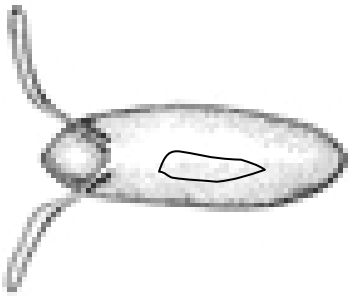

$\frac{whnt^{308}}{}$; $\frac{Dp(1;2)4FRDup}{+}$

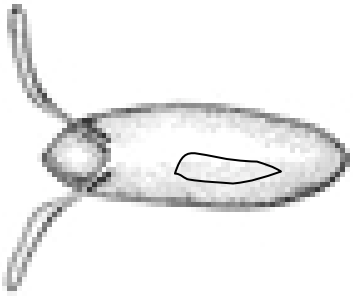

$\frac{whnt^{308}}{tub^{GAL80\text{-}LL1}}$; $\frac{Dp(1;2)4FRDup}{+}$

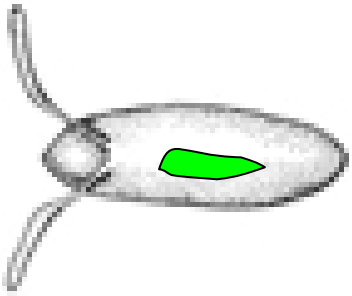

$\frac{whnt^{308}}{}$; $\frac{CyO,Kr^{GAL4}+UAS\text{-}GFP}{+}$

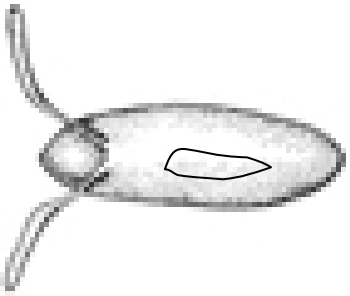

$\frac{whnt^{308}}{tub^{GAL80\text{-}LL1}}$; $\frac{CyO,Kr^{GAL4}+UAS\text{-}GFP}{+}$

2.4 Embryo fixation

Embryos were collected on grape juice agar plates at 25°C. The embryos were washed off the plate into a mesh using PBT and dechorionated in 50% commercial bleach for 3 mins. The embryos were then flushed with distilled water to remove any residual bleach, and transferred to the fixative in a glass scintillation vial. Fixative was composed of 1:1 mixture of heptane to 3.7% formaldehyde (made from 37% histological grade formaldehyde in 1X PBS). Heptane creates holes in the vitelline membrane of the embryos allowing the fixative to enter the embryo. Embryos were incubated in the fixative for 10 mins for TUNEL and α-HNT dual staining protocol, and 20 mins for RNA *in-situ* hybridization with constant shaking. For α-HNT staining, the fixative was composed of 1:1 mixture of heptane and methanol. Upon completion of fixation period, the formaldehyde (lower layer) was replaced with methanol. Vigorous shaking for 30 secs removes the vitelline membrane of the embryos, and embryos sink into the methanol. The embryos were collected and washed with methanol several times. Embryos for RNA *in-situ* hybridization were stored at -20°C in methanol. For TUNEL + α-HNT staining, the embryos were washed twice in 100% ethanol after the methanol washes, and then stored at -20°C in 70% ethanol. Embryos expressing GFP were not stored in methanol.

For α-ARM staining, the hot-methanol fixation procedure was used. Embryos were collected and dechorionated as described above. Embryos were flushed with distilled water and then incubated in hot PBT (heated to 90°C) for 30 secs. Embryos were then transferred to chilled PBT (on ice) for 2 mins. Embryos were then transferred to a 1:1 mixture of heptane and methanol, and shaken vigorously for 30 secs. Embryos

were allowed to settle in the methanol. They were then collected and washed several times with methanol. The hot-methanol fixation procedure extracts most of the cytoplasmic ARM protein, but maintains the plasma membrane bound form of the protein (Muller and Wieschaus, 1996).

2.5 RNA *in-situ* hybridization

An amnioserosa specific probe, CG12011, was used to visualize the presence or absence of the AS tissue in various backgrounds. The probe was generated from cDNA clones housed in pFLC-1 vector obtained from the Canadian *Drosophila* Microarray Center. All steps for RNA *in-situ* hybridization were performed as described by Henry M. Krause (accessed 2008 November 23). Whole mount embryos were viewed using Zeiss Axiovert 200 microscope, and images were captured using the OpenLab Software by Improvision.

2.6 Confocal Live Imaging

Embryos were collected on grape juice agar plates at 3 hour intervals using the FlyMax Automated Egg Collector (FlyMax Scientific Equipment Ltd.). The embryos were allowed to age to the desired stage at 25°C. Approximately a half hour before imaging, the embryos were hand-dechorionated by rolling on double-sided sticky tape using forceps as described by Reed *et al.* (2004) and Mohseni *et al.* (2009).

Live imaging performed on the Zeiss Axiovert 100 confocal microscope had embryos mounted on a double-sided sticky tape on a gas permeable membrane in halocarbon oil (1:1 mixture of series 56: series 700). Images were captured every 2 mins

using the LSM510 software. NIH ImageJ software was used to process the image stacks and compile AVI movies. NIH ImageJ software was also used to make montages of the AVI movies.

Live imaging performed on the Nikon Eclipse confocal microscope had dechorionated embryos mounted in a drop of halocarbon oil on a glass coverslip. The coverslip was inverted over a polycarbonate depression slide and secured in place with tape. The halocarbon oil formed a hanging drop in which the embryos floated to the top to touch the surface of the coverslip. Two holes were cut into the tape on either side of the coverslip to allow for ventilation within the depression. Images were captured as z-stacks with 6 slices of 2μm increments at 2 or 4 minute intervals using the EZ-C1 software. The software was also used to project the z-stacks, process the image stacks and compile AVI movies. NIH ImageJ software was used to make montages of the AVI movies.

2.7 Antibody staining

Embryos were collected, fixed and stored as described above. Embryos in methanol were serially re-hydrated in PBS, and incubated in blocking solution (9:1 mixture of 0.5% Bovine Serum Albumin (BSA) to 1% Normal Goat Serum) for 2 hrs at room temperature. Embryos were then incubated overnight at 4°C in primary antibody diluted in blocking solution (mouse monoclonal α-HNT 27B8 1G9 in a 1:20 dilution or mouse monoclonal α-ARM in a 1:400 dilution). After the incubation period, the primary antibody was removed and embryos were washed three times with PBT for 15 mins each. Embryos were incubated at room temperature for 2 hrs in secondary antibody (TRITC

conjugated goat α-mouse or FITC conjugated goat α-mouse) in a 1:500 mixture for α-HNT and 1:400 for α-ARM staining with blocking solution. Secondary antibody was removed at the end of the incubation period and embryos were washed three times with PBT for 15 mins each, and once with PBS. Embryos were allowed to settle overnight in a fluormount (DABCO). Embryos were mounted on a glass slide in the fluoromount, and visualized using either the Zeiss Axiovert 100 confocal microscope or the Nikon Eclipse confocal microscope.

2.8 TUNEL and α-HNT dual staining

The TUNEL assay is a simple method of labelling the ends of fragmented DNA present in apoptotic cells with fluorescent molecules (Potten and Wilson, 2004). Embryos were collected, fixed, and stored as described above. Embryos were re-hydrated by immersion in 30% ethanol for 10 mins and then two washes in PBS. Staining was performed by following a protocol from Krieser *et al.*, (2007), using the primary antibody (α-HNT) at a 1:20 dilution and secondary antibody (TRITC-conjugated) at 1:500 dilution. The In situ cell death detection kit, Fluorescein kit (Roche) was used to perform the TUNEL assays.

Embryos were mounted on a glass slide in fluoromount (DABCO) and visualized using the Zeiss Axiovert 100 confocal microscope. Images were captured using the LSM510 software, and processed using NIH ImageJ software.

Chapter 3 – Results

Previous work using amorphic (null) alleles showed that the AS dies prematurely in *hnt* mutants (Frank and Rushlow, 1996). The main objective of this study was to analyze and determine the cause of premature AS loss that is associated with *hnt* mutants. Most experiments in this study used the hypomorphic mutant allele, hnt^{308}, rather than amorphic alleles (such as hnt^{XE81}, a known protein null allele). The hnt^{308} allele has reduced HNT protein expression in all tissues where *hnt* is expressed, and this effect of reduced expression is particularly noticeable in the AS (Reed, Wilk, and Lipshitz, 2001). Having reduced HNT expression in the AS, the hnt^{308} allele is attractive for studies relating to phenotypic suppression. That is to say, given a phenotype that is intermediate between the null and wild type, suppression by backgrounds that alter programmed cell death pathways may be more easily detected. The first objective of this study was, therefore, to revisit the hnt^{308} phenotype with particular attention to the fate of the AS.

3.1 Revisiting the *hindsight* phenotype

The hnt^{308} mutant stock was initially examined to address the question of the penetrance and expressivity of the mutant phenotype. The hnt^{308} mutation itself is associated with the insertion of a *P*-element in the 5' upstream regulatory region of *hnt* (Reed, Wilk and Lipshitz, 2001). The *P*-element construct itself was designed as an enhancer trap that expresses *bride-of-sevenless* (*boss*); hnt^{308} mutants, while being recessive for embryonic lethality, are also associated with a dominant rough eye phenotype. This rough eye phenotype serves as a convenient marker for the presence of

the *hnt*^{308} allele in heterozygotes. The *hnt*^{308} mutant is maintained as a balanced heterozygous stock using standard balancer chromosomes. Since *hnt* maps to the X chromosome, hemizygous male (*hnt/Y*) progeny of heterozygous females (*hnt/FM7*) show the embryonic lethal phenotype. At full penetrance (100% embryonic lethality) these embryos are expected to represent 25% of all progeny. Previous analysis of *hnt*^{308} measured just over 10% of total progeny as embryonic lethal, which corresponds to 41% embryonic lethality associated with the *hnt*^{308} mutant (Reed, Wilk and Lipshitz, 2001).

To confirm the *hnt*^{308} phenotype, cuticle preparations were performed on embryos collected from heterozygous *hnt*^{308}/+ females mated to "wild type" males (following the convention of many *Drosophila* research labs, our lab uses a stock which carries the genetic markers *yellow white* (*yw*) as a wild type reference) (Figure 3.1). In these cuticle preparations, numerous embryos displayed "twisted" phenotypes (Figure 3.1b), GBR failures, or dorsal holes (Figure 3.1c). The completion of GBR in presumptive heterozygous control siblings (sibs) is evident by the ventral position of all eight abdominal segments (Figure 3.1a). These observations confirm that the genetic stock had not accumulated any modifiers that could alter the previously reported phenotype.

Although cuticle preparations provided evidence of GBR failure as well as DC failure, the AS cannot be visualized by this method. RNA *in-situ* hybridization using a probe to detect transcripts of the gene *CG12011*, whose expression is highly AS-specific, was performed on 12-15 hr staged embryo collections (embryo collection was as described for cuticle preparation) (Figure 3.2). In control sibs (representative of wild type), normal AS degeneration was evident in late stage 15 embryos which are recognized by midgut morphology (Figure 3.2a). The CG12011 signal appears in cells

Figure 3.1: Cuticle preparations on *hnt*^{308} mutants The *hnt*^{308} stock is maintained as a heterozygous stock, therefore only 25% of the embryos illustrate the *hnt* mutant phenotype. (a) Heterozygous siblings were used as a control for cuticle preparations. The black arrows indicate the eight abdominal segments (denticle bands) found on the ventral surface of the embryo. The red arrow indicates the telsons – the terminal tail structure. (b) A *hnt*^{308} mutant embryo that illustrates a "twisted" phenotype. Since the embryo proper is twisted within the vitelline membrane, the abdominal segments are not visible, making it difficult to distinguish between structures. (c) A *hnt*^{308} mutant embryo that has failed in GBR and illustrates a large dorsal hole. The red arrow indicates the telsons which are located more anteriorly than in control embryos (a) indicating GBR failure. The black dashes surround the dorsal hole in the embryo. Embryos collected from females of stock 4 crossed to males of stock 1 (See Materials and Methods). All embryos are oriented with the anterior to the left and dorsal side up.

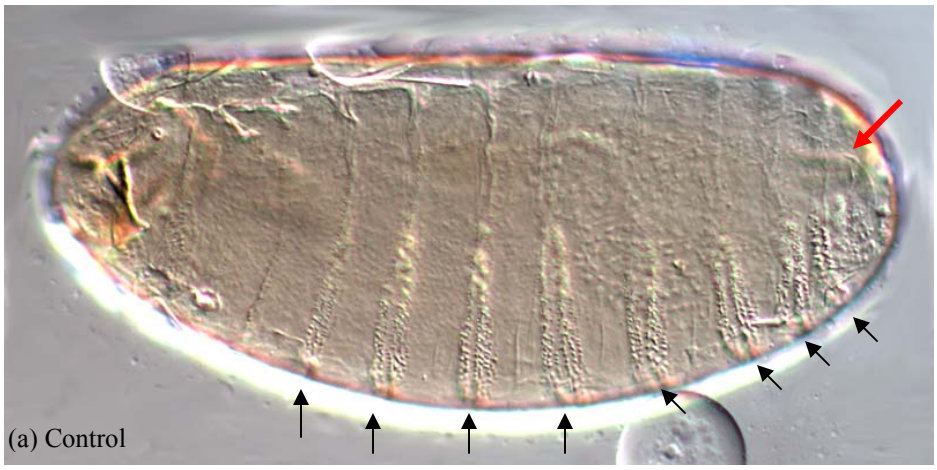

(a) Control

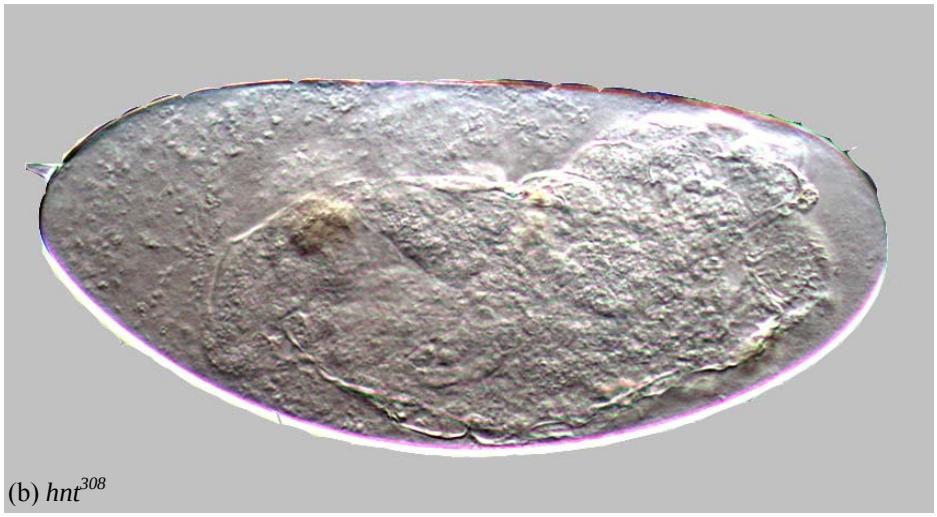

(b) *hnt*^{308}

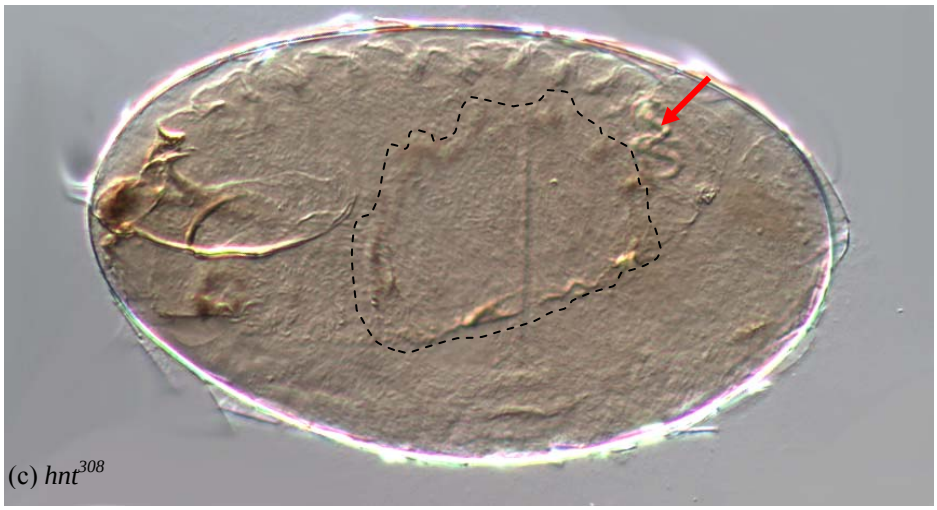

(c) *hnt*^{308}

Figure 3.2: RNA *in-situ* hybridization on *hnt*^{308} embryos. The black arrow indicates AS cells that were labelled with probe for the AS-specific gene *CG12011*. RNA *in-situ* hybridization was performed on 12-15 hr stage embryo collections. (a) Control embryos exhibit normal tissue degeneration where apoptotic corpses are seen surrounding the AS tissue. (b and c) *hnt*^{308} mutants that have failed in GBR and lack CG12011 AS staining, indicating premature AS loss (red arrow). Embryos were collected from females of stock 4 crossed to males of stock 1 (See Materials and Methods). All embryos are oriented with the anterior to the left and dorsal side up.

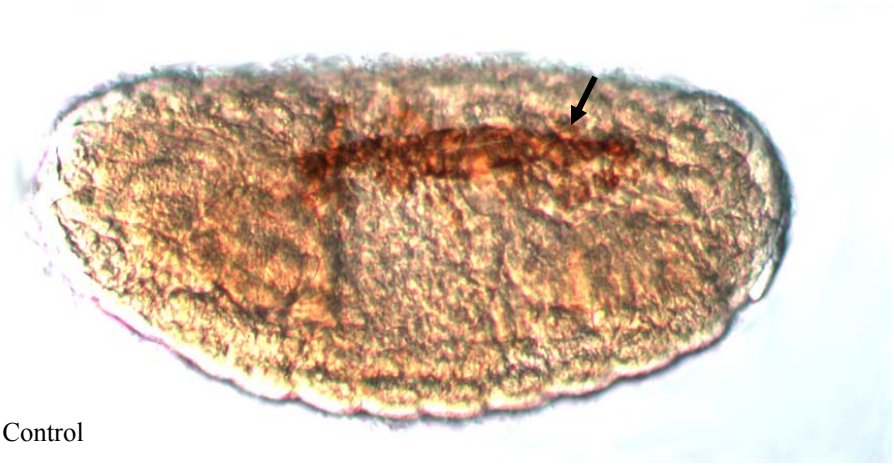

(a) Control

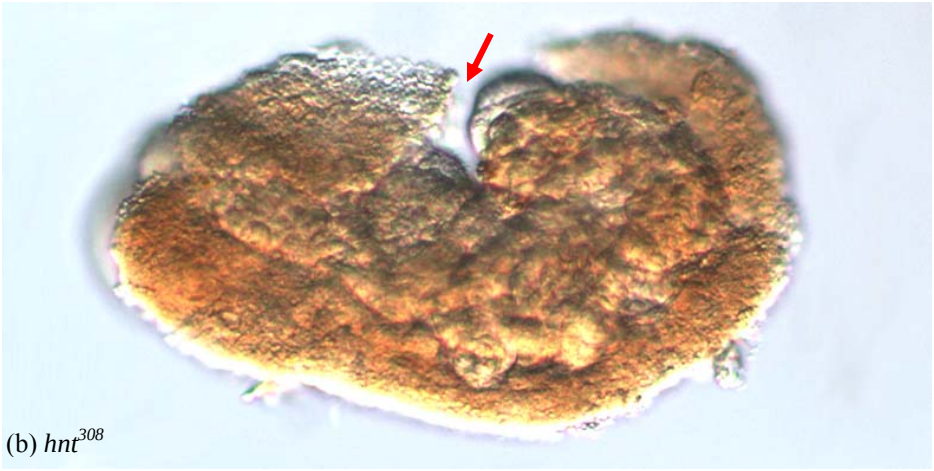

(b) *hnt*^{308}

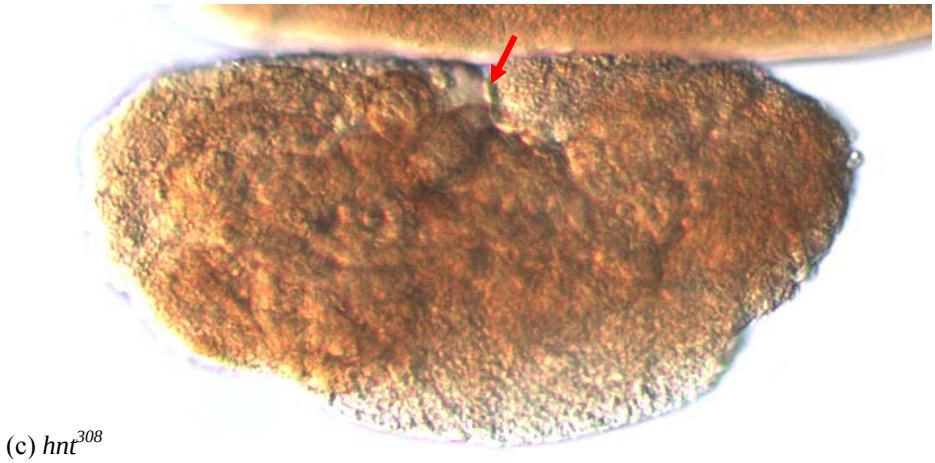

(c) *hnt*^{308}

that have dissociated from the AS tissue most likely indicative of AS apoptotic corpses that have been engulfed by phagocytic macrophages. These are particularly visible at the anterior and posterior of the degenerating tissue (Figure 3.2a). On the other hand, *hnt*^{308} mutant embryos, which in this experiment are recognized by GBR failure, lack signal associated with the CG12011 probe (Figure 3.2b; Figure3.2c). This observation suggests that like the null allele, *hnt*^{308} is also associated with premature AS loss. Of all embryos examined in these experiments, 8.4% were associated with GBR or DC failure, and all such embryos lacked CG12011 signal, indicative of AS loss. This corresponds to a penetrance of 33.6% of AS loss in *hnt*^{308} mutants. This confirms the hypomorphic nature of the *hnt*^{308} allele and that the AS loss phenotype is also hypomorphic.

3.2 Visualizing premature Amnioserosa death in *hindsight* mutants

Techniques such as cuticle preparations and RNA *in-situ* hybridization of whole mount embryos are limited to working with dead or fixed embryos. In order to perform more detailed phenotypic analysis, GFP-based live imaging was used. Live imaging analysis during GBR stage (7 – 9 hrs AEL) was used to further characterize the AS tissue in the *hnt*^{308} mutants. Using green fluorescent protein (GFP) with a nuclear localizing signal (*UAS-GFP*^{nls}), confocal live imaging was performed to visualize the AS in *hnt*^{308} mutants (Figure 3.3). In these experiments *UAS-GFP*^{nls} was expressed in the epidermis as well as the AS, and GFP expressing embryos were selected at stages prior to the onset of *hnt* related phenotypes. In the course of live imaging, embryos were determined as being *hnt*^{308} mutants based on their terminal phenotype. By examining the live imaging

Figure 3.3: Confocal live image sequences of *hnt*^{308} mutants. The AS tissue (using

the *LP-1*^{GAL4} driver), as well as the epidermis (using the *cMar14*^{GAL4} driver), is visualized by detection of GFP localized to the nuclei of cells. Live imaging was performed using the Zeiss Axiovert 100 at 40X objective. Images were captured at 2 minute intervals. Embryos that lacked the *hnt* phenotype were considered as controls. The AS is indicated by the yellow arrow, and the germband is indicated by the red arrow. (a) Progression of GBR (stage 13) in control embryos. The AS stretches out, covering the dorsal surface of the embryo. (b) Progression of GBR (stage 13) in *hnt*^{308} mutants. The AS collapses from the germband, and does not cover the dorsal surface. The germband fails to retract to its final posterior position. Embryos were collected from females of stock 8 crossed to males of stock 7 (See Materials and Methods). All embryos were oriented with the anterior at the top left and the dorsal side facing top right.

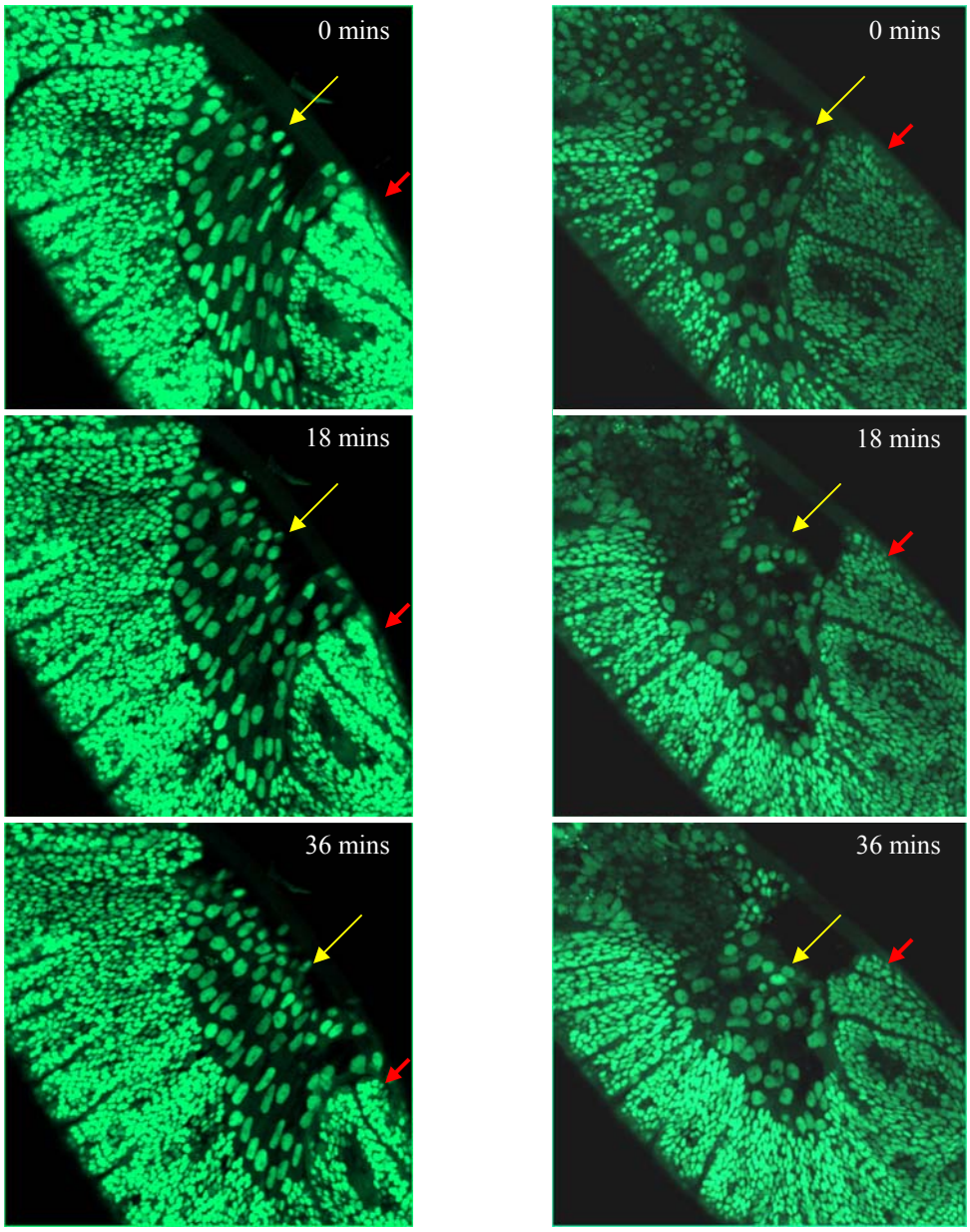

(a) Control **(b) *hnt*^{308}**

Figure 3.4: Nuclear fragmentation of amnioserosa cells in *hnt*^{308} mutants. Two AS nuclei, indicated by the white asterisks, from *hnt*^{308} mutant embryos, that undergo complete nuclear fragmentation within 16 minutes. Image sequence montage illustrated is from the *hnt*^{308} mutant embryo shown in Figure 3.3b. Live imaging was performed using the Zeiss Axiovert 100 confocal microscope.

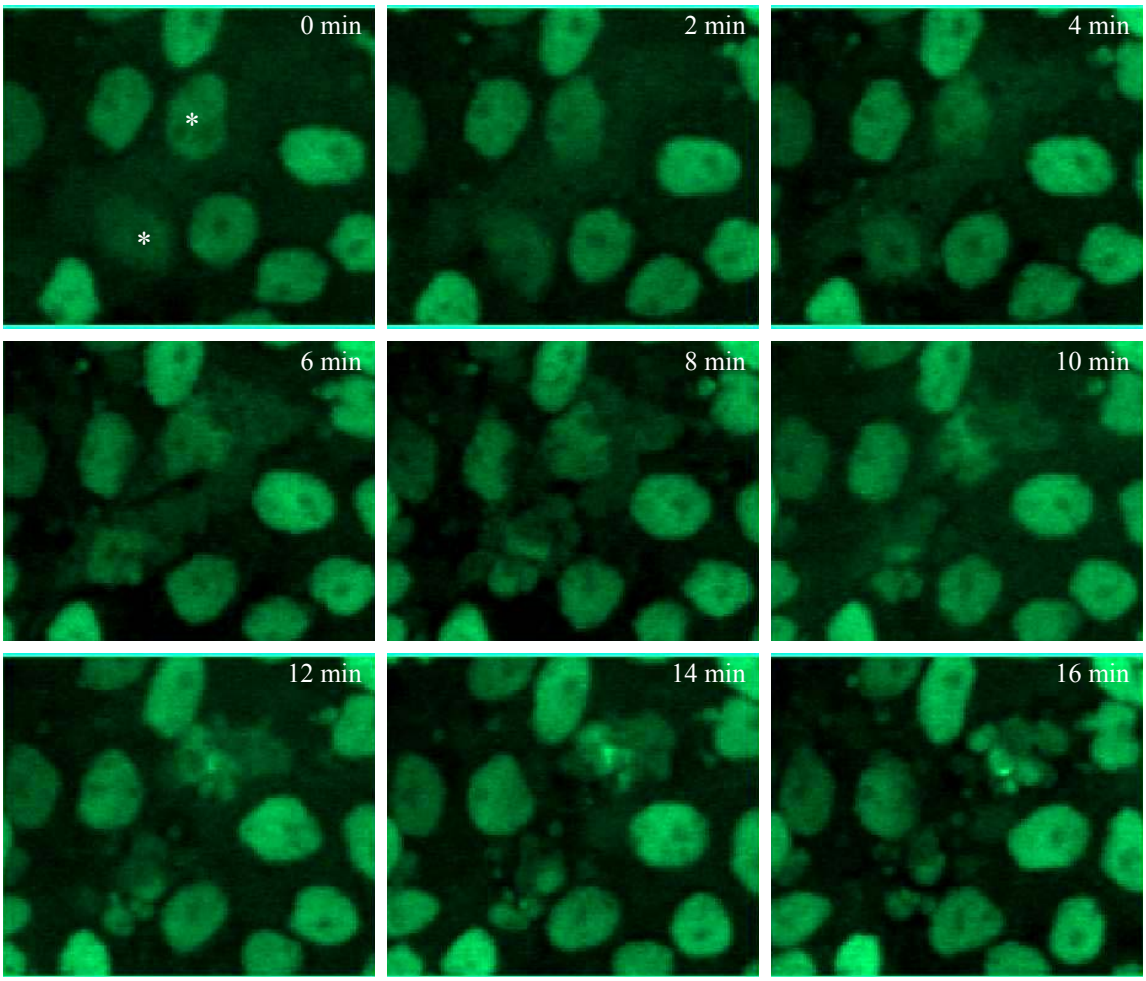
0 min
2 min
4 min
6 min
8 min
10 min
12 min
14 min
16 min

sequences of *hnt*^{308} mutants detected in this manner, the early onset of AS phenotype was characterized. Using this approach, the first indication of an abnormality in *hnt*^{308} mutants was seen at mid-GBR stage embryos. Compared to wild type development, the AS appears to collapse into the gap that is found between the posterior cephalic region and the tip of the retracting germband (Figure 3.3). Concomitant to this collapse of the AS, AS nuclei can been seen in live imaging to undergo nuclear fragmentation, a characteristic typically associated with apoptotic cell death (Figure 3.4).

In wild type development, approximately 10% of AS cells are basally extruded from the epithelium. These extrusion events are readily observed in live imaging analysis using GFP-tagged membrane markers. Since genetic backgrounds that are associated with the absence of cell death lack these extrusion events, it has been suggested that extrusion is the consequence of apoptosis (Mohseni *et al.*, 2009). It was therefore of interest to determine if *hnt* mutant embryos are associated with extensive AS extrusion. To address this question, an RNAi mediated knock down approach was used. HNT expression was reduced along parasegment boundaries that run through the AS by means of a *UAS-hnt*^{RNAi} stock crossed to a stock carrying a *fushi* tarazu GAL4 (*ftz*^{GAL4}) driver. This allowed for a comparison of AS cells having endogenous levels of HNT expression (those AS cells not in the *ftz* stripe) to AS cells in which HNT expression is reduced (those AS cells within the *ftz* stripe). GFP markers also used in this experiment were *Ubi-DEcad*^{GFP} to visualize apical membranes, and nuclear GFP (*UAS-GFP*^{nls}) (see Materials and Methods for stock descriptions). The result of downregulating HNT expression was an increase in the number of extrusion events that occurred during 100 minute intervals in mid-DC staged embryos. Control embryos on average showed only

Figure 3.5: Scoring extruding amnioserosa cells in *UAS-hnt^{RNAi}* embryos. The nuclei of AS cells were visualized using the *ftz^{GAL4}* driver and *UAS-GFP^{nls}*. The background also contained *Ubi-DEcad^{GFP}* which allows for the detection of cell membranes. Confocal live imaging was performed on the Nikon Eclipse confocal microscope using 20X objective. Embryos were 10 hrs old (shown) and imaged for 100 minutes, at 2 minute intervals. (a) Indicated by the pink dot, only one extrusion was observed in the control embryos (lacking *UAS-hnt^{RNAi}*). (b) Indicated by the pink dots, an increase in the number of extrusions was detected in embryos expressing *UAS-hnt^{RNAi}*. The extrusions were detected closer to the anterior of the AS tissue. Embryos were collected from females of stock 1 crossed to males of stock 11 (a) and from females of stock 12 crossed to males of stock 11 (b) (See Materials and Methods). These embryos are oriented with the anterior to the left and dorsal side up.

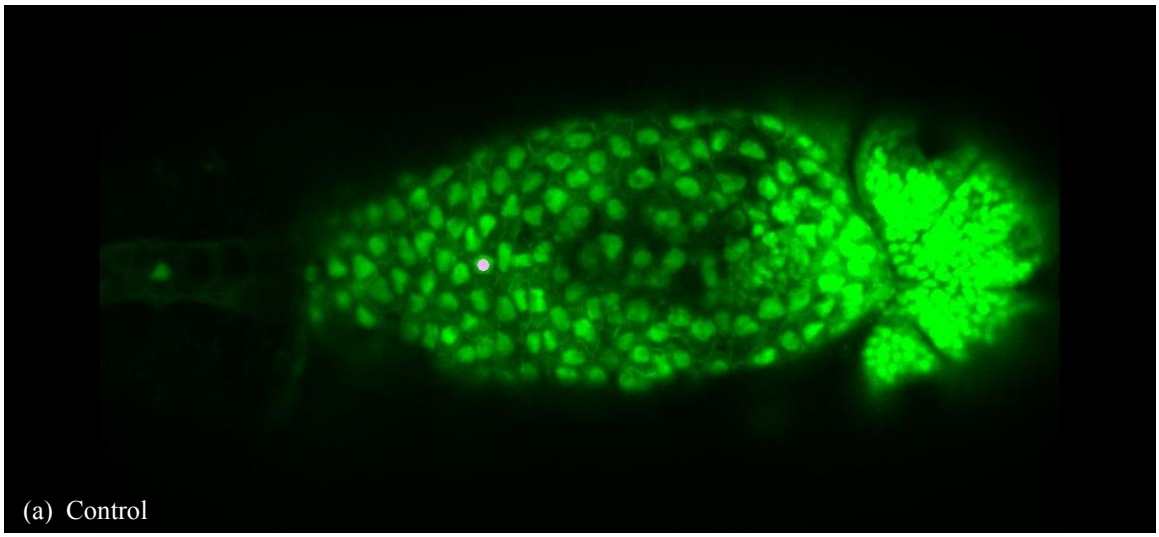

(a) Control

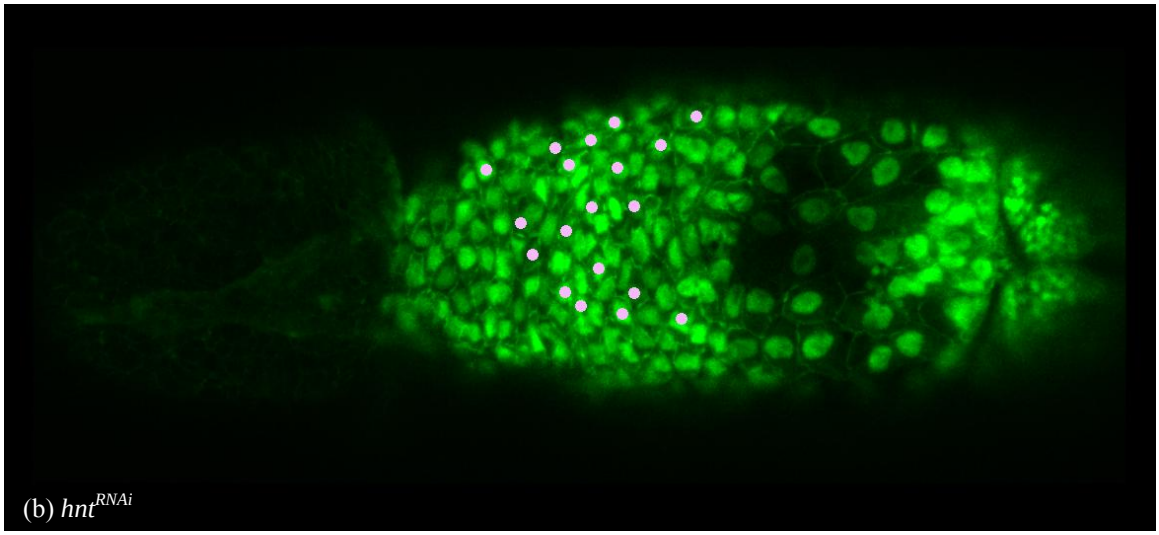

(b) *hnt*^{RNAi}

Figure 3.6: Extrusion and nuclear fragmentation in *UAS-hnt^{RNAi}* expressing embryo. Indicated by the white asterisks, two AS cells, from *UAS-hnt^{RNAi}* expressing embryo, shrink in size as they extrude from the epithelium. These cells were visualized using by *Ubi-DEcad^{GFP}*, and the nuclei visualized using *UAS-GFP^{nls}*. Nuclear fragmentation of the cells begins 4 minutes after extrusion. Image sequence montage illustrated is from the *UAS-hnt^{RNAi}* expressing embryos in Figure 3.5b. Live imaging was performed using the Nikon Eclipse confocal microscope.

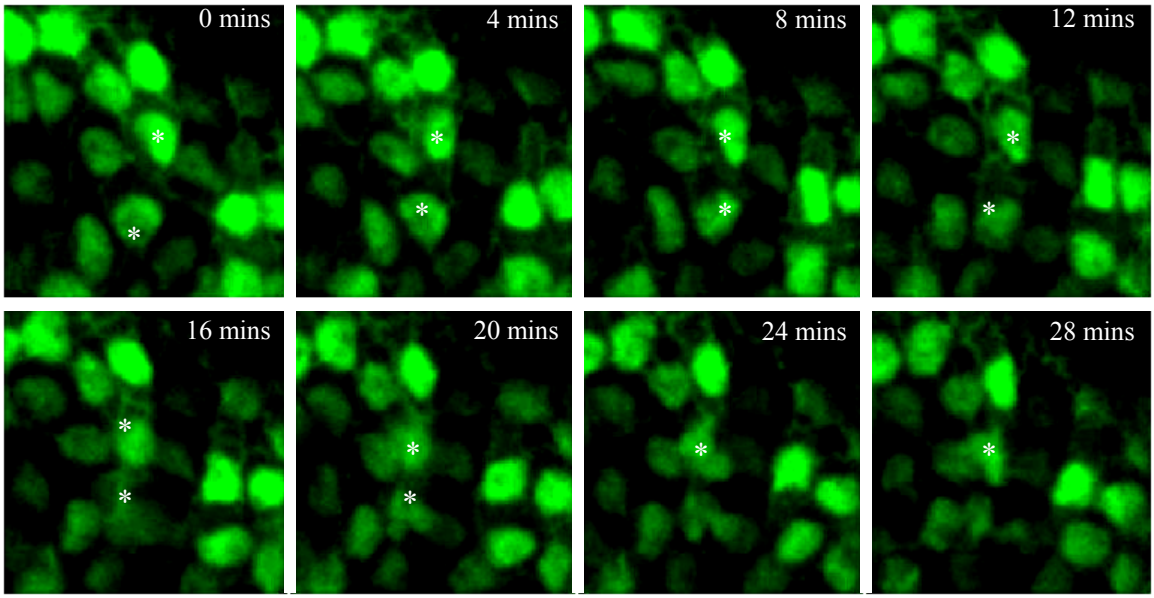
0 mins
4 mins
8 mins
12 mins
16 mins
20 mins
24 mins
28 mins

Table 3.1: Extrusion scores in *hnt*^{RNAi} embryos. The numbers of cells that extrude from the AS surface and undergo nuclear fragmentation were counted (See Figure 3.5 and Figure 3.6). The average number of extrusions in *hnt*^{RNAi} embryos is significantly increased when compared to control embryos.

Genotype	No. of embryos	Average no. of extrusions
Control	2	1
hnt^{RNAi}	6	17

one extrusion event whereas the *UAS-hnt*^{RNAi} expressing embryos had an average of 17 extrusions (Table 3.1). The extrusion events of the *UAS-hnt*^{RNAi} expressing embryos were spatially restricted to the anterior half of the AS (Figure 3.5). Extrusion events did not correspond to stripes of *ftz*^{GAL4} expression, but neither did the *UAS-GFP*^{nls} expression in the AS, although *ftz*-GFP stripes were evident in the lateral epidermis. Also in this background, the extruded cells were observed to undergo nuclear fragmentation (Figure 3.6). These RNAi results are consistent with the *hnt*^{308} mutant phenotype and suggest that AS loss could be associated with premature or inappropriate induction of apoptosis.

3.3 Macrophage activity in *hindsight* mutants

It is well established that apoptotic corpses are engulfed by phagocytic macrophages. To determine if the extrusion and nuclear fragmentation of the AS cells in *hnt* embryos is due to apoptosis, macrophage activity in null *hnt* mutants was examined using live imaging. Macrophages are readily visualized using a macrophage specific driver, *croquemort*^{GAL4} (*crq*^{GAL4}) in combination with *UAS-myristoylatedCD8*^{GFP} (*UAS-mCD8*^{GFP}) from stage 13 onwards. In control embryos, macrophages were visible in the head region as well as around the AS tissue. Macrophage activity was evident as vacuoles were observed in the macrophage cells, seen as big black spots in the cytoplasm of these cells (Figure 3.7).

In *hnt* null mutants (*hnt*^{1142}), macrophages were localized near the anterior region of the embryo where they tended to remain concentrated during development (Figure 3.8). This pattern of localization of the macrophages suggested that they were associated with the degenerating AS. Looking at the mutant embryo using DIC, GBR failure was

Figure 3.7: Confocal live image sequence illustrating macrophage activity. A macrophage specific driver, crq^{GAL4}, was used to detect active macrophages by labelling the cytoplasm of macrophages with $UAS\text{-}mCD8^{GFP}$, indicated by yellow arrows. Live imaging was performed using the Ziess Axiovert 100 confocal microscope. Images were captured using the 40X objective at 2 minute intervals. GFP expression was initially visible at stage 13, and expression remained until late stages of embryogenesis. Engulfment of apoptotic corpses was seen by the appearance of black vacuoles in the cytoplasm of the macrophages. Macrophages were present and active in the head region and around the AS tissue throughout the late stages of embryogenesis. Embryos were collected from females of stock 1 crossed to males of stock 14 (See Materials and Methods). All embryos were oriented with the anterior located at the top left corner and dorsal side facing up.

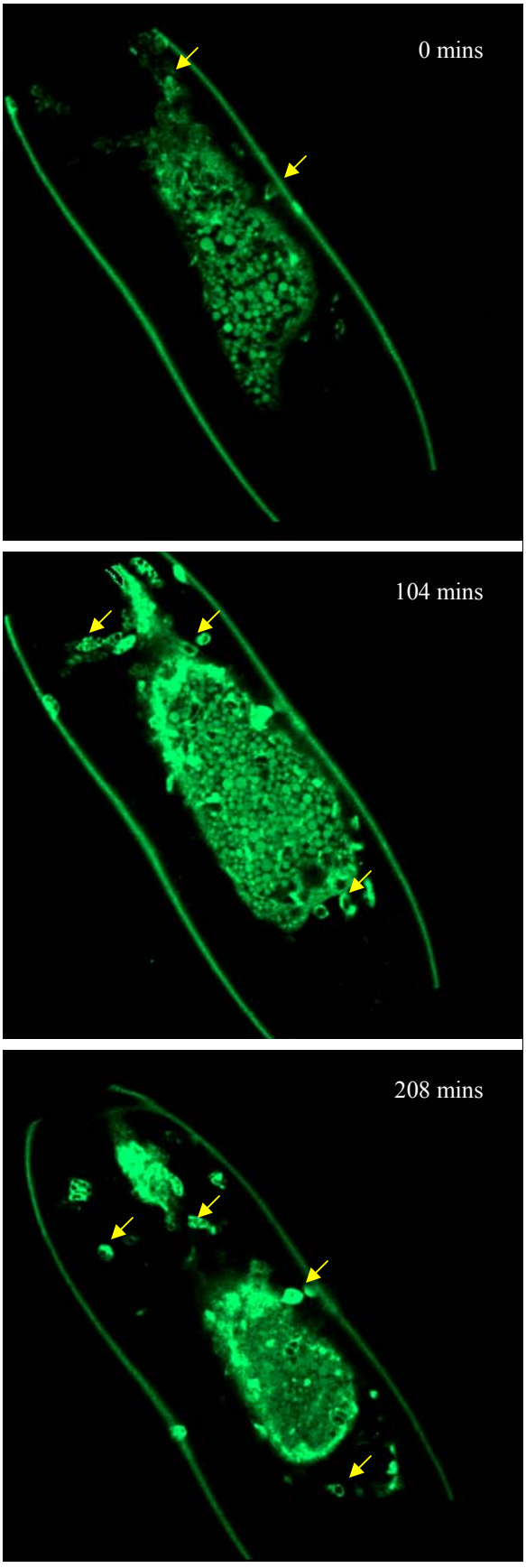
0 mins
104 mins
208 mins

Figure 3.8: Confocal live image sequence of macrophage activity in *hnt*^{1142} mutants. The macrophage specific driver, *crq*^{GAL4}, was used to detect macrophage activity in *hnt*^{1142} mutants by labelling the macrophage cytoplasm with *UAS-mCD8*^{GFP} (yellow arrows). Live imaging was performed using the Ziess Axiovert 100 confocal microscope. Images were captured using the 40X objective at 2 minute intervals. Embryos were aged to 10 hours prior to imaging. The majority of active macrophages were detected in the anterior region of the embryo. Embryos were collected from females of stock 13 crossed to males of stock 14 (See Materials and Methods). These embryos were oriented with the anterior located at the top left corner and dorsal side facing up.

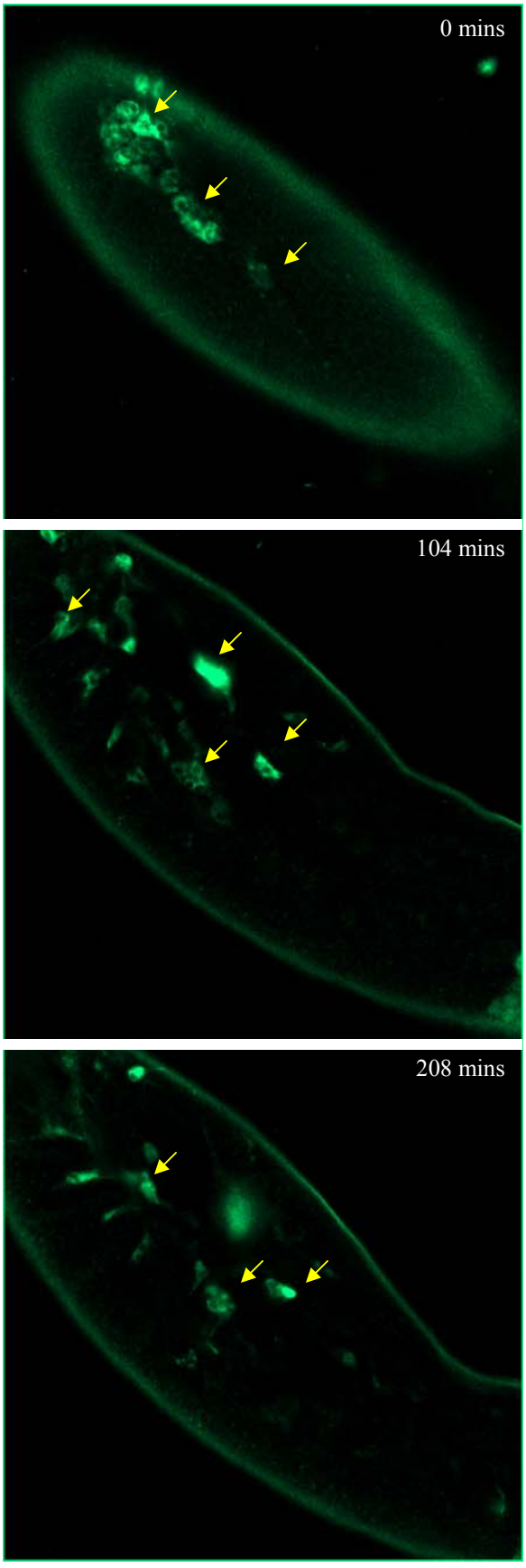
0 mins
104 mins
208 mins

Figure 3.9: Macrophage localization in *hnt*^{1142} mutants. (a) Confocal z-stack projection of *hnt* null mutant showing the pattern of macrophage localization through the embryo (yellow arrows). (b) DIC image of same embryo to confirm the GBR failure in the embryo. White arrow illustrates the caudal end of the germband. These images were taken with Ziess Axiovert 100 confocal microscope using the 40X objective. These embryos were oriented with the anterior located at the top left corner and dorsal side facing up.

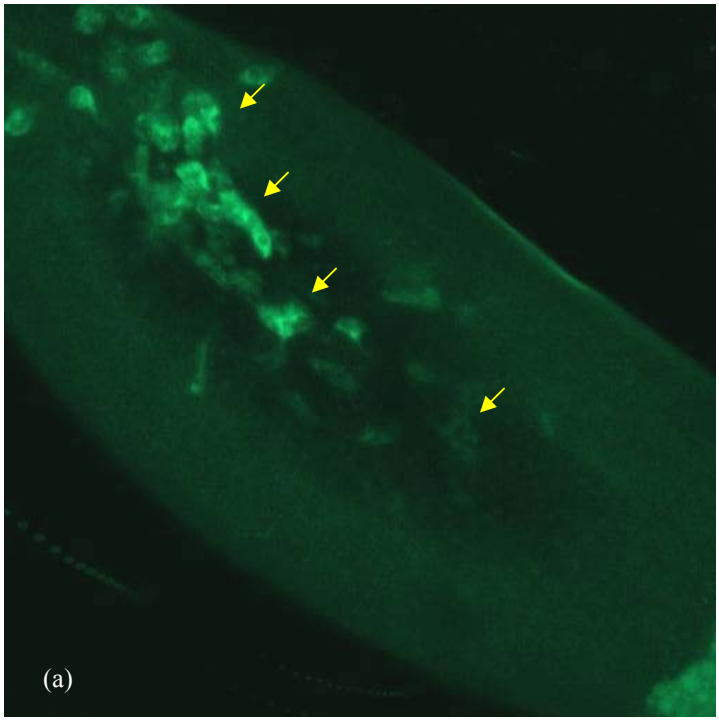
(a)

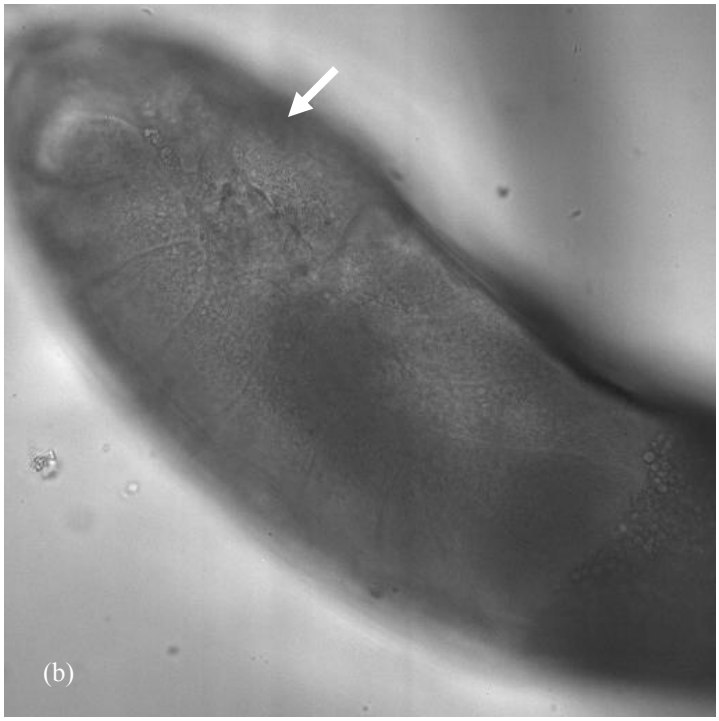
(b)

confirmed (Figure 3.9b). The macrophages had enlarged vacuoles in their GFP-expressing cytoplasm. The presence of vacuoles as well as the movement of the macrophages suggested that they were active and engulfing apoptotic corpses. These observations support the interpretation that the degeneration of the AS in *hnt* mutants is associated with the production of apoptotic corpses.

3.4 Deleting pro-apoptotic genes in *hindsight* mutants

Examination of the AS by RNA *in-situ* hybridization, live imaging analysis, or the examination of macrophage activity suggests that the loss of the AS in *hnt* mutants is associated with either premature or inappropriate activation of apoptosis. Previous studies in our lab have established that the degeneration of the AS during wild type development is inhibited in mutants that lack the pro-apoptotic genes, *hid*, *grim*, and *rpr* (Mohseni *et al.*, 2009). Chromosomal deficiencies *Df(3L)H99* (*H99*) and *Df(3L)ED225* (*ED225*) are deleted for these three genes, and either deficiency, when homozygous, or the trans-heterozygous (*H99/ED225*) is associated with a persistent AS phenotype. This persistent AS typically adopts an elongated "tube-like" structure that is readily observed beneath the dorsal epidermis along the midline of the embryo. It was therefore of interest to determine if the *hnt* mutant phenotype and, in particular, the premature loss of the AS in *hnt* mutants is rescued by the *H99* or *ED225* deficiencies. To address this question, a genetic strategy was devised that would allow *hnt* mutants to be unambiguously identified as also being *H99/ED225*. Briefly, in this experiment, α-HNT labelling permits identification of the hnt^{308} mutant by virtue of decreased HNT expression while only the

Figure 3.10: Anti-HNT antibody staining in apoptotic deficient *hnt* mutants. Staining using α-HNT antibody labels the nuclei of all cells (TRITC). The apoptotic deficient background, *H99/ED225* embryos were detected by the presence of cytoplasmic GFP in the AS using the AS specific driver, $LP\text{-}1^{GAL4}$. The hnt^{308} mutants were detected by the absence of α-HNT staining in the AS. Images were captured using the Ziess Axiovert 100 confocal microscope at 40X objective. The AS tissue is indicated by the yellow arrows. (a) Control embryos show strong α-HNT staining in the AS and an absence of GFP. (b) *H99/ED225*: Embryo illustrate strong α-HNT staining and GFP expression in the AS. (c) *H99/ED225*: Embryo at a late stage of development with a persistent AS in a "tube-like" structure. (d and e) *hnt;H99/ED225*: Double mutant embryos were detected by GFP expression in the AS, and a lack of α-HNT staining. Embryos were collected from females of stock 16 crossed to males of stock 17 (See Materials and Methods). Control and *H99/ED225* embryos were oriented with the anterior located at the top right and dorsal side facing up. The double mutants were oriented with the dorsal side facing the top left corner (d and e).

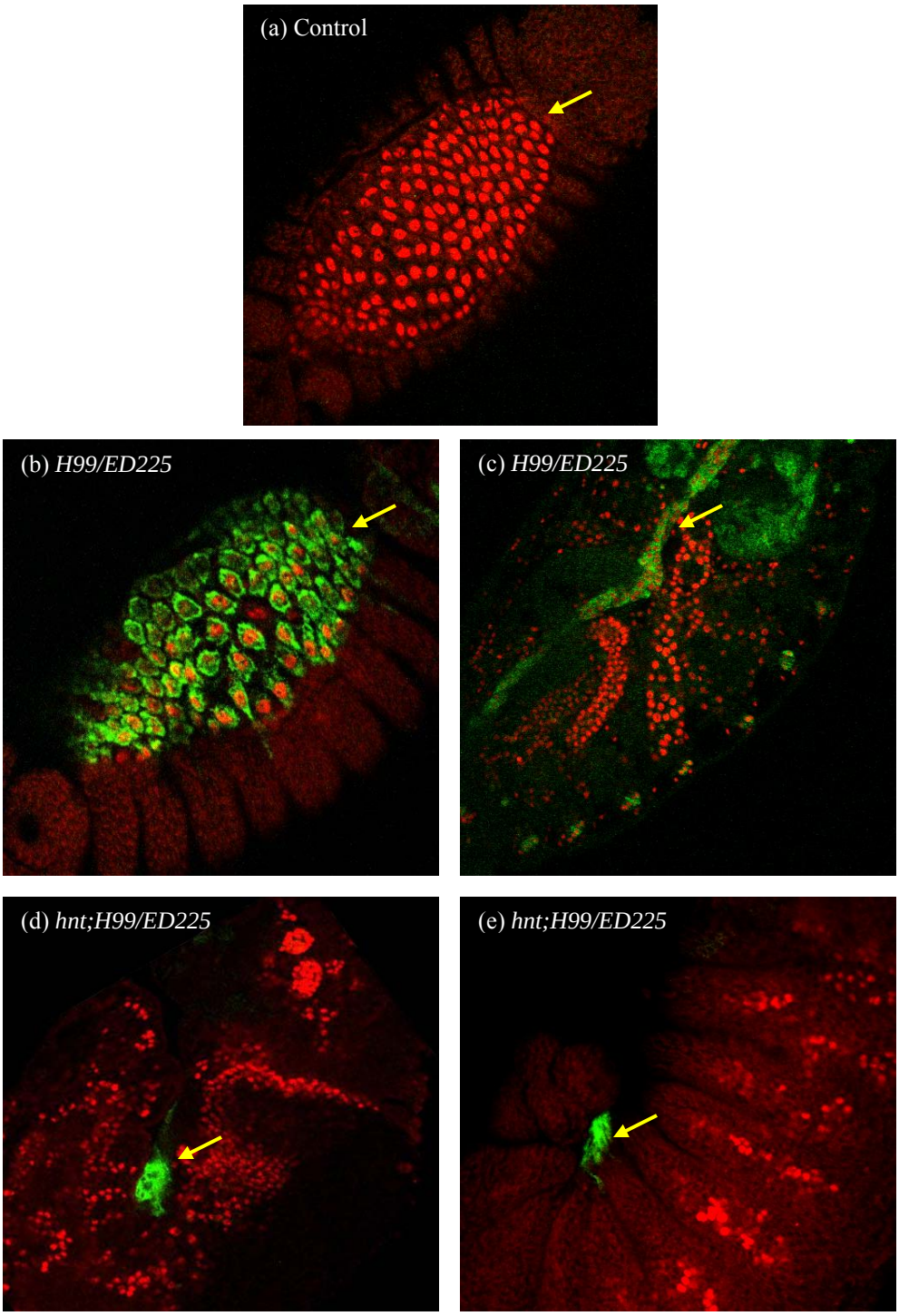
(a) Control
(b) *H99/ED225*
(c) *H99/ED225*
(d) *hnt;H99/ED225*
(e) *hnt;H99/ED225*

H99/ED225 embryos carry the necessary GAL4 and UAS constructs to result in GFP expression (See Materials and Methods, Figure 2.2).

As seen in Figure 3.10, hnt^{+} sibs that are not *H99/ED225* show strong α-HNT staining of the AS which lacks GFP expression. In contrast, the *H99/ED225* mutants show strong GFP expression in the AS, and the AS is present in late stage embryos which have normally completed AS elimination (Figure 3.10b; Figure 3.10c). hnt^{308} mutants, which in this experiment, were unambiguously recognized on the basis of reduced α-HNT staining (although this is not apparent in Figure 3.10 due to different confocal settings used in acquiring the images) showed strong GBR defects regardless of whether or not they were also *H99/ED225* (data not shown). Two examples of hnt^{308} + *H99/ED225* double mutant embryos are shown in Figure 3.10d and Figure 3.10e. In these embryos, the AS is observed as a small remnant. Based on these observations, it can be concluded that the AS degeneration in *hnt* mutants is independent of the pro-apoptotic activators, *hid*, *grim* and *rpr*.

3.5 Blocking caspases in *hindsight* mutants

Although the pro-apoptotic genes were removed in the above experiment, it remained possible for cell death to occur as a consequence of an alternative pathway for caspase activation. Ultimately, apoptotic cell death requires activated caspases. Another approach for inhibiting apoptosis involves the use of the baculovirus derived pan-caspase inhibitor p35. Embryos expressing *UAS-p35* under the control of the $daughterless^{GAL4}$ driver (da^{GAL4}) show a persistent AS phenotype very similar to the *H99* phenotype (Figure 3.11). The absence of apoptotic activity in this *p35* expressing background was

Figure 3.11: TUNEL staining on embryos with ectopic p35 expression. TUNEL staining was used to detect apoptotic cells in embryos during the late stages of DC (late stage 15), when the AS begins to degenerate *en masse*. The AS was detected by α-HNT staining seen in red. (a) Wild type embryos (*yw*) embryos show TUNEL stained cells in green (white arrows) surrounding the AS near the anterior and posterior regions. Embryos collected from stock 1 (See Materials and Methods). (b) *p35*: Embryos ubiquitously expressing *p35* through the use of da^{GAL4} driver (females of stock 3 crossed to males of stock 18 (See Materials and Methods)). These embryos show no TUNEL stained cells near the AS. The AS is persistent, and the morphology of the AS resembles that of the *H99* phenotype. The AS has been flanked on both sides with white asterisks. Images were captured using the Ziess Axiovert 100 confocal microscope and 40X objective. Both embryos were oriented with the anterior facing the top right corner and dorsal side facing up.

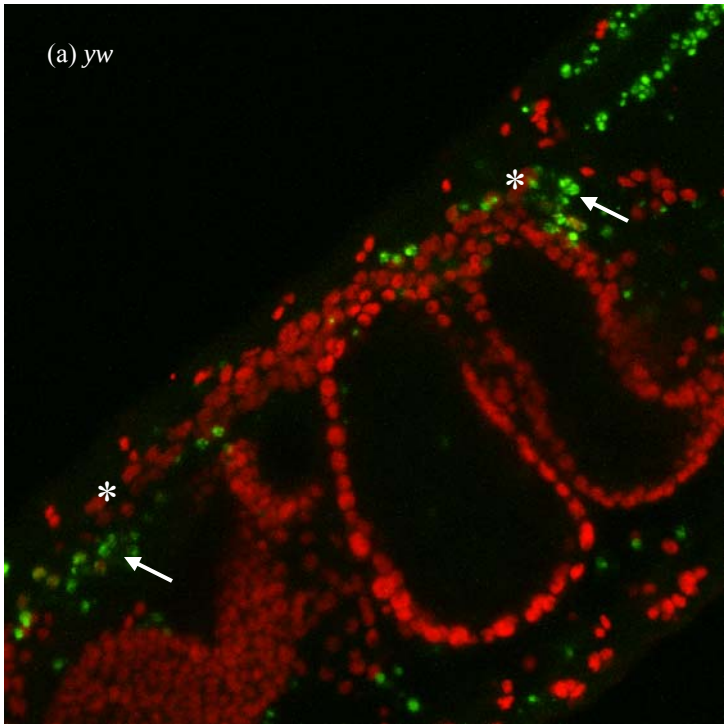
(a) *yw*
*
*

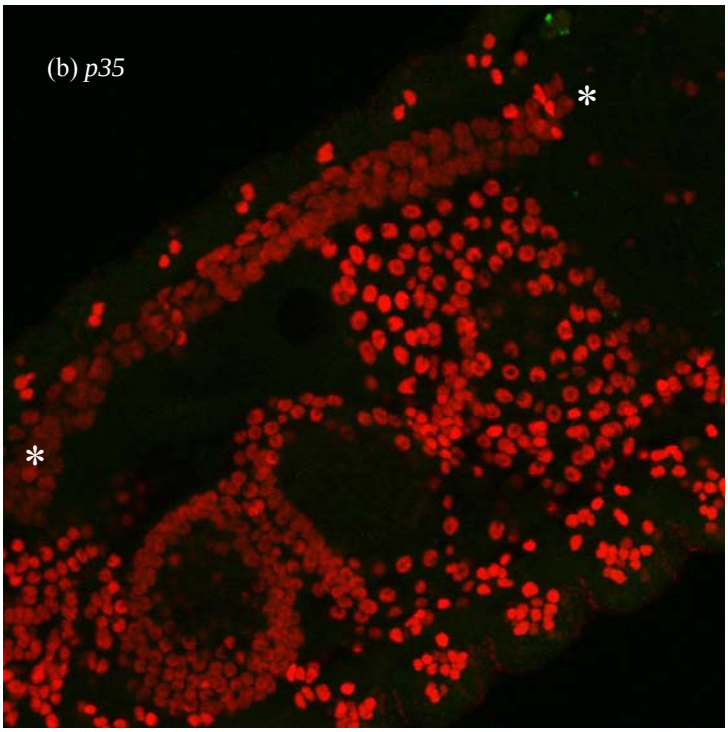
(b) *p35*
*
*

confirmed using the TUNEL staining protocol (absence of TUNEL signal compared to wild type control). To examine the effect of caspase inhibition, the AS was examined by CG12011 RNA *in-situ* hybridization in *hnt* mutants that also carried da^{GAL4} + *UAS-p35*. In this experiment, hnt^{308} mutants were recognized by GBR/DC failure (as seen in Figure 3.2b). Very similar to the *H99/ED225* observation, the AS in the *p35* expressing background was also reduced to a small remnant (Figure 3.12). Control sibs showed a prominent persistent AS phenotype.

Further analysis involved quantification and comparison of the mutant phenotypes associated with the following genotypes: hnt^{308}; *UAS-p35* expression alone; and hnt^{308} + *UAS-p35* expression. While it might have been expected that *p35* expression could rescue the *hnt* mutant, the data surprisingly indicated an increase in GBR and DC failure from 8.4% to 17% (these values refer to the total number of embryos examined with the maximum possible value being 25%) (Table 3.2). Clearly, *p35* expression does not rescue GBR or DC failure of *hnt* mutants. A consistent feature observed in the hnt^{308} + *UAS-p35* embryos, which was not observed in the hnt^{308} mutants without *p35* expression, was the presence of AS tissue as detected by CG12011 RNA *in-situ* hybridization. The interpretation of these observations is that there is a loss of AS integrity in *hnt* mutants that is independent of caspase-dependent apoptotic cell death.

The previous experiment, although intriguing, used a ubiquitously expressed GAL4 driver, and relied on GBR/DC defects for the identification of *hnt* mutants. This work was, therefore, repeated using a live imaging approach which incorporated a genetic system to unambiguously identify hnt^{308} mutants, without relying on the expression of the mutant phenotypes. Briefly, this approach uses the GAL80 repressor in combination with

Figure 3.12: RNA *in situ* hybridization on *hnt*^{308} mutants expressing *p35*. RNA *in-situ* hybridization was performed using the probe for the AS-specific *CG12011* gene (black arrow) on 12-15 hr old embryo collections. (a) *p35*: Embryos ectopically expressing *p35* using the *da*^{GAL4} driver show a persistent AS phenotype, illustrated as a "tube-like" structure during late stages of embryogenesis. Embryos collected from females of stock 3 crossed to males of stock 18 (See Materials and Methods). (b and c) *hnt*^{308}*;p35*: Ectopic *p35* expression in a *hnt*^{308} mutant background with *da*^{GAL4} driver. The AS has fallen off the tail and the embryo has failed GBR. The GBR failure resembles that seen in *hnt*^{308} mutants (refer to Figure 3.2b), though *hnt*^{308} mutants expressing *p35* have AS tissue present. Embryos were collected from females of stock 4 crossed to males of stock 18 (See Materials and Methods). Embryos are oriented with the anterior to the left and dorsal side up.

(a) *p35*

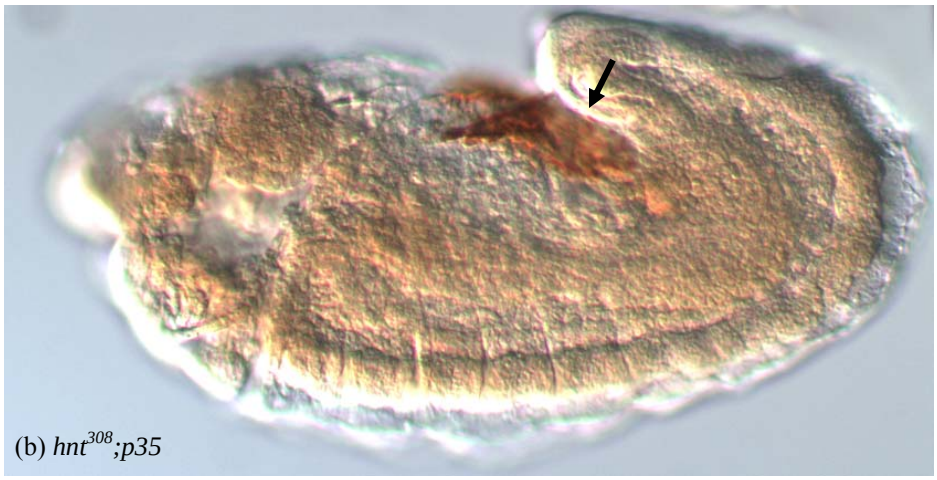

(b) *hnt*^{308}*;p35*

(c) *hnt*^{308}*;p35*

Table 3.2: Summary of RNA *in-situ* hybridization on *hnt*^{308} with ectopic *p35* expression. Embryos expressing ectopic *p35* do not fail in GBR. The ectopic expression of *p35* fails to rescue the GBR failure observed in *hnt*^{308} mutants. RNA *in-situ* hybridization was performed on 12-15 hour old embryos. The *hnt*^{308} embryos were collected from females of stock 4 crossed to stock 1; the *p35* embryos were collected from females of stock 3 crossed to stock 18; and the *hnt*^{308}*; p35* embryos were collected from females of stock 4 crossed to stock 18 (See Materials and Methods).

Genotype	*hnt*^{308}	*p35*	*hnt*^{308}*;p35*
Total embryos	**95**	**194**	**183**
% Persistent AS (completed GBR and DC)	**0%**	**40%**	**56%**
% GBR + DC failure	**8.4%**	**0%**	**17%**

GAL4/*UAS-GFP* backgrounds such that only hemizygous hnt^{308} mutant embryos express GFP (See Materials and Methods Figure 2.3). In addition, the *GAL4* drivers used in this design are associated with elevated AS expression. The live imaging results confirm the interpretation that *p35* expression does not rescue the *hnt* mutant phenotype. Remarkably, in this live imaging analysis, the AS of hnt^{308} + *UAS-p35* embryos, although abnormal in appearance, was persistent as evidenced by the onset of somatic muscular innervation (which occurs at stage 16) (Figure 3.13). Interestingly, all of these embryos which were recognized independent of GBR mutant phenotypes do, in fact, show GBR defects. This key observation confirmed that GBR failure is not a direct or indirect consequence of premature AS death.

3.6 Analysis of cell behaviour in *hindsight* mutants

The previous section established that it was possible to recover a *hnt* mutant with a persistent AS through caspase inhibition. It was, therefore, of interest to examine AS cell shapes and behaviour at earlier stages of development when *hnt* mutants (without *p35* expression) are normally associated with premature AS loss. Unlike the previous live imaging analysis which used a nuclear GFP (Figure 3.3), these experiments used cytoplasmic GFP expression, which better facilitates examination of cell shape changes and cellular extensions. Mid-GBR stage embryos were examined representing the following genotypes: wild type, AS-specific *UAS-p35* expression, hnt^{308}, and hnt^{308} + AS-specific *UAS-p35* expression (Figure 3.14). In both the wild type and the AS-specific *UAS-p35* expressing embryos, the posterior-most AS cells form prominent lamellipodia and show contact with the epidermal cells of the extended tip of the germband. In both,

Figure 3.13: Visualization of the AS in various backgrounds. The AS, indicated by white arrow, is visualized using the kr^{GAL4} driver with *UAS-GFP*. The germband is labelled with a white asterisk. Images were captured using the Nikon Eclipse confocal and 20X objective. Embryos were at late stage 15, the stage prior to muscle twitching. (a) Control: The AS tissue degenerates and apoptotic corpses are seen surrounding the tissue. Embryos collected from females of stock 19 crossed to stock 1 (See Materials and Methods) (b) *p35*: Embryos ectopically expressing *p35* exhibit a persistent AS. Embryos were collected from females of stock 19 crossed to stock 18 (See Materials and Methods) (c) hnt^{308}*; p35* : The hnt^{308} embryos with ectopic *p35* expression results in an AS that remains intact but does not rescue GBR failure. Embryos were collected from females of stock 20 crossed to stock 22 (See Materials and Methods). Embryos are oriented with the anterior to the left and dorsal side up.

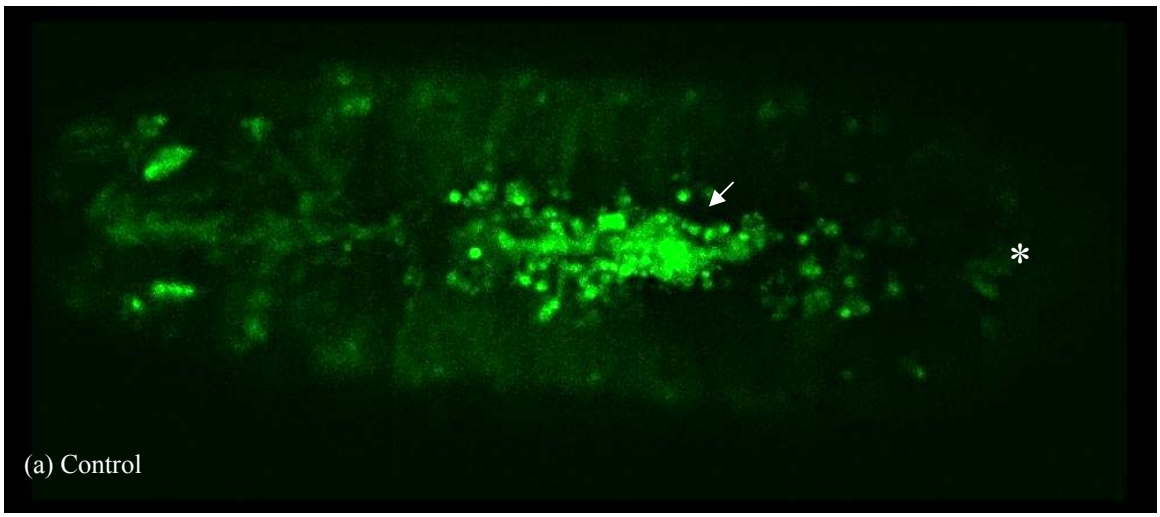
(a) Control

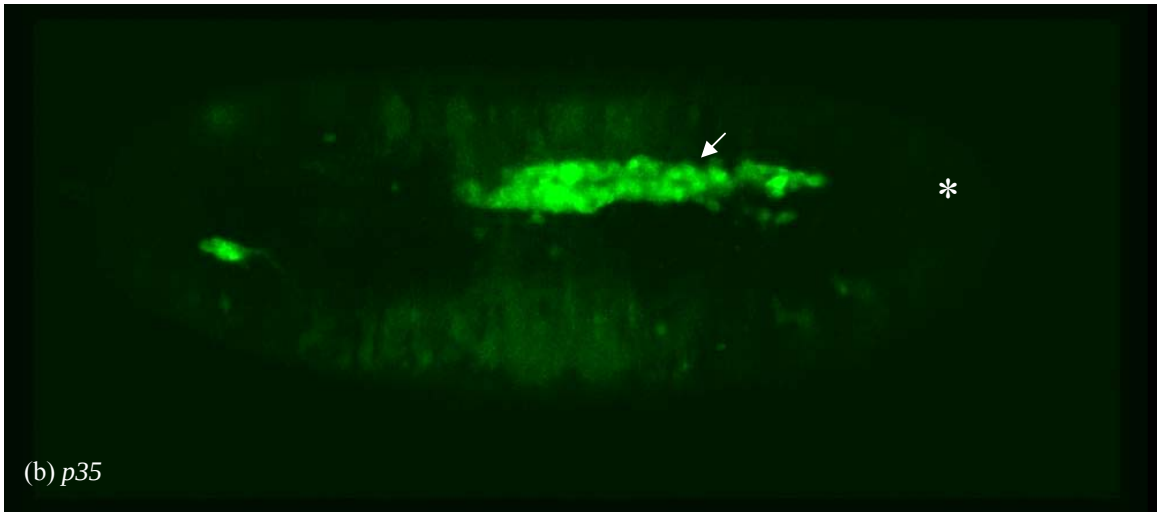
(b) *p35*

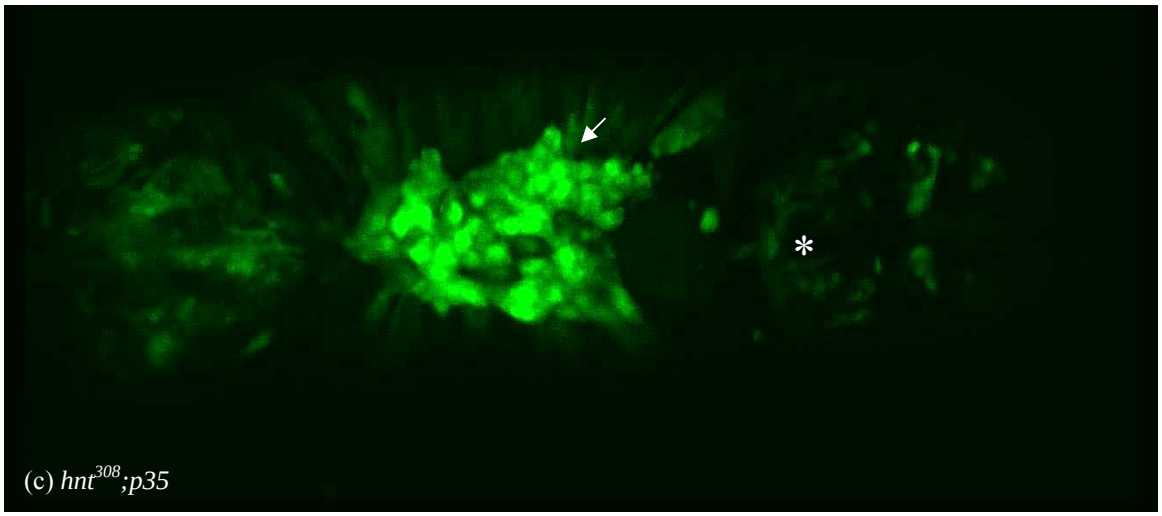
(c) *hnt^{308};p35*

Figure 3.14: Amnioserosa cell behaviour in various backgrounds. The AS, indicated by yellow arrow, is visualized using the kr^{GAL4} driver with *UAS-GFP*. The germband is labelled with a white asterisk. Images were captured using the Nikon Eclipse confocal and 20X objective. Embryos were at mid-GBR stage. (a) Control: The posterior-most AS cells form prominent lamellipodia (white arrows) and contact the extended germband. Embryos were collected from females of stock 19 crossed to stock 1 (See Materials and Methods). (b) hnt^{308}: In *hnt* mutants, the lamellipodia extensions are not observed, indicating a lack of contact between the AS cells and the germband. Embryos were collected from females of stock 20 crossed to stock 24 (See Materials and Methods). (c) *p35*: Embryos expressing *p35* show lamellipodia extending from the AS cells, as seen in the control embryos (a). Embryos were collected from females of stock 19 crossed to stock 18 (See Materials and Methods). (d) hnt^{308}*; p35*: The *hnt* mutant embryos expressing *p35* lack the lamellipodia extensions, resembling hnt^{308} embryos, suggesting no rescue of the phenotype. Embryos were collected from females of stock 20 crossed to stock 22 (See Materials and Methods). All embryos are oriented with the anterior to the left and the dorsal side up.

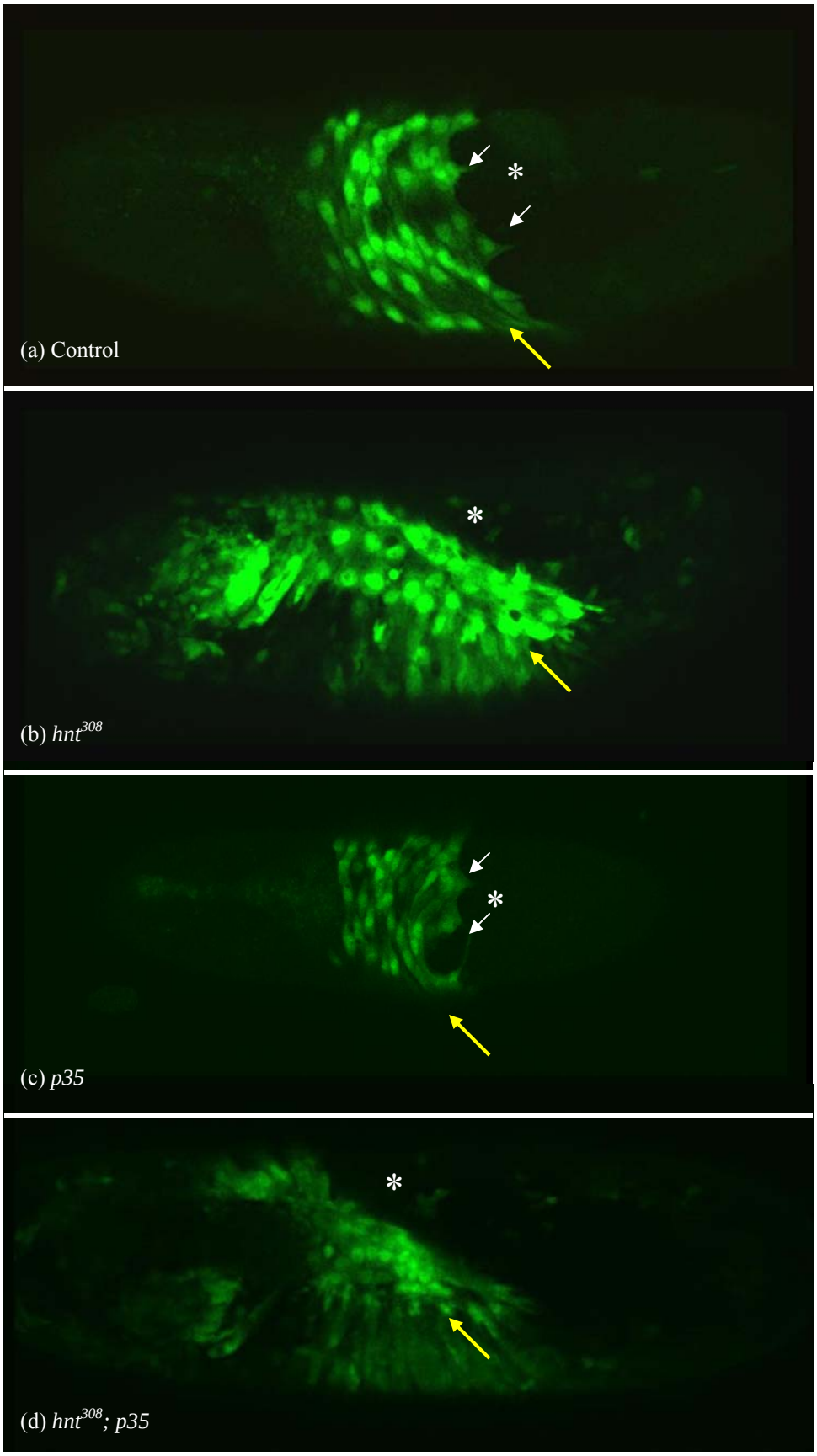
(a) Control
(b) hnt308
(c) p35
(d) hnt308; p35

the *hnt*^{308} mutant and the *hnt*^{308} + AS-specific *UAS-p35* expressing embryos, the posterior most AS cells were not maintained in this position and no lamellipodia were observed. Subsequently, over a period of 160 min, the AS of the *hnt*^{308} mutant was eliminated with evidence of apoptotic cell death (*i.e.* rapid cell fragmentation). Over the same time period, the *hnt*^{308} + AS-specific *UAS-p35* expressing embryos did not show any evidence of similar AS elimination or apoptosis. These observations suggest that the earliest manifestations of the *hnt* mutant phenotype involve a localized loss of contact between the AS and epidermal cells; it is likely that this loss of contact is the primary defect associated with *hnt* mutants and that it leads to activation of apoptosis and premature AS loss.

3.7 Analysis of Armadillo in *hindsight* mutant and Hindsight overexpression embryos

A recently published study implicated *hnt* as a regulator of the levels of Armadillo (β-catenin) and shotgun (DE-cadherin) in the anterior ovarian follicular cells. In this study, somatic mosaics were generated in the follicular epithelium such that patches of follicular cells were recovered that were mutant for *hnt*. These mutant patches were found to show elevated levels of Armadillo (hereafter referred to as ARM) and shotgun (Melani *et al.*, 2008). The same study also demonstrated reductions in the levels of these cell adhesion molecules in follicular cells overexpressing HNT (Melani *et al.*, 2008). It was, therefore, of obvious interest to test if similar alterations of the levels of these cell adhesion molecules could be observed in the AS of *hnt* mutants and HNT overexpressing embryos. This section describes experiments that were done to address the levels of

ARM in these backgrounds (DE-cad was not examined).

Antibody staining using the mouse monoclonal antibody for ARM N27A1 (hereafter referred to as α-ARM) proved to be an excellent membrane marker on whole mount embryos fixed using hot-methanol fixation procedure (Figure 3.15). The hot-methanol fixation procedure extracts most of the cytoplasmic form of ARM, while maintaining the tightly membrane-bound form of ARM (Muller and Wieschaus, 1996). In comparing α-ARM stained wild type and *hnt* mutant embryos, no appreciable differences could be observed in membrane-bound ARM protein levels (Figure 3.15). The *hnt* mutant used in this experiment was the hnt^{1142} allele, a HNT protein null. The hnt^{1142} mutants were recognized on the basis of mutant phenotype which included failure of GBR and AS collapse. The *hnt* mutants were examined at early stages of GBR failure where ample AS tissue was still present.

In addition to examining loss of function *hnt* mutants, HNT overexpressing backgrounds were also stained for ARM. This included collections in which 50% of the embryos were expected to carry the ftz^{GAL4} driver and the *UAS-*hnt^{6-1} construct. In examining numerous embryos (>100) of this background that were at mid-DC stages, no alterations in membrane-bound ARM protein could be detected (Figure 3.15). This was done with particular attention to examination of the lateral epidermis where the ftz^{GAL4} driver is known to have strong expression at parasegment boundaries. No embryos were found to show any changes in the staining of ARM that would correspond to parasegment boundaries.

Figure 3.15: Antibody staining using α-ARM on various backgrounds. A hot-methanol fixation method was used to visualize plasma membranes in the embryos. The AS tissue is indicated by the yellow arrows. Images were captured using the Zeiss Axiovert 100 confocal microscope using the 40X objective and identical confocal settings. (a and b) *yw*: α-ARM staining on control embryos (stage 14) allow the AS to be seen throughout DC. Embryos collected from stock 1 (See Materials and Methods). (c and d) $hnt^{1142}/FM7$: α-ARM staining on heterozygous siblings of hnt^{1142} show similar levels of staining as *yw*. Embryo is at stage 12 (early GBR) where the AS cells show an overlap with the germband (c). At late stage 13, the AS is exposed on the dorsal surface of the embryo (d). Embryos were collected from females of stock 13 crossed to stock 1 (See Materials and Methods). (e and f) hnt^{1142}: The hnt^{1142} mutants (hemizygous males) were recognized by the AS collapse phenotype where the AS slips off the germband. α-ARM staining on the mutants show similar levels of staining as their heterozygous siblings. Embryos were aged to 7-10 hrs (stage 12 and 13). Embryos were collected from females of stock 13 crossed to stock 1 (See Materials and Methods). (g) ftz^{GAL4}: α-ARM staining on the ftz^{GAL4} driver (stage 14) yielded similar levels of the antibody staining compared to *yw* (a). Embryos were collected from females of stock 1 crossed to stock 30 (See Materials and Methods). (h) ftz^{GAL4};*UAS-*hnt^{6-1}: Embryos (stage 14) overexpressing HNT protein yielded similar staining levels as previous controls. Embryos were collected from females of stock 31 crossed to stock 30 (See Materials and Methods). From this cross, 50% of the progeny carry the ftz^{GAL4} driver. All embryos are oriented with the anterior located at the top right and dorsal side up, except in (a and g) where the dorsal side is facing down.

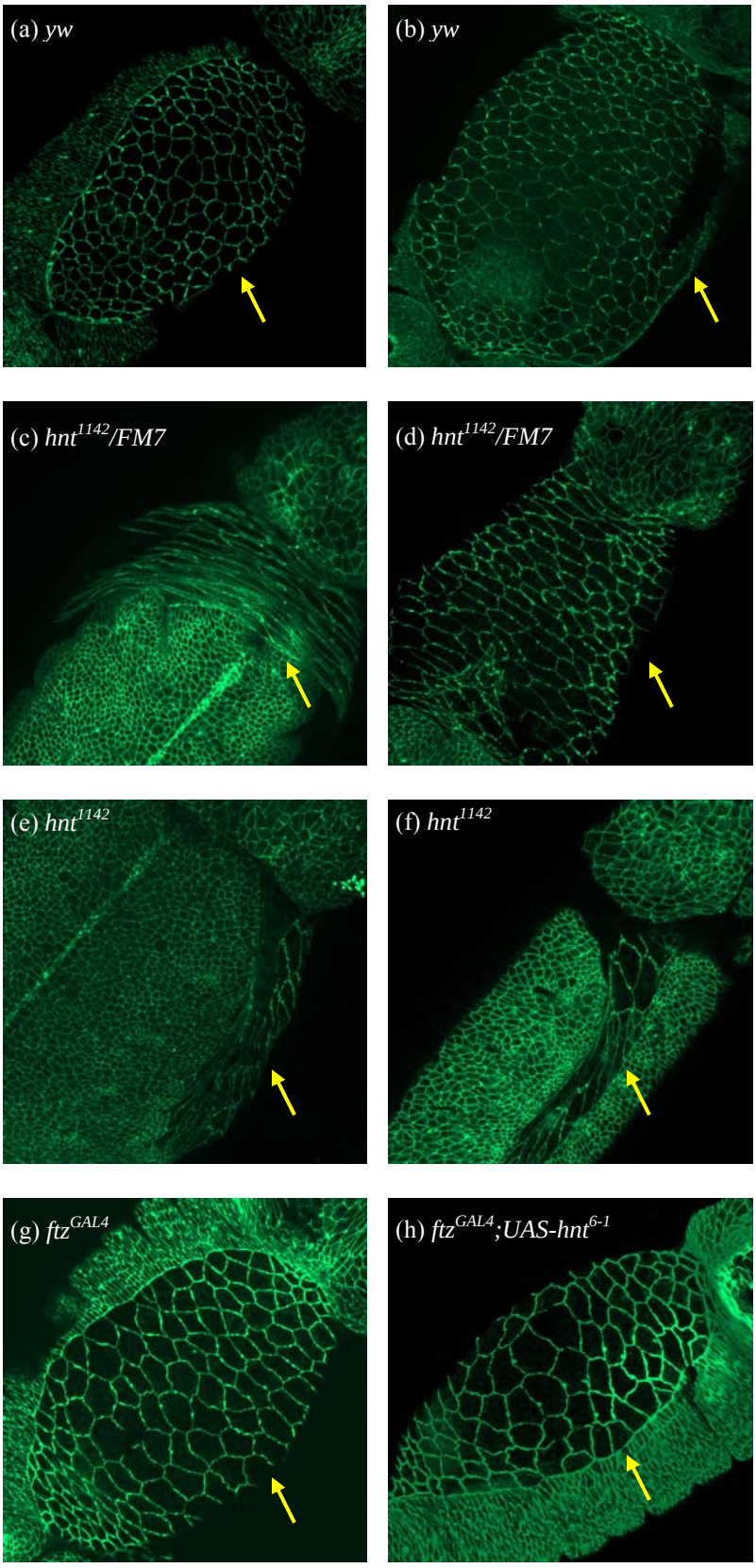
(a) yw
(b) yw
(c) hnt1142/FM7
(d) hnt1142/FM7
(e) hnt1142
(f) hnt1142
(g) ftzGAL4
(h) ftzGAL4;UAS-hnt6-1

In the above experiment it was not possible to recognize those embryos carrying the *GAL4 + UAS* constructs because the *ftz*^{GAL4} stock is not homozygous viable. This experiment was repeated using a different *ftz*^{GAL4} recombinant stock that carries *UAS-actin*^{GFP} in addition to the *Ubi-DEcad*^{GFP} (abbreviated hereafter as *ftzUA*). Progeny of *ftzUA* stock crossed to *UAS-hnt*$^{6-1}$ can be confirmed as carrying *ftz*^{GAL4} and *UAS-hnt*$^{6-1}$ by virtue of the stripes of *UAS-actin*^{GFP} expression (surprisingly, actin^{GFP} was found to maintain fluorescence following the hot-methanol fixation in antibody staining procedure). Control embryos collected from *ftzUA* stock crossed to *yw*, as well as embryos collected from *ftzUA* crossed to *UAS-hnt*$^{6-1}$ were fixed, stained and examined in parallel using identical conditions and confocal settings. Again, with particular attention to the lateral epidermal cells, no alterations in ARM protein levels were detected (Figure 3.16; Figure 3.17).

The antibody staining procedure above examined the ARM protein levels in embryos having reduced and increased HNT expression. The mechanism of the regulation of ARM protein levels by HNT in the ovarian study was not elucidated. Given that HNT is a transcription factor, it is possible that this regulation could occur at the level of transcriptional activation/repression. To test this, an armadillo reporter construct (*arm*$^{GFParm[83]}$) was used. The *arm*$^{GFParm[83]}$ expresses ARM-GFP fusion protein under the control of the *arm* promoter. The *arm*$^{GFParm[83]}$ is a good marker for cell membranes, and appears to be an accurate reporter of endogenous ARM expression and protein localization (Figure 3.18a). Live imaging was performed on control embryos collected from *ftz*^{GAL4} + *arm*$^{GFParm[83]}$ crossed to *yw*, as well as embryos collected from *ftz*^{GAL4} + *arm*$^{GFParm[83]}$ crossed to *UAS-hnt*$^{6-1}$. Like the previous experiment, only 50% of progeny

Figure 3.16: α-ARM staining on *ftzUA* embryos. Confocal images (captured using the Nikon Eclipse confocal using 40X objective) of embryos collected at various stages are shown. The Y-axis indicates the genotype of the embryo, and the X-axis indicates the *Ubi-DEcad*^{GFP} as well as the *UAS-actin*^{GFP} detected in green, and the α-ARM staining is in red (TRITC). Embryos were collected from females of stock 1 crossed to stock 32 (See Materials and Methods). (a) Embryos lacking expression of *ftzUA* do not have GFP expression. (b) Early GBR stage embryo shows *ftzUA* expression seen as green stripes in the epidermis. The intensity of α-ARM staining is similar to the embryos lacking *ftzUA* expression (a). (c) Mid-DC stage embryo with *ftzUA* expression seen in the epidermis as green stripes. The levels of α-ARM antibody are similar to the previous staged embryos. The embryos are oriented with the anterior located at the top left and dorsal side facing upwards.

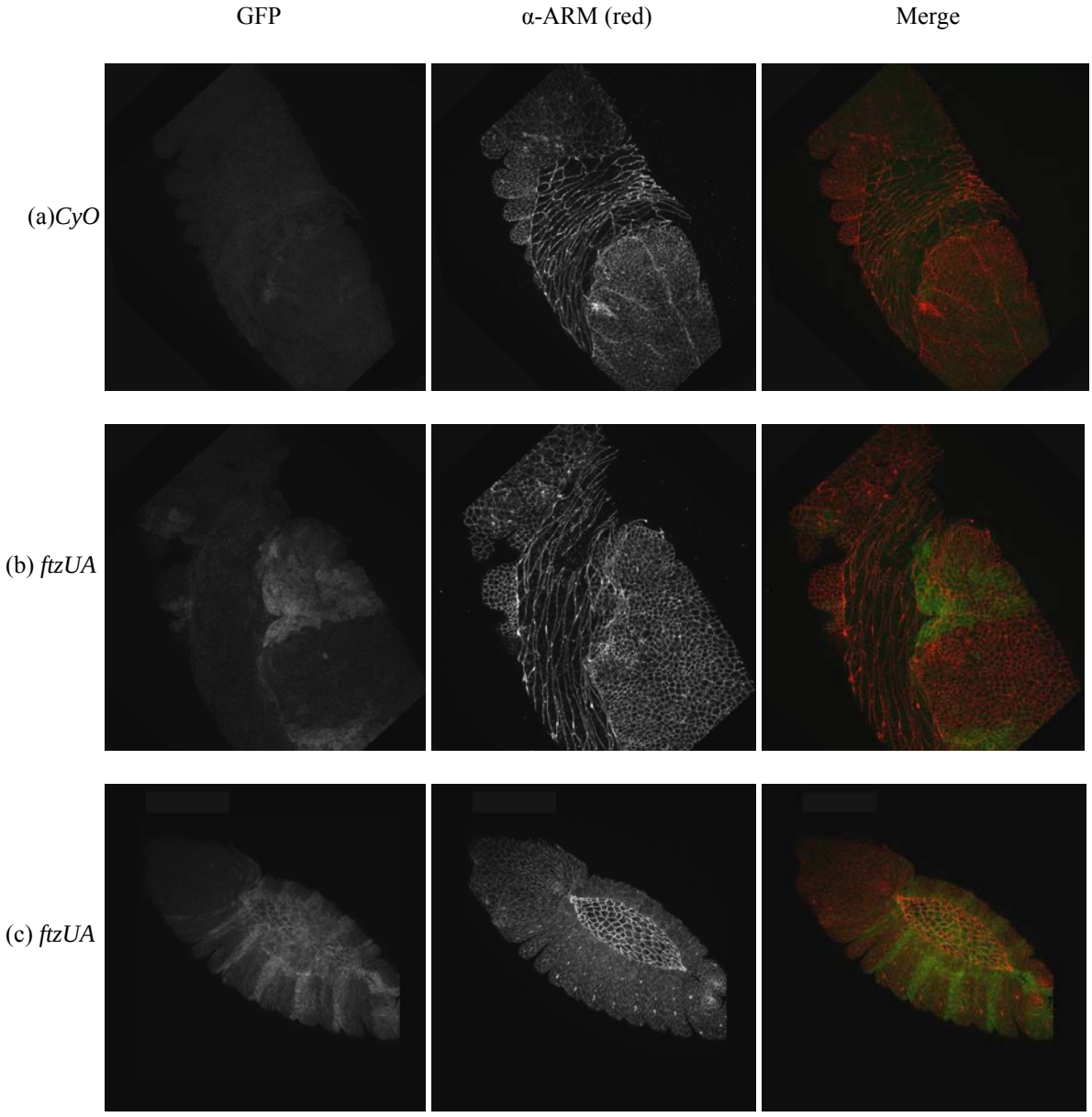
GFP
α-ARM (red)
Merge
(a)*CyO*
(b) *ftzUA*
(c) *ftzUA*

Figure 3.17: α-ARM staining on embryos overexpressing HNT. Confocal images (captured using the Nikon Eclipse confocal using 40X objective) of embryos collected at various stages are shown. Embryos were collected from females of stock 31 crossed to stock 32 (See Materials and Methods). The Y-axis indicates the genotype of the 2nd chromosome in the embryo, and the X-axis indicates the *Ubi-DEcad*^{GFP} as well as the *UAS-actin*^{GFP} detected in green, and the α-ARM staining is in red (TRITC). HNT was overexpressed in embryos using the *UAS-hnt*$^{6-1}$ construct with the *ftzUA* driver. (a) Embryos lacking *ftzUA* do not express GFP. (b) Embryo overexpressing HNT show no changes in α-ARM staining through out the embryo during early GBR stage. (c) Embryo overexpressing HNT show no alterations in ARM staining during late GBR stage. When compared to non-GFP expressing stripes, the α-ARM staining does not differ from the GFP expressing stripes. All embryos are oriented with the anterior located at the top left and dorsal side upwards.

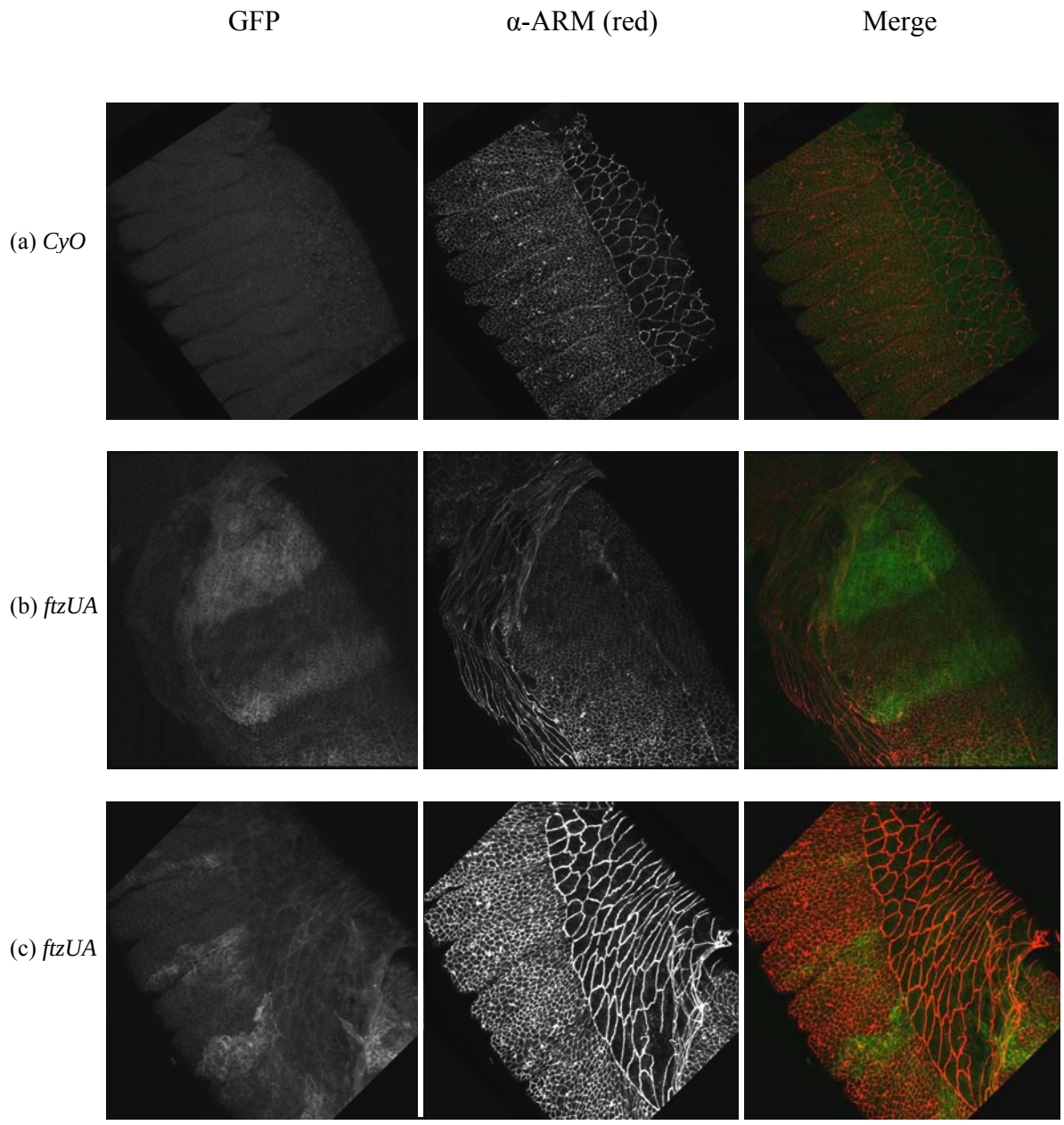
GFP
α-ARM (red)
Merge
(a) *CyO*
(b) *ftzUA*
(c) *ftzUA*

of these crosses carry the ftz^{GAL4} driver since this driver is not homozygous viable. In terms of gross morphology, there was no phenotype observed among these embryos; live imaging analysis showed no detectable alterations in $arm^{GFParm[83]}$ expression in either the epidermis or the AS of eight embryos examined (Figure 3.18).

In summary, a number of approaches were used to address the question of *hnt*'s role in regulating the levels of ARM. These approaches included the analysis of antibody staining in *hnt* loss of function mutants and HNT overexpressing embryos, and embryos carrying the $arm^{GFParm[83]}$ reporter in the HNT overexpressing background. The observations of these experiments support the interpretation that ARM levels are unaffected by alterations in HNT expression in embryos.

3.8 Blocking autophagy in *hindsight* mutants

Recent work from our lab has established that cellular autophagy is a pre-requisite for the activation of caspase-dependent AS cell death during wild type development (Mohseni *et al.*, 2009). Persistent AS phenotypes result when autophagy is inhibited by the expression of activated InR ($UAS\text{-}dInR^{ACT}$) or activated Ras ($UAS\text{-}Ras^{V12}$) using AS-specific GAL4 drivers. It was of interest to examine the AS phenotype associated with these expression backgrounds in the *hnt* mutant to determine if they achieved rescue of AS loss and/or AS cell shape changes. Using the genetic crossing scheme that was used to unambiguously recognize and obtain live images of hnt^{308} mutant embryos expressing *p35*, hnt^{308} mutant embryos having AS specific expression of $UAS\text{-}dInR^{ACT}$ and $UAS\text{-}Ras^{V12}$ were similarly imaged. As described in Materials and Methods (section 2.2), these crosses used males of stocks carrying tub^{GAL80} with the $UAS\text{-}dInR^{ACT}$ or the

Figure 3.18: Confocal images of *arm*$^{GFParm[83]}$ in various backgrounds. Images of embryos at mid-DC stage are shown. The AS tissue is indicated by the yellow arrow. (a) The *arm*$^{GFParm[83]}$ marks the cell membranes in the embryo. Embryos collected from females of stock 1 crossed to stock 33 (See Materials and Methods). (b) *ftz*^{GAL4} driver in *arm*$^{GFParm[83]}$ background has similar levels of GFP throughout the embryo. Embryos collected from females of stock 1 crossed to stock 34 (See Materials and Methods). (c) Embryos overexpressing HNT using *ftz*^{GAL4} driver in *arm*$^{GFParm[83]}$ background do not show any differences in GFP expression throughout the embryo. Embryos were collected from females of stock 31 crossed to stock 34 (See Materials and Methods). Images were captured using the Ziess Axiovert 100 confocal microscope (40X objective) in (a), while the Nikon Eclipse confocal microscope (40X objective) was used for (b) and (c). Similar confocal settings were used to capture all images. The embryos are oriented with the anterior to the left and dorsal side up.

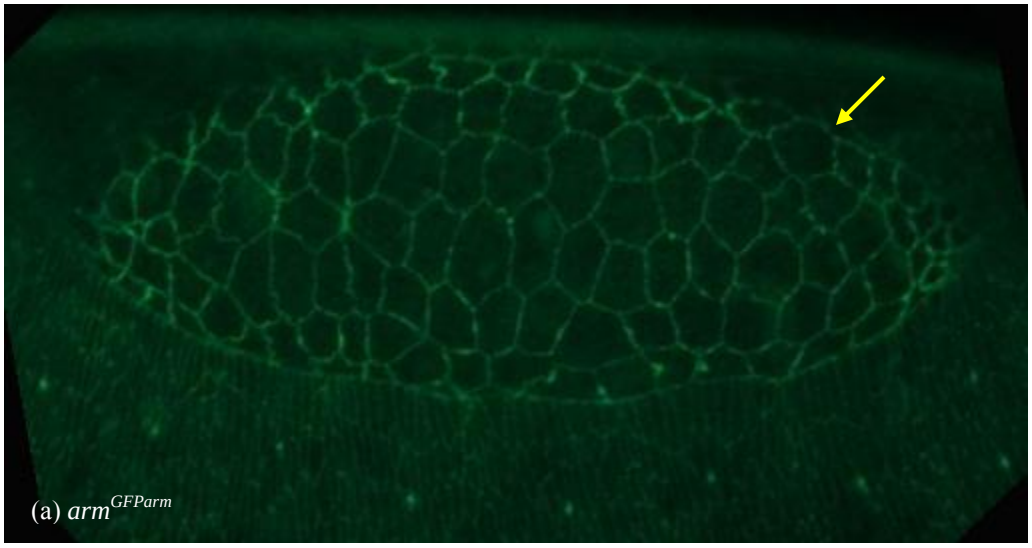
(a) *arm*^{GFParm}

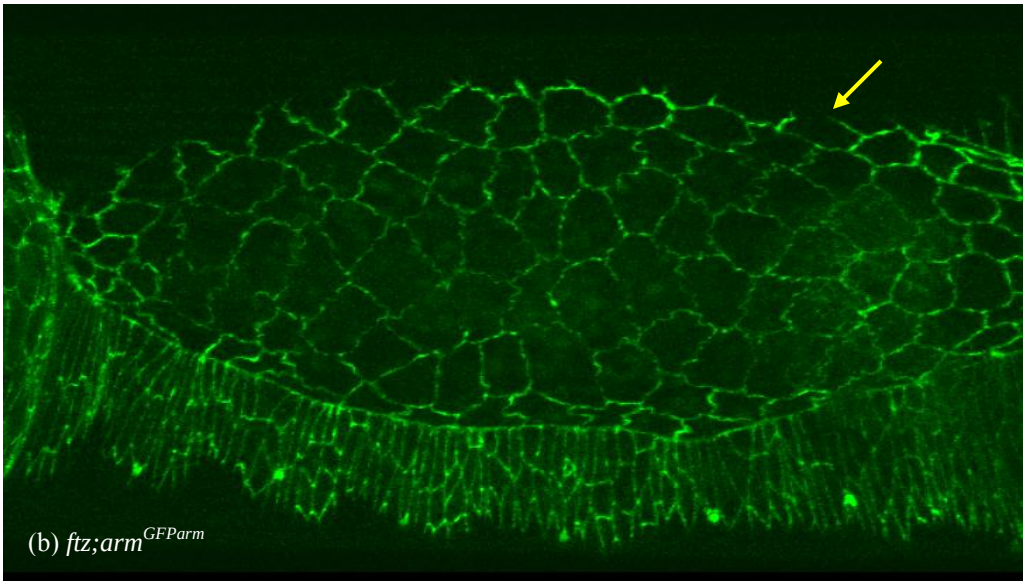
(b) *ftz;arm*^{GFParm}

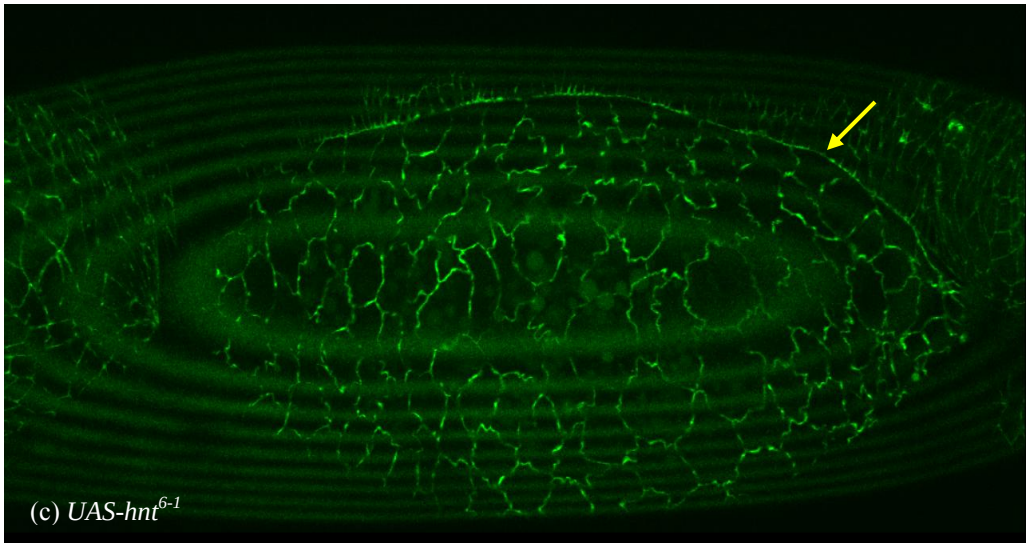
(c) *UAS-hnt*$^{6-1}$

UAS-Ras^{V12} constructs. Five embryos selected at extended germband stages of development, prior to the manifestation of any *hnt* mutant phenotype, were imaged from each background. In the background of AS-specific expression of activated InR, three of the five embryos successfully completed GBR while two failed to complete GBR. In the two embryos which failed to complete GBR, there was some evidence of AS cells in apoptosis as determined by rapid cellular fragmentation. These two embryos also displayed large cytoplasmic black spots interpreted as vacuoles (Figure 3.19a). All three embryos of this background that completed GBR showed cellular morphologies typically associated with wild type, and that are absent in *hnt*^{308} mutants (see Section 3.6 above). Specifically, large cellular projections associated with lamellipodia in the posterior-most AS cells, normally absent in *hnt*^{308} mutants, were observed (Figure 3.19b). These embryos proceeded to show wild type development and normal progression of DC. In contrast to the two embryos that failed to complete GBR, these embryos displayed fewer and less prominent vacuoles. The appearance of the lamellipodia projections in mutant embryos clearly indicates that this aspect of the *hnt* mutant phenotype can be rescued by activation of the InR pathway.

In examining *hnt*^{308} mutant embryos that were expressing activated Ras in the AS, a similar rescue effect was observed. Of the five embryos imaged, two showed gross morphological defects possibly associated with rupture of the yolk sac—and these were difficult to interpret. The remaining three embryos, which did not display gross morphological abnormalities, displayed the prominent lamellipodia normally seen in wild type development, thus indicating rescue of this aspect of the *hnt* mutant phenotype (Figure 3.20a). In this *hnt* rescued background, however, GBR was initiated but did not

Figure 3.19: Visualization of AS in *hnt*^{308} mutants with *UAS-dInR*^{ACT} expression. The AS, indicated by yellow arrow, is visualized using the *kr*^{GAL4} driver with *UAS-GFP*. The germband is labelled with a white asterisk. Images were captured using the Nikon Eclipse confocal and 20X objective. Embryos were at mid-GBR stage, collected from females of stock 20 crossed to stock 27 (See Materials and Methods). (a) Embryos which fail in GBR show presence of vacuoles in the AS cells, and lack extensions from the posterior-most AS cells. (b) Embryos, which successfully complete GBR and have normal DC completion, have prominent lamellipodia, indicated by white arrows, in the posterior-most AS cells, similar to those seen in wild type (Figure 3.14a). Embryos are oriented with the anterior to the left and dorsal side up.

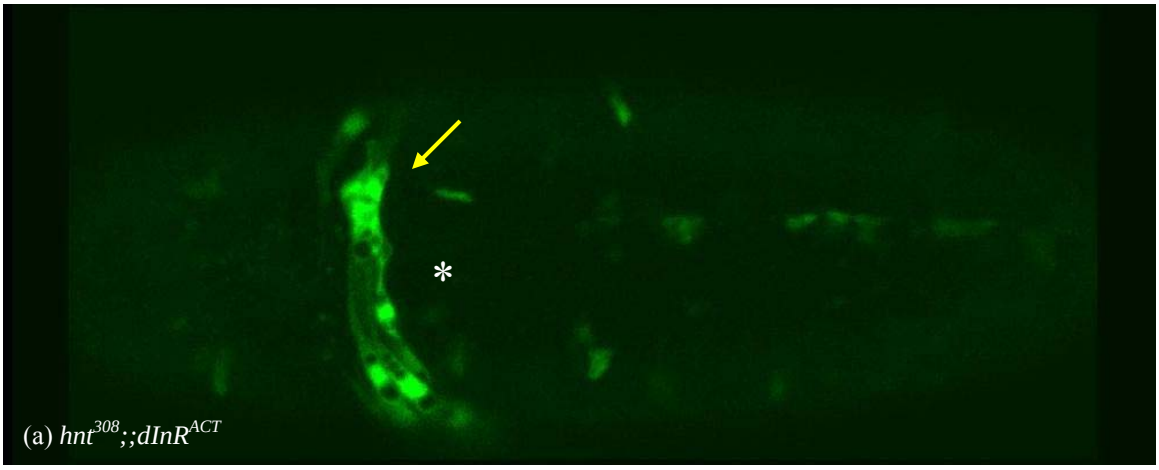
(a) hnt308;;dInRACT

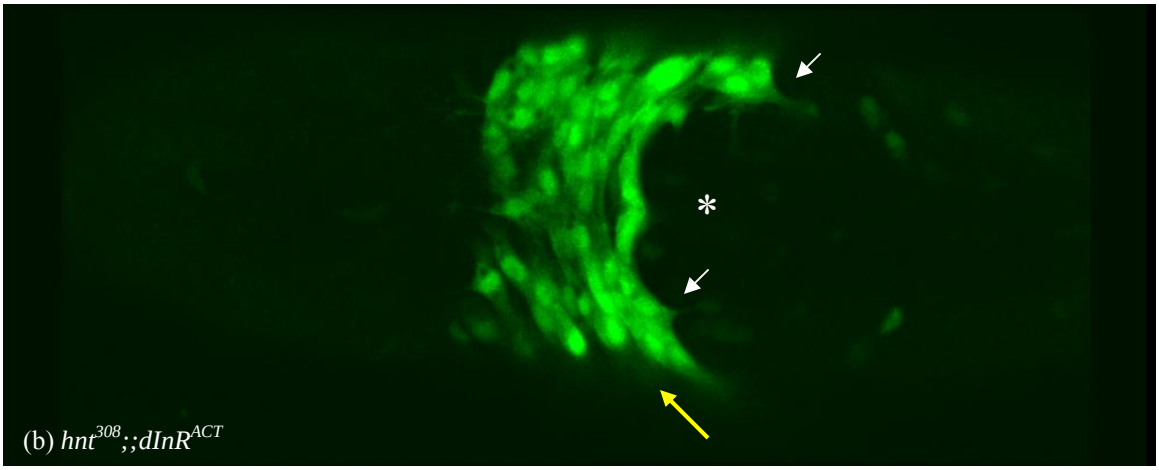
(b) hnt308;;dInRACT

reach completion. The point at which GBR stalled or failed correlated with an apparent loss of contact between the posterior-most AS cells and the tip of the retracting germband; as evidenced by a sudden anterior movement of this group of AS cells (Figure 3.20b).

To summarize, these experiments establish that the behaviour of AS cells in *hnt*^{308} mutant embryos is rescued by either activation of InR signalling pathway or Ras. At this point, however, the mechanism of this rescue is not understood. Further experiments will be necessary to determine if autophagy, *per se*, or if other consequences of activating these pathways are responsible for the observed rescue. While InR and Ras signalling pathways have been implicated in the regulation of autophagy, it is also possible that these pathways may have additional effects on the regulation of cell shape changes and cell adhesion properties that are independent of their roles in regulating autophagy.

Figure 3.20: Visualization of the AS in *hnt*^{308} mutants with *UAS-Ras*^{V12} expression. The AS, indicated by yellow arrow, is visualized using the *kr*^{GAL4} driver with *UAS-GFP*. The germband is labelled with a white asterisk. Images were captured using the Nikon Eclipse confocal and 20X objective. Embryos were collected from females of stock 20 crossed to stock 29 (See Materials and Methods). (a) During mid-GBR, the embryos show prominent lamellipodia, indicated by the white arrows, associated with the posterior-most AS cells extending to contact the tip of the germband. This resembles the extensions seen in wild type embryos (Figure 3.14a). (b) During late GBR, the posterior-most AS cells attempt to contact the retracting germband as the AS moves in an anterior direction. This anterior movement suggests a loss of contact between the AS and the germband. The embryo fails in GBR. Embryos are oriented with the anterior to the left and dorsal side up.

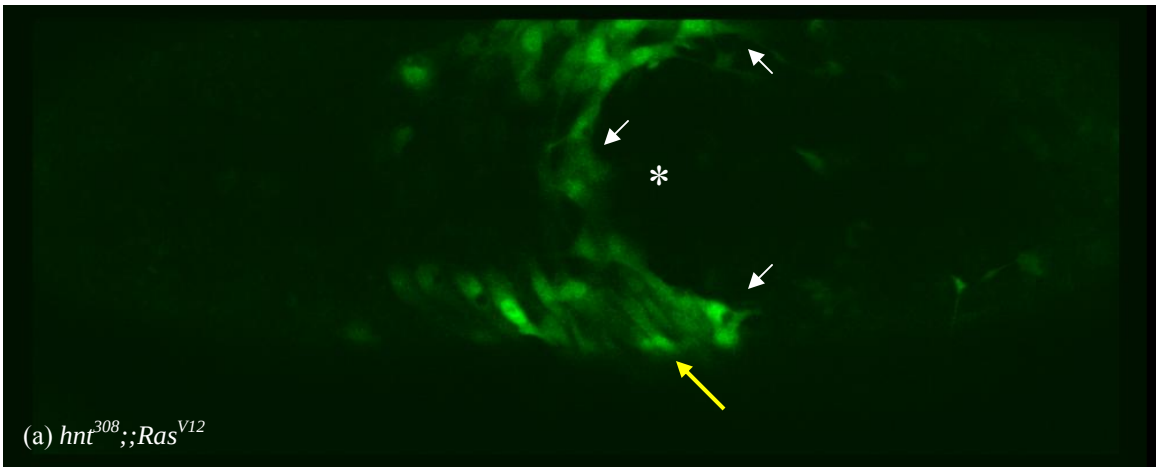
(a) hnt308;;RasV12

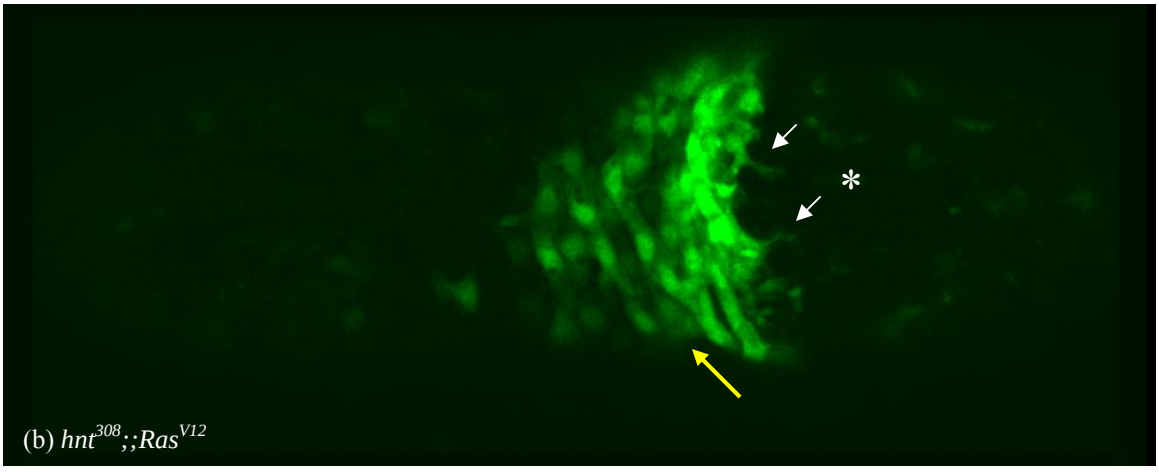
(b) hnt308;;RasV12

Chapter 4 – Discussion

The main objective of this study was to better characterize the AS behaviour in *hnt* mutants. The AS, a squamous epithelial monolayer, plays an important role in GBR and DC morphogenetic processes (Reed *et al.*, 2004). The *hindsight* (*hnt*) gene encodes a nuclear zinc-finger protein that is expressed in the amnioserosa (AS). The *hnt* mutants display germband retraction failure associated with premature AS loss (Frank and Rushlow, 1996). The cause of the premature loss of the AS tissue in *hnt* mutants was unclear prior to this study.

4.1 Amnioserosa death does not cause the *hnt* GBR phenotype

Premature loss of the AS tissue in *hnt* mutants was believed to be a consequence of *reaper*-mediated apoptosis (Frank and Rushlow, 1996). Using RNA *in-situ* hybridization, Frank and Rushlow (1996) demonstrated a concentration of *rpr* positive cells within the AS, suggesting a premature apoptotic death of the tissue. Another study on *hnt* mutants showed that GBR failure was not rescued by the genetic removal of apoptotic cell death using the homozygous deficiency *H99* background (Lamka and Lipshitz, 1999). Using an *hnt* null allele (hnt^{XE81}), Lamka and Lipshitz (1999) showed that *hnt* function in the AS is required for proper GBR completion. In these experiments, TUNEL staining was used to confirm the absence of apoptosis in this background which still showed a GBR failure (Lamka and Lipshitz, 1999). The authors looked at the gross morphology of the AS tissue rather than AS cell behaviour in *hnt* mutants.

In this study, the morphology of the AS tissue, as well as AS cell shapes and

behaviours were further analyzed in *hnt* mutants using high resolution confocal microscopy in combination with live imaging techniques. Using a hypomorphic allele (*hnt*^{308}) that is associated decreased HNT expression, particularly in the AS, the AS behaviour was analyzed in several backgrounds. These included the direct inhibition of apoptosis using the homozygous deficiency *H99*, as well as the expression of the caspase inhibitor p35. In addition, *hnt* phenotypes were examined in backgrounds that lack AS PCD through the inhibition of autophagy.

Consistent with previously published data, the results presented in this thesis confirm that GBR failure in *hnt* mutants is not rescued by *H99*. Moreover, it was shown that *p35* expression resulted in an identical outcome. The high resolution microscopy used in this study establishes that the "rescued" AS tissue, although persistent, is associated with abnormal morphology and behaviour during development. The spatial positioning and the overall morphology of the persistent AS tissue in *hnt* mutants (in apoptotic deficient backgrounds) differed greatly when compared to apoptotic deficient backgrounds alone. In *hnt*^{308} + *p35* expressing embryos, the persistent AS was found to collapse between the head and the tail, while in *p35* expressing embryos, the AS formed a "tube-like" structure under the dorsal epidermis.

4.2 The inhibition of autophagy shows partial rescue of GBR and complete rescue of AS cell morphology in *hnt* mutants

During GBR, the posterior most AS cells contact and migrate over the germband via lamellipodia extensions (Schöck and Perrimon, 2002). In live imaging experiments using GFP-tagged proteins, *hnt* mutants were observed to lack these lamellipodia

extensions to the epithelia of the germband during GBR and, as a consequence, the AS lost contact with the germband and collapsed. A similar phenotype of no lamellipodia extensions was also observed in *hnt* mutants with ectopic *p35* expression. The loss of extensions in *hnt* mutants phenocopies maternal/zygotic mutants of the *Drosophila* homolog of βPS integrin, *myospheroid* (*mys*) (Schöck and Perrimon, 2003). Embryos mutant for maternal/zygotic *mys* also display a GBR failure phenotype with early AS loss (Schöck and Perrimon, 2003). The resemblance in phenotypes between *hnt* mutants and *mys* mutants suggest that the premature AS death in *hnt* mutants is due to cell-matrix or cell-cell adhesion loss, which would best be described as anoikis.

Strikingly, the inhibition of PCD in the *hnt* mutants using expression backgrounds associated with the inhibition of autophagy ($dInR^{ACT}$ and Ras^{V12} expression) gave partial rescue of GBR defects. Moreover, the absence of AS lamellipodia in *hnt* mutants, which is a novel observation of these studies, was completely rescued in these expression backgrounds. Previous studies have implicated the expression of the insulin receptor in rescue of the GBR defect of *hnt* mutants (Lamka and Lipshitz, 1999). This study used a wild type insulin receptor under the control of a heat-shock promoter, and reported a partial rescue of GBR without any rescue of premature AS death. This lead to the interpretation that the AS produces a diffusible signal that is transduced by the insulin receptor in the lateral epidermis, and that subsequent cell shape changes in the lateral epidermis drive GBR (Lamka and Lipshitz, 1999). One obvious difference in this study and that of Lamka and Lipshitz (1999) is the use of an activated form of InR which was expressed specifically in the AS. Another difference between this study and that of Lamka and Lipshitz (1999) is the use of different hypomorphic alleles; it is possible that

combined differences between the use of wild type and activated insulin receptor in these different allelic backgrounds could be responsible for the contradictory observations concerning the rescue of premature AS loss in *hnt* mutants.

4.3 Amnioserosa cell extrusion

During DC, approximately 10% of AS cells are basally extruded (Mohseni *et al.*, 2009). Extruding AS cells display activation of apoptosis prior to extrusion, and it has been suggested that the removal of AS cells from the epithelium contributes to the ability of the AS to generate the mechanical force required for DC (Toyama *et al.*, 2008). In experiments performed using the *UAS-hnt*^{RNAi} construct, the observed increase in the average number of extrusions during early DC likely reflects an increase in the number of cells entering apoptosis. The analysis of *hnt* mutants, however, suggests that *hnt* does not function directly to suppress apoptosis. The increased rate of extrusion in the *hnt* knockdown embryos is, therefore, likely to reflect loss of appropriate cell-cell contacts and could be a useful paradigm for anoikis. Future experiments to examine extrusion rates in embryos that co-express *p35* and *UAS-hnt*^{RNAi} will possibly be able to confirm the relevance of AS extrusion to study of anoikis.

AS extrusion events in *hnt*^{RNAi} expressing embryos were restricted to the anterior half of the AS. One possible explanation for this observation may relate to different levels of HNT that result from the use of the *ftz*^{GAL4} driver, the expression of which is not uniform across the tissue. Possible interactions between cells expressing HNT and cells lacking HNT (through *hnt*^{RNAi}) may be the underlying cause of the spatial restriction of extrusion events. A precedent for subdivisions within the AS in terms of cell shape and

behaviour is found in embryos that overexpress a protein of the adherins junction complex, crumbs (Harden *et al.*, 2002). In such embryos, there is a clear boundary demarking anterior cells that undergo premature constriction and posterior AS cells that remain unconstricted. Curiously, this anterior region corresponds well to the region that shows elevated extrusion rates in *UAS-hnt*^{RNAi} expressing embryos.

The cell-matrix detachment of MDCK cells is a model system for studying anoikis. MDCK cells that lose integrin-mediated contacts with the matrix undergo anoikis, and are associated with an increase in JNK signalling activity (Cardone *et al.*, 1997). Since, *hnt* mutants are associated with elevated JNK signalling in the AS at the onset of GBR (Reed, Wilk and Lipshitz, 2001), it is interesting to speculate that premature AS loss is fundamentally similar to anoikis described in mammalian systems.

4.4 Armadillo expression in hindsight mutants

In *Drosophila* ovarian follicular cells mutant for *hnt*, an increase in ARM levels was observed, while follicle cells overexpressing HNT displayed a 2-fold decrease in ARM levels (Melani *et al.*, 2008). The HNT overexpressing follicle cells were also observed to lack motility. Using genetic modifications to decrease or increase HNT levels in *Drosophila* embryos, no significant changes were observed in ARM expression levels.

Based on the observations of ovarian follicular cells that are mutant for *hnt*, one might expect the same to be true of the AS. An increase in ARM, however, seems contrary to what one would expect in the anoikis-like death observed in the AS of *hnt* mutants. A difference in constructs used in the two systems could account for the lack of

alterations in ARM levels in *Drosophila* embryos in this study. The alterations in ARM levels observed in follicle cells of *Drosophila* ovaries with overexpression of HNT was performed using an enhancer trap line hnt^{EP55} (Melani *et al.*, 2008). The construct used for overexpression of HNT in *Drosophila* embryos was *UAS-*hnt^{6-1}. In addition, any comparison of the AS with the ovarian follicular epithelium may not be pertinent to the effects of HNT on the levels of ARM. In particular, the loss of HNT in the AS results in premature cell death where as the mutant patches of follicle cells remain viable. Clearly, these two tissues respond very differently to alterations in *hnt*.

4.5 Conclusion

The experiments described in this study illustrate that the germband retraction defect of *hnt* mutants is independent of the premature AS death. *hnt* mutants were found to lack lamellipodia extensions emanating from AS cells and contacting the germband during the process of retraction. Activation of either InR or Ras in the AS of *hnt* mutants rescued this defect. Overall, the death of AS cells in *hnt* mutants and HNT knockdown backgrounds may represent a new paradigm for anoikis.

Appendix I

Genetic manipulations of the *hnt* mutant was used to study the AS cell shape and behaviour in various backgrounds. Some of the backgrounds used for manipulations of the *hnt* mutant required extensive genetic crosses to build stable stocks. The crossing schemes used to build multiple insertion stocks used in this study are illustrated in this Appendix. The parental stocks used to build the multiple insertion stocks are listed in the figure heads. Newly eclosed adult females (virgin females) were used for all crosses.

Figure A.1: Crossing scheme used to build stock 4. The parental stocks include stock 2 and stock 3 (See Materials and Methods). The resulting stock 4 requires maintenance through selection of females carrying the *hnt*^{308} by selecting adult rough eye phenotype associated with this allele.

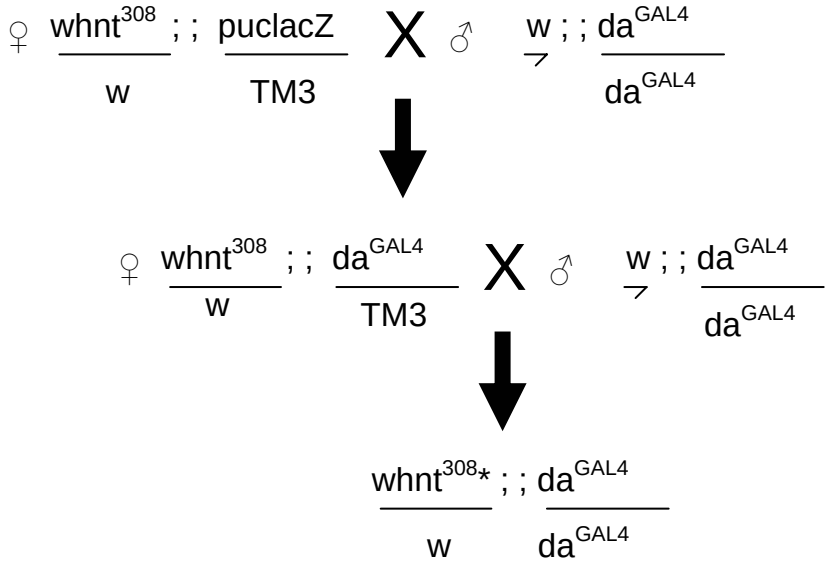

* requires selection

Figure A.2: Crossing scheme used to build stock 7. The parental stocks include stock 5 and stock 6 (See Materials and Methods).

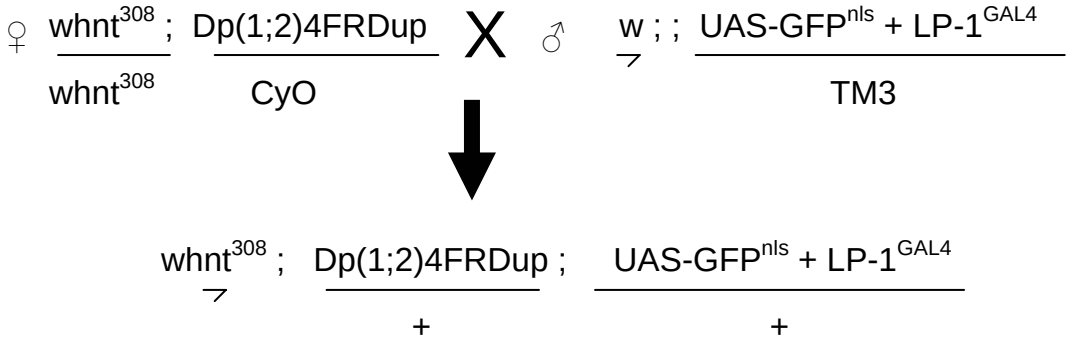
♀ whnt308 ; Dp(1;2)4FRDup X ♂ w ; ; UAS-GFPnls + LP-1GAL4
whnt308 CyO TM3
whnt308 ; Dp(1;2)4FRDup ; UAS-GFPnls + LP-1GAL4
+ +

Figure A.3: Crossing scheme used to build stock 11. The parental stocks used in this crossing scheme include stock 9 and stock 10 (See Materials and Methods).

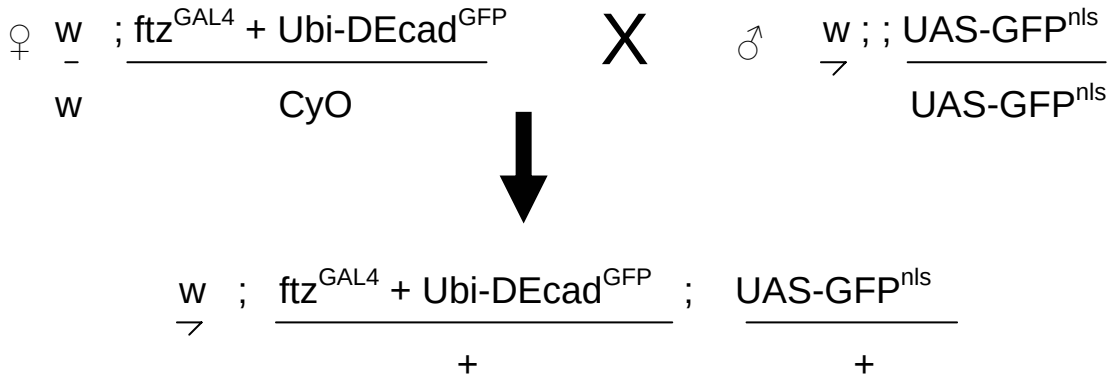
♀ w / w ; ftz^GAL4 + Ubi-DEcad^GFP / CyO
X
♂ w / ; ; UAS-GFP^nls / UAS-GFP^nls
w / ; ftz^GAL4 + Ubi-DEcad^GFP / + ; UAS-GFP^nls / +

Figure A.4: Crossing scheme used to build stock 16. The parental stocks used included stock 2 and stock 15 (See Materials and Methods). The maintenance of stock 16 as stable stock requires the selection of females with hnt^{308} using the adult rough eye phenotype associated with this allele.

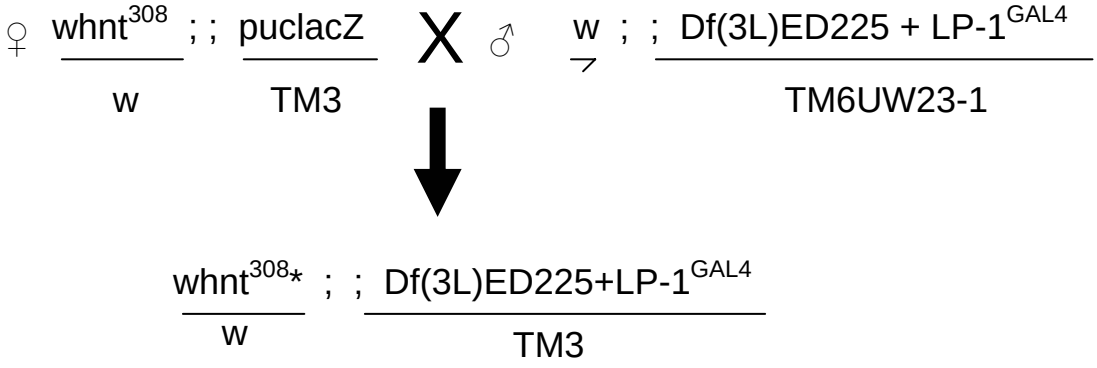

* requires selection

Figure A.5: Crossing scheme used to build stock 20. The parental stocks used in this crossing scheme include stocks 19 and stock 5 (See Materials and Methods).

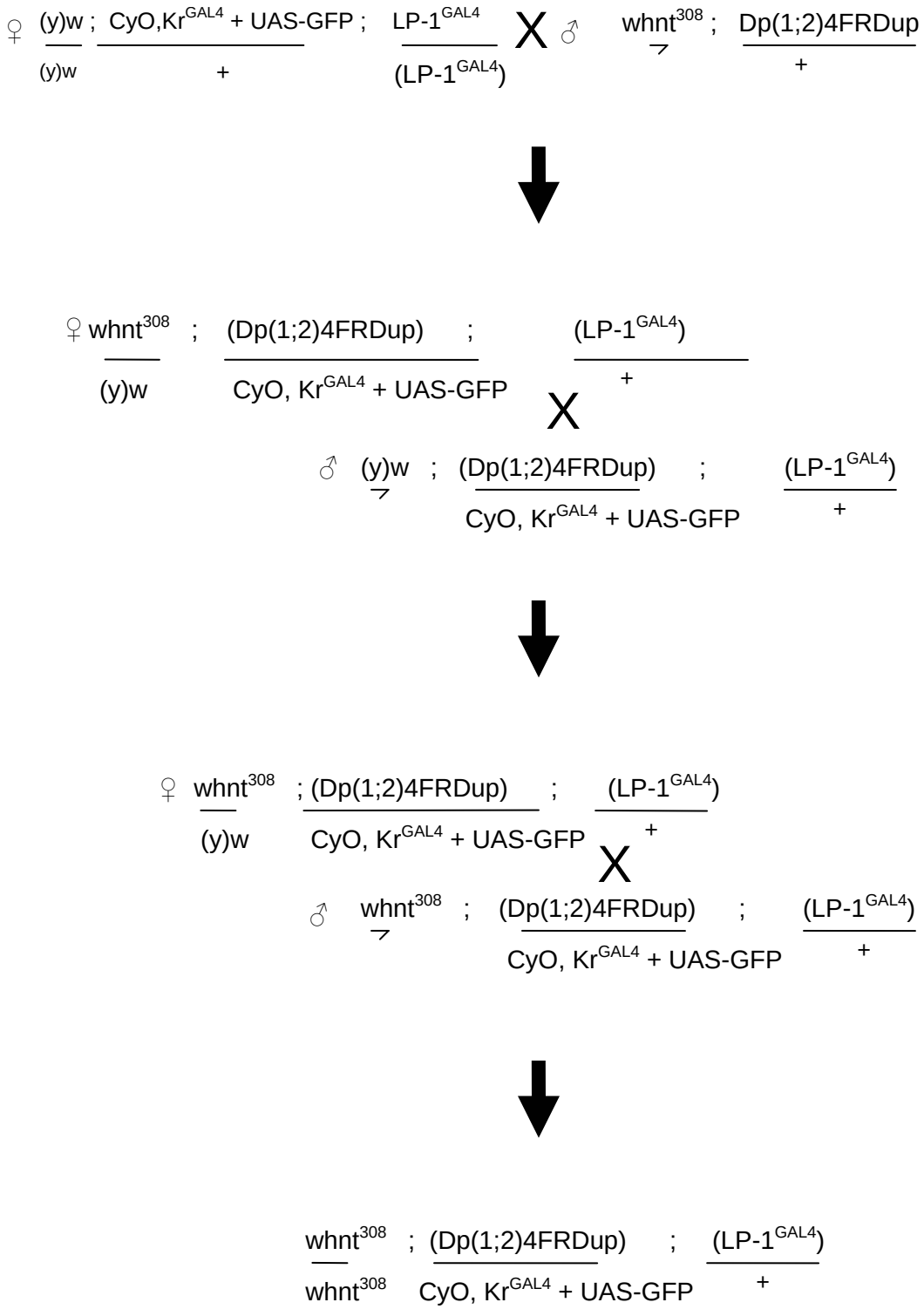
♀ (y)w / (y)w ; CyO,Kr^GAL4 + UAS-GFP / + ; LP-1^GAL4 / (LP-1^GAL4) X ♂ whnt^308 / ; Dp(1;2)4FRDup / +
♀ whnt^308 / (y)w ; (Dp(1;2)4FRDup) / CyO, Kr^GAL4 + UAS-GFP ; (LP-1^GAL4) / + X ♂ (y)w / ; (Dp(1;2)4FRDup) / CyO, Kr^GAL4 + UAS-GFP ; (LP-1^GAL4) / +
♀ whnt^308 / (y)w ; (Dp(1;2)4FRDup) / CyO, Kr^GAL4 + UAS-GFP ; (LP-1^GAL4) / + X ♂ whnt^308 / ; (Dp(1;2)4FRDup) / CyO, Kr^GAL4 + UAS-GFP ; (LP-1^GAL4) / +
whnt^308 / whnt^308 ; (Dp(1;2)4FRDup) / CyO, Kr^GAL4 + UAS-GFP ; (LP-1^GAL4) / +

Figure A.6: Crossing scheme used to build stock 22. The parental stocks used included stock 21 and stock 18 (See Materials and Methods).

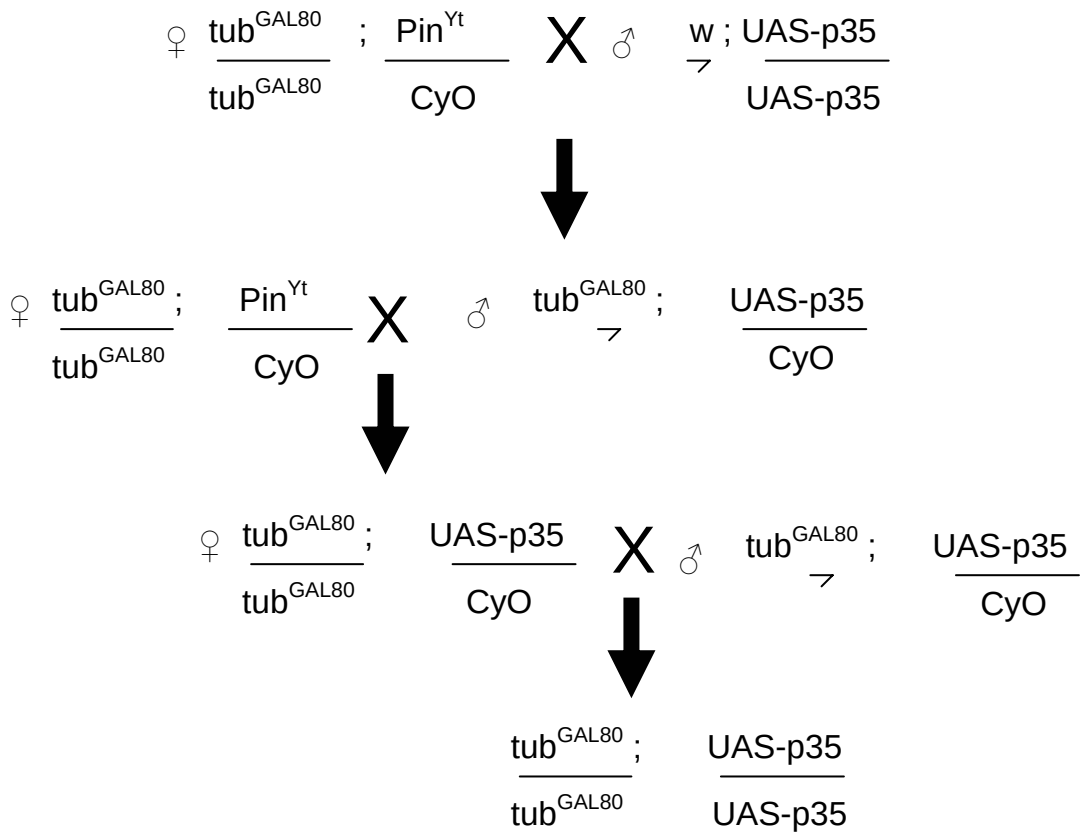
♀ tub^GAL80 / tub^GAL80 ; Pin^Yt / CyO X ♂ w ; UAS-p35 / UAS-p35
♀ tub^GAL80 / tub^GAL80 ; Pin^Yt / CyO X ♂ tub^GAL80 ; UAS-p35 / CyO
♀ tub^GAL80 / tub^GAL80 ; UAS-p35 / CyO X ♂ tub^GAL80 ; UAS-p35 / CyO
tub^GAL80 / tub^GAL80 ; UAS-p35 / UAS-p35

Figure A.7: Crossing scheme used to build stock 26. The parental stocks used in this crossing scheme include stock 24 and stock 25 (See Materials and Methods).

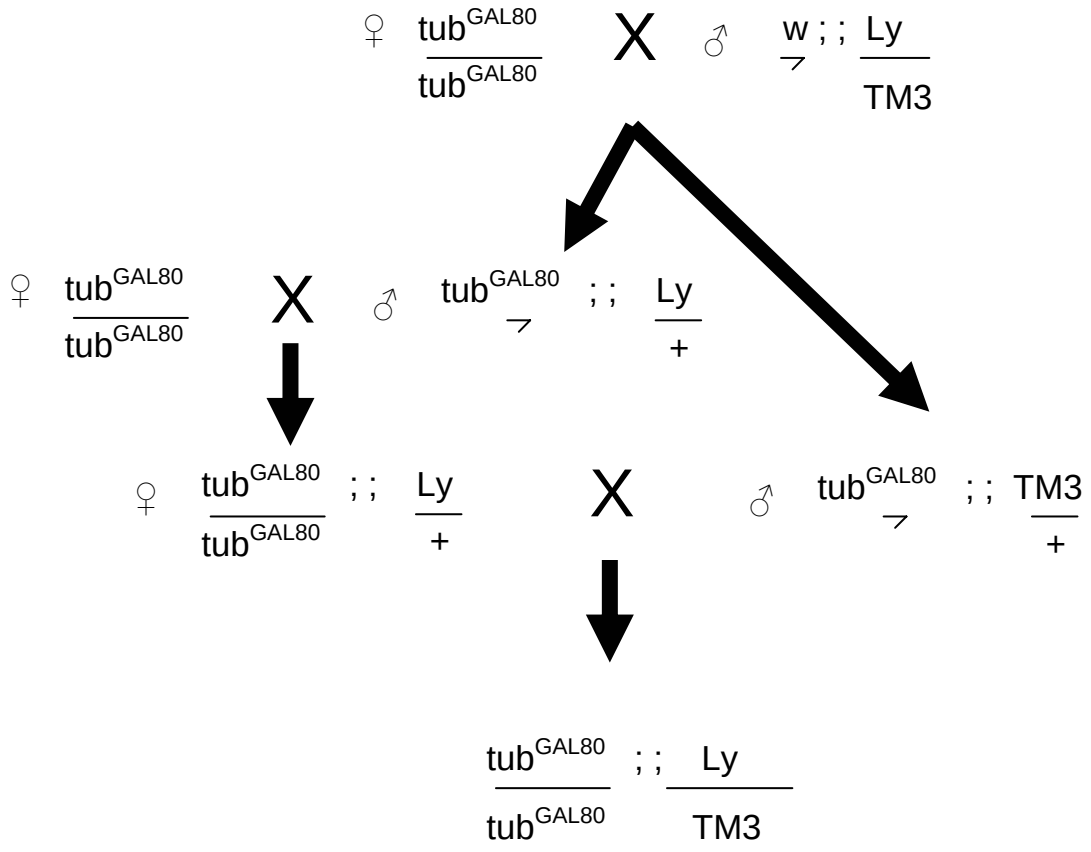
♀ tub^GAL80 / tub^GAL80 X ♂ w ; ; Ly / TM3
♀ tub^GAL80 / tub^GAL80 X ♂ tub^GAL80 / ; ; Ly / +
♀ tub^GAL80 / tub^GAL80 ; ; Ly / + X ♂ tub^GAL80 / ; ; TM3 / +
tub^GAL80 / tub^GAL80 ; ; Ly / TM3

Figure A.8: Crossing scheme used to build stock 27. The parental stocks used in this crossing scheme include stock 23 and stock 26 (See Materials and Methods).

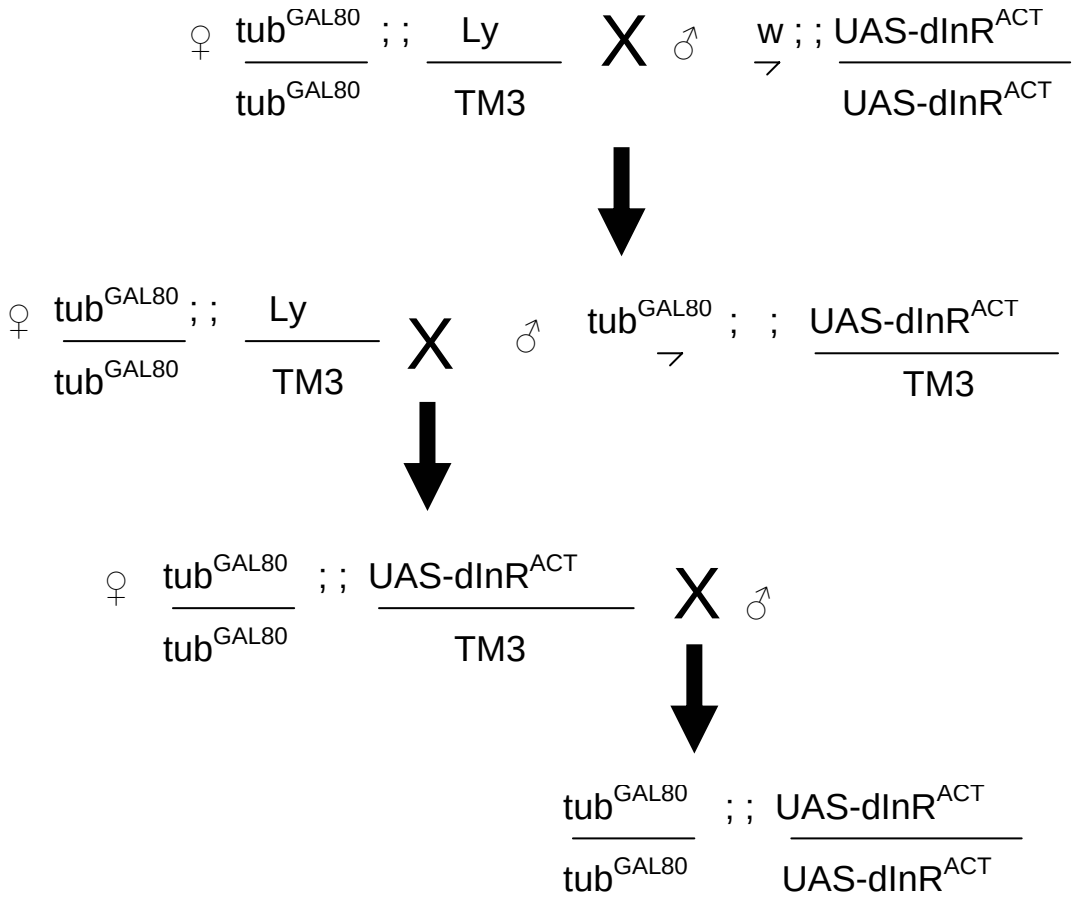
♀ tub^GAL80 / tub^GAL80 ; ; Ly / TM3 X ♂ w ; ; UAS-dInR^ACT / UAS-dInR^ACT
♀ tub^GAL80 / tub^GAL80 ; ; Ly / TM3 X ♂ tub^GAL80 ; ; UAS-dInR^ACT / TM3
♀ tub^GAL80 / tub^GAL80 ; ; UAS-dInR^ACT / TM3 X ♂
tub^GAL80 / tub^GAL80 ; ; UAS-dInR^ACT / UAS-dInR^ACT

Figure A.9: Crossing scheme used to build stock 29. The parental stocks used in this crossing scheme include stock 26 and stock 28 (See Materials and Methods).

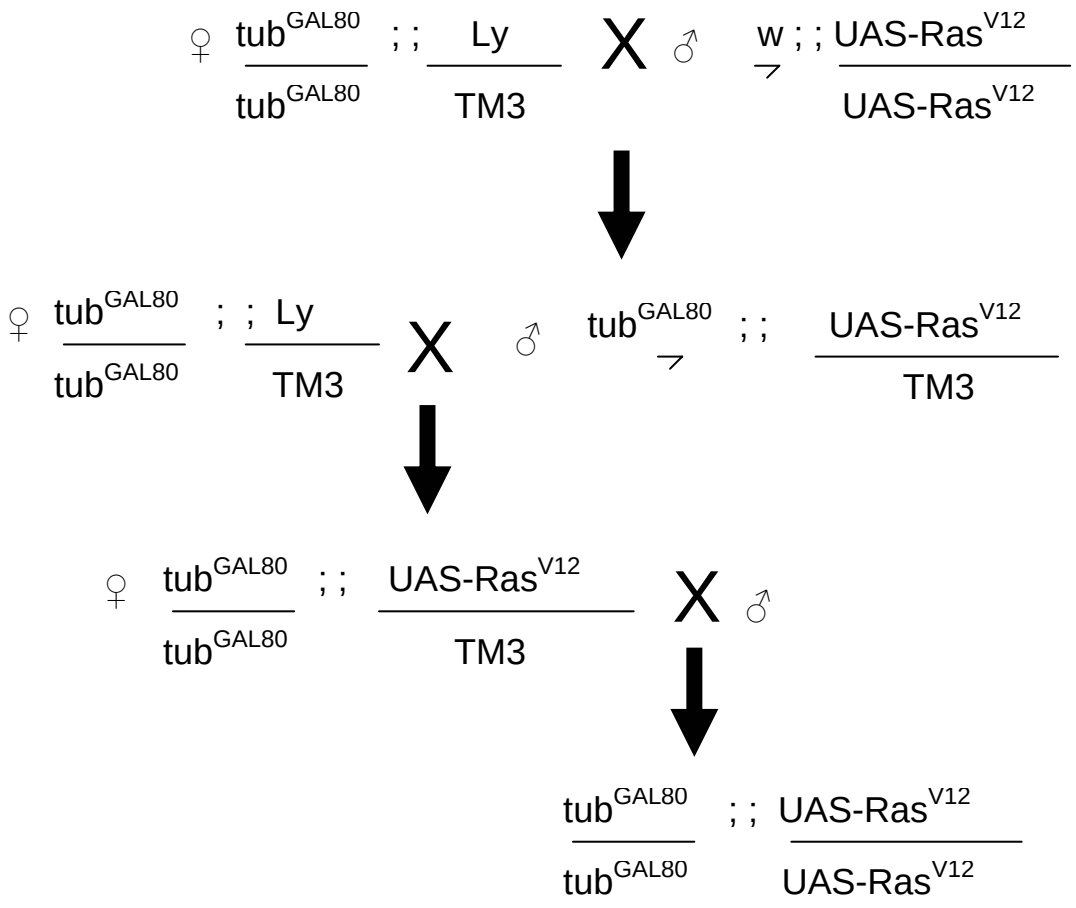
♀ tub^GAL80 / tub^GAL80 ; ; Ly / TM3 X ♂ w ; ; UAS-Ras^V12 / UAS-Ras^V12
♀ tub^GAL80 / tub^GAL80 ; ; Ly / TM3 X ♂ tub^GAL80 ; ; UAS-Ras^V12 / TM3
♀ tub^GAL80 / tub^GAL80 ; ; UAS-Ras^V12 / TM3 X ♂
tub^GAL80 / tub^GAL80 ; ; UAS-Ras^V12 / UAS-Ras^V12

References

Alberts,B ., Johnson, A., Lewis, J., Raff, M., Roberts, K., Walter, P. (2008). Molecular Biology of the Cell. Fifth Ed. Garland Science. NY. USA. 1115-1128.

Ashburner, M. (1989). *Drosophila*: A Laboratory Handbook. Cold Spring Laboratory Press. Cold Spring Harbor, NY. USA. 157-171.

Baehrecke, E. H. (2002). How Death Shapes Life during Development. *Nat. Rev. Mol. Cell Biol.* **3,** 779-787.

Baehrecke, E. H. (2005). Autophagy: Dual Roles in Life and Death? *Nat. Rev. Mol. Cell Biol.* **6,** 505-510.

Bangs, P., Franc, N. and White, K. (2000). Molecular Mechanisms of Cell Death and Phagocytosis in Drosophila. *Cell Death Differ.* **7,** 1027-1034.

Berry, D. L. and Baehrecke, E. H. (2007). Growth Arrest and Autophagy are Required for Salivary Gland Cell Degradation in Drosophila. *Cell* **131,** 1137-1148.

Brand, A. H. and Perrimon, N. (1993). Targeted Gene Expression as a Means of Altering Cell Fates and Generating Dominant Phenotypes. *Development* **118,** 401-415.

Britton, J. S., Lockwood, W. K., Li, L., Cohen, S. M. and Edgar, B. A. (2002). Drosophila's insulin/PI3-Kinase Pathway Coordinates Cellular Metabolism with Nutritional Conditions. *Dev. Cell.* **2,** 239-249.

Cardone, M. H., Salvesen, G.S., Widmann, C., Johnson, G., and Frisch, S.M. (1997). The Regulation of Anoikis: MEKK-1 Activation Requires Cleavage by Caspases. *Cell*. **90,** 315-323.

Cashio, P., Lee, T. V. and Bergmann, A. (2005). Genetic Control of Programmed Cell Death in Drosophila Melanogaster. *Semin. Cell Dev. Biol.* **16,** 225-235.

Casso, D., Ramirez-Weber, F. and Kornberg, T. B. (2000). GFP-Tagged Balancer Chromosomes for Drosophila Melanogaster. *Mech. Dev.* **91,** 451-454.

Codogno, P. and Meijer, A. J. (2005). Autophagy and Signaling: Their Role in Cell Survival and Cell Death. *Cell Death Differ.* **12 Suppl 2,** 1509-1518.

da Silva, S. M. and Vincent, J. P. (2007). Oriented Cell Divisions in the Extending Germband of Drosophila. *Development* **134,** 3049-3054.

Davies, J.A., (2005). Mechanisms of Morphogenesis: The Creation of Biological Form. Elsevier Academic Press, MA. USA. 329-345.

Debnath, J., Baehrecke, E. H. and Kroemer, G. (2005). Does Autophagy Contribute to Cell Death? *Autophagy* **1,** 66-74.

Foe, V. E. (1989). Mitotic Domains Reveal Early Commitment of Cells in Drosophila Embryos. *Development* **107,** 1-22.

Franc, N. C., Dimarcq, J. L., Lagueux, M., Hoffmann, J. and Ezekowitz, R. A. (1996). Croquemort, a Novel Drosophila hemocyte/macrophage Receptor that Recognizes Apoptotic Cells. *Immunity* **4,** 431-443.

Frank, L. H. and Rushlow, C. (1996). A Group of Genes Required for Maintenance of the Amnioserosa Tissue in Drosophila. *Development* **122,** 1343-1352.

Frisch, S. M. and Screaton, R. A. (2001). Anoikis Mechanisms. *Curr. Opin. Cell Biol.* **13,** 555-562.

Gilbert, S.F. (2003). Developmental Biology Seventh Edition. Sinauer Associates Inc., MA.USA. 263-304.

Gorfinkiel, N. and Arias, A. M. (2007). Requirements for Adherens Junction Components in the Interaction between Epithelial Tissues during Dorsal Closure in Drosophila. *J. Cell. Sci.* **120,** 3289-3298.

Harden, N., Ricos, M., Yee, K., Sanny, J., Langmann, C., Yu, H., Chia, W. and Lim, L. (2002). Drac1 and Crumbs Participate in Amnioserosa Morphogenesis during Dorsal Closure in Drosophila. *J. Cell. Sci.* **115,** 2119-2129.

Hay, B. A. and Guo, M. (2006). Caspase-Dependent Cell Death in Drosophila. *Annu. Rev. Cell Dev. Biol.* **22,** 623-650.

Irvine, K. D. and Wieschaus, E. (1994). Cell Intercalation during Drosophila Germband Extension and its Regulation by Pair-Rule Segmentation Genes. *Development* **120,** 827-841.

Jacinto, A. and Martin, P. (2001). Morphogenesis: Unravelling the Cell Biology of Hole Closure. *Curr. Biol.* **11,** R705-7.

Kiehart, D. P., Galbraith, C. G., Edwards, K. A., Rickoll, W. L. and Montague, R. A. (2000). Multiple Forces Contribute to Cell Sheet Morphogenesis for Dorsal Closure in Drosophila. *J. Cell Biol.* **149,** 471-490.

Klionsky, D. J. (2007). Autophagy: From Phenomenology to Molecular Understanding in Less than a Decade. *Nat. Rev. Mol. Cell Biol.* **8,** 931-937.

Kornbluth, S. and White, K. (2005). Apoptosis in Drosophila: Neither Fish nor Fowl (nor Man, nor Worm). *J. Cell. Sci.* **118,** 1779-1787.

Krause, H.M. (Accessed 2008 November 23). http://www.utoronto.ca/krause/FISH.html FISH Protocols for *Drosophila*.

Krieser, R. J., Moore, F. E., Dresnek, D., Pellock, B. J., Patel, R., Huang, A., Brachmann, C. and White, K. (2007). The Drosophila Homolog of the Putative Phosphatidylserine Receptor Functions to Inhibit Apoptosis. *Development* **134,** 2407-2414.

Lamka, M. L. and Lipshitz, H. D. (1999). Role of the Amnioserosa in Germ Band Retraction of the Drosophila Melanogaster Embryo. *Dev. Biol.* **214,** 102-112.

Levine, B. and Yuan, J. (2005). Autophagy in Cell Death: An Innocent Convict? *J. Clin. Invest.* **115,** 2679-2688.

Lodish, H., Berk, A., Matsudaira, P., Kaiser, C.A., Krieger, M., Scott, M.P., Zipursky, S.L., Darnell, J. (2004). Molecular Cell Biology. Fifth Ed. W. H. Freeman and Company. NY. USA. 588.

Martin, D. N. and Baehrecke, E. H. (2004). Caspases Function in Autophagic Programmed Cell Death in Drosophila. *Development* **131,** 275-284.

Melani, M., Simpson, K. J., Brugge, J. S. and Montell, D. (2008). Regulation of Cell Adhesion and Collective Cell Migration by Hindsight and its Human Homolog RREB1. *Curr. Biol.* **18,** 532-537.

Mohseni, N., McMillan, S. C., Chaudhary, R., Mok, J. and Reed, B. H. (2009). Autophagy Promotes Caspase-Dependent Cell Death during Drosophila Development. *Autophagy* **5,**.

Muller, H. A. and Wieschaus, E. (1996). Armadillo, Bazooka, and Stardust are Critical for Early Stages in Formation of the Zonula Adherens and Maintenance of the Polarized

Blastoderm Epithelium in Drosophila. *J. Cell Biol.* **134,** 149-163.

Pazdera, T. M., Janardhan, P. and Minden, J. S. (1998). Patterned Epidermal Cell Death in Wild-Type and Segment Polarity Mutant Drosophila Embryos. *Development* **125,** 3427-3436.

Perler, F. B. (2004). The Ins and Outs of Gene Expression Control. *Nat. Biotechnol.* **22,** 824-826.

Pick, L. (1998). Segmentation: Painting Stripes from Flies to Vertebrates. *Dev. Genet.* **23,** 1-10.

Pickup, A. T., Lamka, M. L., Sun, Q., Yip, M. L. and Lipshitz, H. D. (2002). Control of Photoreceptor Cell Morphology, Planar Polarity and Epithelial Integrity during Drosophila Eye Development. *Development* **129,** 2247-2258.

Pope, K. L. and Harris, T. J. (2008). Control of Cell Flattening and Junctional Remodeling during Squamous Epithelial Morphogenesis in Drosophila. *Development* **135,** 2227-2238.

Reed, B. H., Wilk, R. and Lipshitz, H. D. (2001). Downregulation of Jun Kinase Signaling in the Amnioserosa is Essential for Dorsal Closure of the Drosophila Embryo. *Curr. Biol.* **11,** 1098-1108.

Reed, B. H., Wilk, R., Schock, F. and Lipshitz, H. D. (2004). Integrin-Dependent Apposition of Drosophila Extraembryonic Membranes Promotes Morphogenesis and Prevents Anoikis. *Curr. Biol.* **14,** 372-380.

Rusconi, J. C., Hays, R. and Cagan, R. L. (2000). Programmed Cell Death and Patterning in Drosophila. *Cell Death Differ.* **7,** 1063-1070.

Schock, F. and Perrimon, N. (2002). Cellular Processes Associated with Germ Band Retraction

in Drosophila. *Dev. Biol.* **248,** 29-39.

Schock, F. and Perrimon, N. (2003). Retraction of the Drosophila Germ Band Requires Cell-Matrix Interaction. *Genes Dev.* **17,** 597-602.

Scott, R. C., Juhasz, G. and Neufeld, T. P. (2007). Direct Induction of Autophagy by Atg1 Inhibits Cell Growth and Induces Apoptotic Cell Death. *Curr. Biol.* **17,** 1-11.

Shiozaki, E. N. and Shi, Y. (2004). Caspases, IAPs and Smac/DIABLO: Mechanisms from Structural Biology. *Trends Biochem. Sci.* **29,** 486-494.

Stephan, J. S. and Herman, P. K. (2006). The Regulation of Autophagy in Eukaryotic Cells: Do all Roads Pass through Atg1? *Autophagy* **2,** 146-148.

Stronach, B. E. and Perrimon, N. (2001). Investigation of Leading Edge Formation at the Interface of Amnioserosa and Dorsal Ectoderm in the Drosophila Embryo. *Development* **128,** 2905-2913.

Toyama, Y., Peralta, X. G., Wells, A. R., Kiehart, D. P. and Edwards, G. S. (2008). Apoptotic Force and Tissue Dynamics during Drosophila Embryogenesis. *Science* **321,** 1683-1686.

Tschopp, J., Thome, M., Hofmann, K. and Meinl, E. (1998). The Fight of Viruses Against Apoptosis. *Curr. Opin. Genet. Dev.* **8,** 82-87.

Tsujimoto, Y. and Shimizu, S. (2005). Another Way to Die: Autophagic Programmed Cell Death. *Cell Death Differ.* **12 Suppl 2,** 1528-1534.

Turner, F. R. and Mahowald, A. P. (1979). Scanning Electron Microscopy of Drosophila Melanogaster Embryogenesis. III. Formation of the Head and Caudal Segments. *Dev.*

Biol. **68,** 96-109.

VanHook, A. and Letsou, A. (2008). Head Involution in Drosophila: Genetic and Morphogenetic Connections to Dorsal Closure. *Dev. Dyn.* **237,** 28-38.

Wilk, R., Reed, B. H., Tepass, U. and Lipshitz, H. D. (2000). The Hindsight Gene is Required for Epithelial Maintenance and Differentiation of the Tracheal System in Drosophila. *Dev. Biol.* **219,** 183-196.

Yin, V. P. and Thummel, C. S. (2004). A Balance between the diap1 Death Inhibitor and Reaper and Hid Death Inducers Controls Steroid-Triggered Cell Death in Drosophila. *Proc. Natl. Acad. Sci. U. S. A.* **101,** 8022-8027.

Yip, M. L., Lamka, M. L. and Lipshitz, H. D. (1997). Control of Germ-Band Retraction in Drosophila by the Zinc-Finger Protein HINDSIGHT. *Development* **124,** 2129-2141.

Yoshimori, T. (2007). Autophagy: Paying Charon's Toll. *Cell* **128,** 833-836.